UNIVERSIDADE FEDERAL DO PARANÁ

BARBARA MIGLIORETTO MONARO

APPLICATIONS OF THE SCHWINGER MULTICHANNEL METHOD TO THE SCATTERING OF SLOW ELECTRONS BY THE Z, E, N ISOMERS OF C-CYANOMETHANIMINE

CURITIBA

2025

BARBARA MIGLIORETTO MONARO

APPLICATIONS OF THE SCHWINGER MULTICHANNEL METHOD TO THE SCATTERING OF SLOW ELECTRONS BY THE Z, E, N ISOMERS OF C-CYANOMETHANIMINE

Dissertação apresentada ao programa de Pós-Graduação em Física do Setor de Ciências Exatas da Universidade Federal do Paraná, como requisito parcial à obtenção do título de Mestre em física. .

Orientador: Márcio Henrique Franco Bettega

CURITIBA

2025

DADOS INTERNACIONAIS DE CATALOGAÇÃO NA PUBLICAÇÃO (CIP)
UNIVERSIDADE FEDERAL DO PARANÁ
SISTEMA DE BIBLIOTECAS – BIBLIOTECA CIÊNCIA E TECNOLOGIA

Monaro, Barbara Miglioretto
Applications of the Schwinger multichannel method to the scattering of slow electrons by the Z, E, N isomers of C-cyanomethanimine. / Barbara Miglioretto Monaro. – Curitiba, 2025.
1 recurso on-line : PDF.

Dissertação (Mestrado) - Universidade Federal do Paraná, Setor de Ciências Exatas, Programa de Pós-Graduação em Física.

Orientador: Márcio Henrique Franco Bettega

1. Elétrons - Espalhamento. 2. Método Multicanal de Schwinger. 3. Meio interestelar. I. Universidade Federal do Paraná. II. Programa de Pós-Graduação em Física. III. Bettega, Márcio Henrique Franco. IV. Título.

Bibliotecária: Roseny Rivelini Morciani CRB-9/1585

TERMO DE APROVAÇÃO

Os membros da Banca Examinadora designada pelo Colegiado do Programa de Pós-Graduação FÍSICA da Universidade Federal do Paraná foram convocados para realizar a arguição da dissertação de Mestrado de **BARBARA MIGLIORETTO MONARO**, intitulada: **"Applications of the Schwinger Multichannel Method to the Scattering of Slow Electrons by the Z, E, N Isomers of C-Cyanomethanimine"**, sob orientação do Prof. Dr. MARCIO HENRIQUE FRANCO BETTEGA, que após terem inquirido a aluna e realizada a avaliação do trabalho, são de parecer pela sua APROVAÇÃO no rito de defesa.
A outorga do título de mestra está sujeita à homologação pelo colegiado, ao atendimento de todas as indicações e correções solicitadas pela banca e ao pleno atendimento das demandas regimentais do Programa de Pós-Graduação.

CURITIBA, 30 de Outubro de 2025.

Assinatura Eletrônica
30/10/2025 17:13:11.0
MARCIO HENRIQUE FRANCO BETTEGA
Presidente da Banca Examinadora

Assinatura Eletrônica
30/10/2025 17:26:18.0
GISELI MARIA MOREIRA
Avaliador Externo (UNIVERSIDADE ESTADUAL DO CENTRO - OESTE)

Assinatura Eletrônica
31/10/2025 16:23:10.0
SERGIO D´ALMEIDA SANCHEZ
Avaliador Interno (UNIVERSIDADE FEDERAL DO PARANÁ)

Dedico este trabalho a todos aqueles que se empenham em promover uma prática científica acessível, engajada e voltada para a transformação social.

AGRADECIMENTOS

A conclusão deste mestrado um é momento de imensa gratidão, e gostaria de expressar meus sinceros agradecimentos a todos que, de alguma forma, tornaram essa jornada possível.

Primeiramente, minha mais profunda gratidão ao meu orientador, Márcio Henrique Franco Bettega. Sua confiança inabalável, a orientação precisa e o entusiasmo contagiante foram a bússola que guiou esta pesquisa. Agradeço por me desafiar intelectualmente e por me ensinar a pensar de forma crítica e inovadora. E, principalmente, por me acolher em um momento tão conturbado quanto o início deste mestrado.

Agradeço à Universidade Federal do Paraná e ao Programa de Pós Graduação em Física pelo ambiente acadêmico, de certa forma, inspirador e pelos recursos que tive à disposição. Um agradecimento especial aos membros da banca examinadora, por dedicarem seu tempo e conhecimento à leitura e avaliação deste trabalho.

Aos meus colegas e amigos do Grupo de Pesquisa em Física Atômica e Molecular o GFAM, ou como eu gosto de chamar, o GFun, Vitorino, Ed, Francisco, Jhenifer e Pedro. Agradeço pelas discussões, pelo apoio mútuo e pelo companheirismo que tornaram os dias de trabalho mais leves e produtivos.

Aos meus colegas da sala 113, alguns da 116 e melhores amigos Thayna Vaz, Beatriz Tremarin, Nicole Lecheta, Victor Wellington (Cictor), Felipe Magno, Matheus Franco e Sidnei Jr. Agradeço pelas discussões, pela rede de apoio e pelo companheirismo em tantas fases, e situações que renderam certo entretenimento. A vida sempre fica mais bonita quando você encontra pertencimento, e com vocês os dias foram incrivelmente mais belos.

Por fim, e com o coração cheio, agradeço à minha família, o meu porto seguro. A Sandra Miglioretto, minha mãe, Rinaldo Monaro, meu pai e Caroline Miglioretto Monaro, minha irmã que em todo momento possível não deixaram de apoiar este sonho. Não chegaria aqui se não fosse pelos puxões de orelha de voces ao longo do caminho. Agradeço em especial ao João Pedro que foi do companheiro mais singular da 113 para um companheiro de vida. Obrigado por ser casa. Este trabalho é, em grande parte, o reflexo do apoio e da crença de cada um de vocês.

Se era inteligente, não sabia. Ser ou não inteligente dependia muito da instabilidade dos outros.

— CLARICE LISPECTOR

RESUMO

A detecção de moléculas prebióticas em ambientes astrofísicos, especialmente em regiões de formação estelar, é fundamental para a compreensão das origens da vida e da química do meio interestelar (Interestelar Medium-ISM). Entre tais espécies, a C-cianometanimina (HNCHCN) destaca-se por atuar como intermediária na síntese da adenina e como possível precursora de moléculas biologicamente relevantes. Seus três isômeros estruturais (Z, E e N), todos já detectados no ISM, apresentam propriedades de espalhamento eletrônico essenciais para a modelagem de processos induzidos por radiação em ambientes astrofísicos.Esta dissertação apresenta um estudo teórico do espalhamento de elétrons de baixa energia pelos três isômeros da C-cianometanimina. As geometrias de equilíbrio e as energias relativas foram determinadas nos níveis Hartree–Fock [HF/6-31G(d)] e Teoria do Funcional da Densidade (DFT), complementados por métodos de função de onda correlacionada. Os cálculos de espalhamento foram realizados por meio do Método Multicanal de Schwinger (SMC) com pseudopotenciais, nas aproximações estático-troca (SE) e estático-troca mais polarização (SEP). Análises adicionais incluíram a diagonalização do Hamiltoniano de colisão para a caracterização de autovalores próximos às ressonâncias e de seus orbitais associados, bem como o procedimento de complemento de Born para a descrição das interações de longo alcance. Os resultados mostram o isômero Z como mínimo global, enquanto os isômeros E e N apresentam energias mais elevadas, separadas por barreiras de isomerização significativas. Na aproximação SE, cada isômero exibe duas ressonâncias de forma associadas a orbitais π^*: uma de simetria A′ (em aproximadamente 1,66, 1,80 e 2,63 eV para Z, E e N, respectivamente) e outra de simetria A″ (3,73, 3,59 e 3,82 eV). Adicionalmente, identifica-se uma ressonância de forma de baixa energia de simetria A″ (1,15, 1,22 e 0,88 eV), que se torna um estado ligado no tratamento SEP, acompanhado pela redução das energias das demais ressonâncias, comportamento confirmado pela diagonalização do Hamiltoniano de colisão e por cálculos de energia total. Este estudo fornece uma caracterização teórica abrangente do espalhamento eletrônico na C-cianometanimina, contribuindo com dados fundamentais para modelos de astroquímica e de física de plasmas.

Palavras-chaves: Espalhamento de elétrons C-cianometanimina; Meio interestelar; Método Multicanal de Schwinger; Completar com Born.

ABSTRACT

The detection of prebiotic molecules in astrophysical environments, particularly in star-forming regions, is essential for understanding the origins of life and the chemistry of the interstellar medium (ISM). Among such species, C-cyanomethanimine (HNCHCN) stands out as an intermediate in adenine formation and as a potential precursor of biologically relevant molecules. Its three structural isomers (Z, E, and N), all of which have already been detected in the ISM, exhibit electron-scattering properties that are crucial for modeling radiation-induced processes in astrophysical environments. This dissertation presents a theoretical investigation of low-energy electron scattering by the three isomers of C-cyanomethanimine. Equilibrium geometries and relative energies were computed at the Hartree–Fock [HF/6-31G(d)] and Density Functional Theory (DFT) levels, complemented by correlated wave function methods. Scattering calculations were performed using the Schwinger Multichannel Method (SMC) with pseudopotentials, within the static-exchange (SE) and static-exchange plus polarization (SEP) approximations. Additional analyses included collision-Hamiltonian diagonalization to characterize eigenvalues near resonant states and their associated orbitals, as well as Born-completion procedures to describe long-range interactions. The results indicate that the Z isomer is the global minimum, while the E and N isomers lie at higher energies, separated by significant isomerization barriers. Within the SE approximation, each isomer exhibits two shape resonances associated with π^* orbitals: one of A′ symmetry (at approximately 1.66, 1.80, and 2.63 eV for Z, E, and N, respectively) and one of A″ symmetry (3.73, 3.59, and 3.82 eV). An additional low-energy A″ shape resonance (1.15, 1.22, and 0.88 eV) becomes a bound state in the SEP treatment, accompanied by a lowering of the remaining resonance energies, a behavior confirmed through collision-Hamiltonian diagonalization and total-energy calculations. This work provides a comprehensive theoretical characterization of electron scattering in C-cyanomethanimine, offering essential data for astrochemical and plasma-physics modeling.

Key-words: Electron scattering; C-cyanomethanimine; Interstellar medium; Schwinger Multichannel method; Born-closure.

LIST OF FIGURES

SUMMARY

CHAPTER 1

INTRODUCTION

The interaction of low-energy electrons with molecules has attracted growing attention from the scientific community in recent decades, particularly in biological and astrophysical contexts [1]. These studies provide fundamental information on critical scattering phenomena, including elastic, inelastic, ionization processes, and the highly relevant dissociative electron attachment (DEA). A central feature governing these interactions is the formation of temporary negative ions, or resonances, which are associated with the temporary capture of an incident electron by an unoccupied molecular orbital [2–4]. Depending on the molecular orbital involved, these resonances are typically characterized as being of σ^* or π^* character, and their short lifetimes (on the order of 10^{-15}–10^{-14} s) are nonetheless sufficient to drive significant nuclear motion, potentially leading to dissociation of the parent molecule [3, 5, 6].

In the biological domain, pioneering work [7] demonstrated that low-energy electrons can induce single and double-strand breaks in DNA through DEA, even at energies below the ionization threshold. These breaks arise when transient negative ions form in local subunits such as nucleobases or sugar moieties, leading to fragmentation of the phosphodiester backbone. This discovery motivated extensive theoretical and experimental efforts focused on electron interactions with biologically relevant molecules, thereby advancing the understanding of radiation damage at the molecular level [8]. Given the widespread use of ionizing radiation in biomedical applications for both diagnosis and therapy, there is substantial demand for fundamental knowledge regarding the phenomena occurring in human tissue, where accurate determination of electronic excitation cross sections for DNA constituents is crucial for modeling the effects of secondary electrons.

Beyond biological applications, scattering data is highly sought after for technological applications, particularly in understanding and optimizing processing plasmas [9–11]. The generation of these plasmas involves introducing a small amount of gas into a vacuum chamber and subjecting it to an alternating electromagnetic field, promoting partial ionization of the gas. The released electrons then collide with present molecules, generating secondary species, making precise cross-section data essential for modeling plasma dynamics[12–16]. Furthermore, industrial interest is directed toward enhancing the performance of machinery powered by fossil fuels through innovative approaches

like plasma ignition spark plugs, which promote more complete combustion, significantly increasing fuel efficiency while substantially reducing pollutant emissions[17, 18].

From a theoretical standpoint, electron scattering poses a formidable many-body quantum problem whose exact solution remains intractable. To address this, various approximations are employed [19, 20]. The Born-Oppenheimer approximation simplifies the problem by treating the nuclei as fixed due to their much slower motion relative to electrons. At the electronic level, calculations often begin with the static-exchange (SE) approximation, which accounts for the Pauli exchange principle and the electrostatic interaction between the incident electron and the target molecule [20]. However, at low energies, polarization effects become crucial, requiring the more refined static-exchange plus polarization (SEP) approximation. The molecular electronic structure is typically described within the Hartree-Fock framework, while scattering amplitudes can be computed using variational methods such as the Schwinger Multichannel (SMC) method [5, 21–23], which is well-suited for treating elastic, inelastic, and resonant processes for polyatomic molecules.

Beyond terrestrial relevance, electron scattering plays a pivotal role in astrochemistry [1]. The interstellar medium (ISM), though cold and tenuous, is constantly bombarded by cosmic rays that generate secondary electrons. These electrons efficiently drive excitation, ionization, and fragmentation processes that would otherwise be too slow under interstellar conditions, profoundly influencing the chemical inventory of space. Accordingly, accurate electron-molecule cross sections are indispensable for astrochemical models designed to explain the origin and evolution of molecular complexity in the universe [1].

Within this context, C-cyanomethanimine (HNCHCN) has emerged as a molecule of profound astrochemical and prebiotic importance [24, 25]. High-accuracy theoretical work [26] established the fundamental quantum chemical properties of its isomers, identifying the Z-isomer as the global minimum, with the E- and N-isomers lying higher in energy by 0.0136 eV and 0.2422 eV, respectively. A large isomerization barrier ($\sim$25 kcal/mol or 1.084 eV) confirmed the kinetic stability of the isomers in the ISM, preventing rapid interconversion. The molecular structures of these isomers are shown in Figure 1.

These theoretical foundations enabled subsequent astronomical detections: the E-isomer was first reported toward Sagittarius B2(N) [27], and the Z-isomer was later detected toward the Galactic Center source G+0.693-0.027 [28]. More recently, the N-cyanomethanimine isomer (H_2CNCN) has also been detected in the same source [29]. Importantly, the Z-isomer was found to be significantly more abundant than the E-isomer under interstellar conditions (T $\approx$ 150 K), consistent with thermodynamic predictions and strongly suggestive of grain-surface formation routes. These findings firmly establish

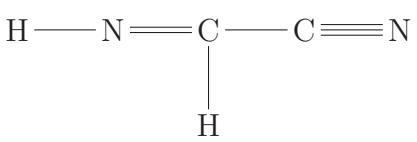

(a) Generic Structure

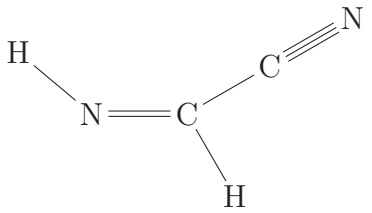

(b) Z-C

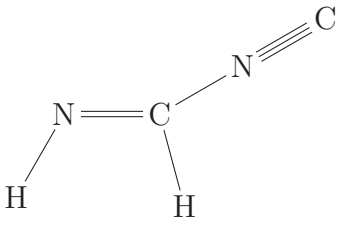

(c) E-C

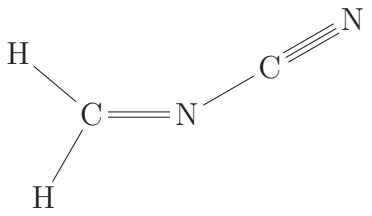

(d) N

FIGURE 1 – 2D chemical structures of C-Cyanomethanimine and its isomers. Source: Author's own work (2025).

cyanomethanimine as a plausible intermediate in the formation of adenine, a nucleobase of DNA and RNA, directly linking its chemistry to the molecular origins of life.

Despite these advances, a critical gap remains: The electron-scattering properties of C-cyanomethanimine have not yet been investigated. Given the dominance of electron-driven chemistry in interstellar environments, knowledge of elastic scattering cross sections and resonant phenomena is essential to model its excitation, stability, and potential fragmentation under astrophysical conditions [24].

This dissertation addresses this significant deficiency by performing a systematic computational study of low-energy electron scattering from C-cyanomethanimine isomers. These molecules are of considerable interest in prebiotic chemistry and are potential precursors to nucleobases in the interstellar medium. This work bridges the existing gap, providing essential input for both astrochemical and plasma physics applications by connecting fundamental scattering theory with the chemistry of the ISM.

To this end, we employ the Schwinger multichannel method in both static-exchange and static-exchange-plus-polarization approximations to accurately capture the physics of transient anion formation. We calculate elastic integral cross sections and, most importantly, identify and characterize resonance features that are directly relevant to processes like dissociative electron attachment. Our results confirm the established energetic ordering of the Z, E, and N isomers and reveal distinct resonance features for each. Furthermore, the presence of these transient anions is confirmed through Hamiltonian diagonalization. This detailed theoretical characterization provides a foundational understanding of how low-energy electrons interact with these key

prebiotic molecules.

The remainder of this dissertation is structured as follows: Chapter 2 outlines the theoretical framework, detailing the quantum theory of the scattering process, the specifics of the Schwinger multichannel method, and the Born-closure and Hamiltonian diagonalization procedures. Chapter 3 introduces the C-cyanomethanimine molecule, detailing its isomers and the computational methods used for electronic structure calculations and scattering calculations. Chapter 4 presents the core results, beginning with the electronic structure determined at the Hartree-Fock level and proceeding through the SE and SEP approximations of the SMC method. Finally, Chapter 5 provides a general conclusion, summarizing the main findings and discussing avenues for future work.

CHAPTER 2

THEORY

This chapter outlines the theoretical framework of our study. We begin by describing the target molecule within the Hartree-Fock method and the Born-Oppenheimer approximation. Subsequently, we address the electron-molecule scattering problem using the Schwinger Multichannel Method (SMC). The discussion of the SMC is followed by an overview of the static-exchange (SE) and static-exchange-plus-polarization (SEP) approximations, improved virtual orbitals (IVOs), modified virtual orbitals (MVOs), pseudopotentials, the Born-closure procedure, and the treatment of resonances. [1]

2.1 TARGET DESCRIPTION

The target molecule is described using the Hartree-Fock method under the Born-Oppenheimer approximation [30]. The usage of the Hartree–Fock approximation is necessary because the Schrödinger equation is not solvable exactly for polyatomic systems. The Born-Oppenheimer approximation decouples nuclear and electronic motion by treating the nuclei as fixed, justified by their significantly greater mass and consequently slower movement compared to electrons [5].

The Hamiltonian for a molecule with N electrons and M nuclei in atomic units is:

$$H_{\text{molecule}} = -\sum_{i=1}^{N}\frac{\nabla_i^2}{2} - \sum_{A=1}^{M}\frac{\nabla_A^2}{2M_A} - \sum_{i=1}^{N}\sum_{A=1}^{M}\frac{Z_A}{r_{iA}} + \sum_{i=1}^{N}\sum_{j>i}^{N}\frac{1}{r_{ij}} + \sum_{A=1}^{M}\sum_{B>A}^{M}\frac{Z_A Z_B}{R_{AB}} \tag{2.1}$$

where r_{iA} is the distance between the i-th electron and the A-th nucleus; r_{ij} is the distance between the i-th and j-th electrons; R_{AB} is the distance between the A-th and B-th nuclei; M_A is the ratio of the mass of nucleus A to the mass of the electron; and Z_A and Z_B are the atomic numbers of nucleus A and nucleus B, respectively.

[1] Throughout this work, we employ atomic units ($\hbar = e = m_e = 1$) [30]. Consequently, the Bohr radius (a_0) is the unit of length, and integral cross-sections are reported in a_0^2. For comparison with the literature, cross-sections are also given in square angstroms (Å^2), using the conversion $a_0 = 0.5291$ Å. All theoretical figures presented in this chapter are based on concepts from theoretical books of reference [20, 30]. The original visualizations were created by L. V. Dalagnol (2025).

The first term is the kinetic energy operator of the electrons; the second term is the kinetic energy operator of the nuclei; the third term is the Coulomb attraction between the electrons and the nuclei; the fourth term is the repulsion between the electrons; and the fifth term is the repulsion between the nuclei.

Given the considerable difference in mass between nuclei and electrons, nuclear dynamics are considerably slower than electronic motion. This permits the assumption of a fixed nuclear framework, thus reducing the problem to solving the electronic Schrödinger equation. Formally, this involves neglecting the nuclear kinetic energy term, leading to the following molecular Hamiltonian:

$$H_{\text{molecule}} = H_{\text{electronic}} + \sum_{A=1}^{M} \sum_{B>A}^{M} \frac{Z_A Z_B}{R_{AB}} \tag{2.2}$$

the second term in Equation (2.2), representing the nuclear repulsion, can be treated as a constant. Thus, we only need to solve the electronic Hamiltonian ($H_{\text{electronic}}$), which is given by:

$$H_{\text{electronic}} = -\sum_{i=1}^{N} \frac{\nabla_i^2}{2} - \sum_{i=1}^{N} \sum_{A=1}^{M} \frac{Z_A}{r_{iA}} + \sum_{i=1}^{N} \sum_{j>i}^{N} \frac{1}{r_{ij}}. \tag{2.3}$$

With the electronic Hamiltonian $H_{\text{electronic}}$ defined, we now proceed to describe the molecular ground state using the variational Hartree-Fock method. In this approach, the antisymmetric trial wave function for an N-electron system is represented by a single Slater determinant, which depends parametrically on the nuclear coordinates:

$$\Phi(\boldsymbol{x}_1, \boldsymbol{x}_2, \ldots, \boldsymbol{x}_N) = \frac{1}{\sqrt{N!}} \begin{vmatrix} \chi_1(\boldsymbol{x}_1) & \chi_2(\boldsymbol{x}_1) & \cdots & \chi_N(\boldsymbol{x}_1) \\ \chi_1(\boldsymbol{x}_2) & \chi_2(\boldsymbol{x}_2) & \cdots & \chi_N(\boldsymbol{x}_2) \\ \vdots & \vdots & \ddots & \vdots \\ \chi_1(\boldsymbol{x}_N) & \chi_2(\boldsymbol{x}_N) & \cdots & \chi_N(\boldsymbol{x}_N) \end{vmatrix} \tag{2.4}$$

where $(N!)^{-1/2}$ is a normalization factor. This determinant is composed of a set of spin orbitals $|\Phi_0\rangle = |\chi_1 \chi_2 \cdots \chi_N\rangle$. These spin orbitals provide the spatial position of the electron $\psi(\boldsymbol{r})$ and its spin: up for $\alpha(\omega)$ and down for $\beta(\omega)$:

$$\chi(\boldsymbol{x}) = \begin{cases} \psi(\boldsymbol{r})\alpha(\omega) \\ \psi(\boldsymbol{r})\beta(\omega), \end{cases} \tag{2.5}$$

where ω corresponds to the spin coordinate, $\boldsymbol{r}$ corresponds to the three spatial coordinates, and $\boldsymbol{x}$ represents the four coordinates, $\boldsymbol{x} = (\boldsymbol{r}, \omega)$.

The variational principle is applied to obtain set of $\chi_j(\boldsymbol{x}_i)$, where the optimal wave function is the one that minimizes the energy:

$$E_0 = \langle \Phi_0 | H_e | \Phi_0 \rangle \tag{2.6}$$

Here, the equation above is a functional of the spin orbitals $\{\chi_j(\boldsymbol{x}_i)\}$. We can express the total energy as a functional of spin orbitals as follows.

$$E_0[\{\chi_j\}] = \sum_{j=1}^{N} [j|h|j] + \frac{1}{2} \sum_{j=1}^{N} \sum_{k=1}^{N} \big([jj|kk] - [jk|kj] \big), \tag{2.7}$$

where $[j|h|j]$ is the notation used for the one-electron integral, and $[jj|kk]$ and $[jk|kj]$ represent two-electron integrals. The Coulomb and exchange integrals, respectively, are written as:

$$[j|h|j] = k_{jj} = \int d\boldsymbol{x}_1 \, \chi_j^*(\boldsymbol{x}_1) \left(-\frac{1}{2} \nabla_1^2 - \sum_A \frac{Z_A}{r_{1A}} \right) \chi_j(\boldsymbol{x}_1), \tag{2.8}$$

$$[jj \mid kk] = J_{jk} = \int d\boldsymbol{x}_1 d\boldsymbol{x}_2 \, \chi_j^*(1) \chi_j(1) \frac{1}{r_{12}} \chi_k^*(2) \chi_k(2), \tag{2.9}$$

$$[jk \mid kj] = K_{jk} = \int d\boldsymbol{x}_1 d\boldsymbol{x}_2 \, \chi_j^*(1) \chi_k(1) \frac{1}{r_{12}} \chi_k^*(2) \chi_j(2), \tag{2.10}$$

where the one-electron integral represents the average kinetic energy and nuclear attraction energy of an electron, the Coulomb integral Equation (2.8) arises from the repulsion between electron clouds, and the exchange integral Equation (2.9) results from the antisymmetric nature of the Slater determinant.

We need to minimize $E_0[\{\chi_j(\boldsymbol{x}_i)\}]$ with respect to the spin orbitals while maintaining their orthonormality to obtain the Hartree-Fock equations That is, subject to the constraint $[j \mid k] - \delta_{jk} = 0$. We then obtain the functional $\mathcal{L}[\{\chi_j(\boldsymbol{x}_i)\}]$ for the spin orbitals, which takes the following form:

$$\mathcal{L}[\{\chi_j(\boldsymbol{x}_i)\}] = E_0[\{\chi_j(\boldsymbol{x}_i)\}] - \sum_{j=1}^{N} \sum_{k=1}^{N} \varepsilon_{kj} \left([j \mid k] - \delta_{jk} \right), \tag{2.12}$$

where the coefficients ε_{kj} are Lagrange multipliers. Since $\mathcal{L}$ is real and $[j \mid k] = [k \mid j]^*$, the Lagrange multipliers must form a Hermitian matrix. By imposing the condition that $\delta\mathcal{L}[\{\chi_j\}]$ be stationary with respect to small variations in the spin orbitals (i.e., $\chi_j \to \chi_j + \delta\chi_j$), and after some manipulations, we arrive at the following equation:

$$f|\chi_j\rangle = \sum_{k=1}^{N} \varepsilon_{jk} |\chi_k\rangle \tag{2.13}$$

where f is called the Fock operator and will be defined later. The expression above is an eigenvalue equation, but it is not in its usual form. To express it in the canonical form, we need to "rotate"the spin orbitals through a unitary transformation U ($U^\dagger = U^{-1}$):

$$\chi'_j = \sum_k \chi_k U_{kj}. \tag{2.14}$$

Through the unitary transformation of the spin orbitals Equation (2.14), the wave function can be rewritten as:

$$|\Phi'_0\rangle = \det(U)\,|\Phi_0\rangle = e^{(i\theta)}\,|\Phi_0\rangle\,, \tag{2.15}$$

where the transformed determinant $|\Phi'_0\rangle$ is expressed in terms of the original determinant $|\Phi_0\rangle$ multiplied by a phase factor. Since the observables of interest depend only on $|\Phi_0|^2$, the original wave function in terms of the spin orbitals $\{\chi_j\}$ and the transformed wave function in terms of the spin orbitals $\{\chi'_j\}$ are identical. If U is a real matrix, the phase factor is ± 1. The Fock operator f is invariant under an arbitrary unitary transformation of the spin orbitals, i.e., $f'(1) = f(1)$.

We now have a system of N coupled nonlinear integro-differential equations called the canonical Hartree-Fock equations, written for the i-th electron occupying the j-th spin orbital:

$$f(i)\chi_j(i) = \varepsilon_j \chi_j(i) \quad (j = 1, \ldots, N) \tag{2.16}$$

Here, ε_j is the eigenvalue corresponding to the orbital χ_j, and $f(i)$ is the Fock operator, defined as:

$$f(i) = -\frac{\nabla_i^2}{2} - \sum_{A=1}^{M} \frac{Z_A}{r_{iA}} + v^{HF}(i) \tag{2.17}$$

The electron's kinetic energy contribution and the electron-nucleus interaction are represented in the first and second term of the equation, respectively, while v^{HF} is called the Hartree-Fock (HF) potential, which depends on the spin orbitals. The HF potential is the term that couples the equations and is expressed in terms of integrals of the eigenfunctions. These are called coupled integro-differential equations because they are differential equations containing integrals, where the Fock operator depends on its own eigenfunctions.

For closed-shell systems (where each occupied orbital contains two electrons with opposite spins - doubly occupied molecular orbitals resulting in an overall singlet

spin state), we can rewrite Equation (2.16). This allows summing the Hartree-Fock equations over all spins, resulting in a set of $N/2$ equations for the spatial orbitals ψ_j:

$$f(\boldsymbol{r}_i)\psi_j(\boldsymbol{r}_i) = \varepsilon_j\psi_j(\boldsymbol{r}_i), \quad (j = 1, ..., N/2) \tag{2.18}$$

where the Fock operator $f(\boldsymbol{r}_i)$ is written as:

$$f(\boldsymbol{r}_i) = -\frac{\nabla_i^2}{2} - \sum_{A=1}^{M}\frac{Z_A}{r_{iA}} + v^{HF}(\boldsymbol{r}_i) \tag{2.19}$$

v^{HF} is the Hartree-Fock potential, which now takes the form

$$v^{HF}(\boldsymbol{r}_i) = \sum_{a=1}^{N/2}[2J_a(\boldsymbol{r}_i) - K_a(\boldsymbol{r}_i)] \tag{2.20}$$

This represents the effective potential experienced by the i-th electron due to all other electrons, where J_a is the Coulomb operator and K_a is the exchange operator, defined respectively as:

$$J_a(\boldsymbol{r}_i)\psi_b(\boldsymbol{r}_i) = \left[\int d\boldsymbol{r}_j\psi_a^*(\boldsymbol{r}_j)\frac{1}{r_{ij}}\psi_a(\boldsymbol{r}_j)\right]\psi_b(\boldsymbol{r}_i) \tag{2.21}$$

$$K_a\left(\boldsymbol{r}_i\right)\psi_b\left(\boldsymbol{r}_i\right) = \left[\int d\boldsymbol{r}_j\psi_a^*\left(\boldsymbol{r}_j\right)\frac{1}{r_{ij}}\psi_b\left(\boldsymbol{r}_j\right)\right]\psi_a\left(\boldsymbol{r}_i\right) \tag{2.22}$$

where the Coulomb operator is local while the exchange operator represents an exchange between electron i and electron j in the spatial orbitals to the right of the r term [30]. Making a math manipulation by substituting equation (2.20) into (2.19), the Fock operator becomes:

$$f\left(\boldsymbol{r}_i\right) = \left[-\frac{\nabla_i^2}{2} - \sum_{A=1}^{M}\frac{Z_A}{r_{iA}}\right] + \sum_{a=1}^{N}\left[2J_a\left(\boldsymbol{r}_i\right) - K_a\left(\boldsymbol{r}_i\right)\right] \tag{2.23}$$

The problem Equation (2.18) can be solved by expressing the spatial orbitals as a linear combination of atomic orbitals (LCAO). That is, each spatial orbital $\psi_i(r)$ is expanded in a basis set $\phi_\mu(r)$ of atomic orbitals. By introducing a basis set, the integro-differential equations can be transformed into a set of algebraic equations [31]. These spatial orbitals are written as:

$$\psi_i = \sum_{\mu=1}^{k} C_{\mu i}\phi_\mu, \tag{2.24}$$

where $C_{\mu i}$ are expansion coefficients representing the contribution of each of the k atomic orbitals to each spatial orbital. This basis set does not necessarily need to be orthonormal, so we can define an overlap integral.

$$S_{\mu\nu} = \int d\boldsymbol{r}_1 \phi_\mu^* (\boldsymbol{r}_1) \, \phi_\nu (\boldsymbol{r}_1) \, . \tag{2.25}$$

These algebraic equations are known as the Hartree-Fock-Roothaan equations, expressed as:

$$\sum_{\nu=1}^{k} F_{\mu\nu} C_{\nu i} = \varepsilon_i \sum_{\nu=1}^{k} S_{\mu\nu} C_{\nu i}, \quad (i = 1, \ldots, k) \tag{2.26}$$

where C is the matrix of expansion coefficients describing the spatial orbital ψ_i, ε_i is the energy associated with orbital i, and F is the Fock matrix. The solution to the Hartree-Fock-Roothaan equations is obtained iteratively and will be discussed later. For now, let's express the Fock operator with two terms:

$$F_{\mu\nu} = H_{\mu\nu}^{\text{core}} + G_{\mu\nu}, \tag{2.27}$$

where $G_{\mu\nu}$ accounts for two-electron interactions (Coulomb and exchange), and $H_{\mu\nu}^{\text{core}}$ represents one-electron interactions (kinetic energy and electron-nucleus attraction), written as:

$$H_{\mu\nu}^{\text{core}} = T_{\mu\nu} + V_{\mu\nu}^{\text{nucl}}, \tag{2.28}$$

The corresponding expressions for the kinetic energy $T_{\mu\nu}$ and nuclear potential energy $V_{\mu\nu}^{\text{nucl}}$ terms are given by:

$$T_{\mu\nu} = \int d\boldsymbol{r}_1 \phi_\mu^* (\boldsymbol{r}_1) \left[-\frac{1}{2} \nabla_1^2 \right] \phi_\nu (\boldsymbol{r}_1) \, , \tag{2.29}$$

and

$$V_{\mu\nu}^{\text{nucl}} = \int d\boldsymbol{r}_1 \phi_\mu^* (\boldsymbol{r}_1) \left[\sum_{A=1}^{M} - \frac{Z_A}{|\boldsymbol{r}_1 - \boldsymbol{r}_A|} \right] \phi_\nu (\boldsymbol{r}_1) \, . \tag{2.30}$$

The term accounting for two-electron interactions can be expressed as:

$$G_{\mu\nu} = \sum_{\lambda=1}^{k} \sum_{\sigma=1}^{k} P_{\lambda\sigma} \left[(\mu\nu|\sigma\lambda) - \frac{1}{2} (\mu\lambda|\sigma\nu) \right], \tag{2.31}$$

where $P_{\lambda\sigma}$ is the charge density matrix, given by:

$$P_{\lambda\sigma} = 2 \sum_{a=1}^{N/2} C_{\lambda a} C_{\sigma a}^*, \tag{2.32}$$

The term $(\mu\nu \mid \lambda\sigma)$ represents the electron-electron repulsion integrals, written as:

$$(\mu\nu \mid \lambda\sigma) = \iint d\boldsymbol{r}_1 d\boldsymbol{r}_2 \phi_\mu^*(\boldsymbol{r}_1)\phi_\nu(\boldsymbol{r}_1)\frac{1}{|\boldsymbol{r}_1 - \boldsymbol{r}_2|}\phi_\lambda^*(\boldsymbol{r}_2)\phi_\sigma(\boldsymbol{r}_2). \tag{2.33}$$

With these mathematical foundations established, the Hartree-Fock-Roothaan equations are solved through a well-defined computational procedure. This process begins with the system definition, where the number of electrons and the coordinates and charges of the atomic nuclei are specified. The next critical step is basis set selection, wherein a set of basis functions ϕ_μ (typically Cartesian-Gaussian functions) is chosen to represent the molecular orbitals as in Equation (2.24). The use of Gaussian functions is particularly advantageous; linear combinations of them can accurately approximate atomic orbitals, and their mathematical properties are highly beneficial for computation. Specifically, the product of two Gaussian functions yields another Gaussian function, a characteristic that enables the analytical evaluation of all necessary integrals, including those for one-particle operators, Coulomb interactions, and exchange interactions.

These Cartesian functions take the form:

$$\lambda_{lmn}^{(\alpha)} = N_{lmn}(x - x_0)^l(y - y_0)^m(z - z_0)^n e^{-\alpha|\boldsymbol{r}-\boldsymbol{r}_0|^2}, \tag{2.34}$$

where $\boldsymbol{r}$ is the spatial position, $\boldsymbol{r}_0 = (x_0, y_0, z_0)$ is the position where the function is center, N is the Normalization factor] , $\{l, m, n\}$ are the cartesian exponents and α is the Gaussian exponent The type of function is determined by the sum $l + m + n$, as shown in Table 1:

TABLE 1 – Cartesian function types

Function Type	$l + m + n$
s	0
p	1
d	2
f	3

The Hartree-Fock self-consistent field (SCF) procedure begins by generating an initial coefficient matrix $C_{\mu i}$, which is used to construct the Fock matrix $F_{\mu\nu}$. Solving the resulting eigenvalue problem yields orbital energies ε_i and an updated set of coefficients $C'_{\mu i}$. These new coefficients are then used to recalculate the Fock matrix $F'_{\mu\nu}$, eigenvalues ε'_i, and further refined coefficients $C''_{\mu i}$ in an iterative cycle.

This process repeats until self-consistency between input and output values is achieved, typically monitored through convergence criteria based on the total system energy. Upon convergence, the final coefficient matrix and eigenvalues fully characterize the molecular orbitals' shapes and energies [30]. With this converged solution,

key properties like the ground state energy can be calculated from the total energy expectation value $E_0 = \frac{1}{2}\sum_{\mu,\nu} P_{\mu\nu}(H_{\mu\nu}^{\text{core}} + F_{\mu\nu}) + V_{nn}$, where V_{nn} represents nuclear repulsion.

The entire procedure leverages the analytical tractability of Gaussian basis functions Equation (2.34) for efficient computation of one- and two-electron integrals.

$$E_0 = \langle \Phi_0 | H | \Phi_0 \rangle \tag{2.35}$$

where the ground state energy E_0 is given by:

$$E_0 = 2\sum_{j}^{N/2} h_{jj} + \sum_{j}^{N/2}\sum_{k}^{N/2}(2J_{jk} - K_{jk}) \tag{2.36}$$

From the definition of the Fock operator presented earlier, we can express:

$$\varepsilon_j = f_{jj} = h_{jj} + \sum_{k}^{N/2}(2J_{jk} - K_{jk}) \tag{2.37}$$

which represents the orbital energy equation. Substituting equation (2.37) into equation (2.36) yields a new expression for E_0 in terms of ε_j:

$$E_0 = \sum_{j}^{N/2}(h_{jj} + \varepsilon_j) \tag{2.38}$$

When we incorporate the basis set expansion from equation (2.25), we obtain the formula for the ground state energy. Thus, the total energy becomes:

$$E_{\text{total}} = E_0 + \sum_{A=1}^{M}\sum_{B>A}^{M}\frac{Z_A Z_B}{R_{AB}} \tag{2.39}$$

E_0 represents the electronic energy, expressed as:

$$E_0 = \frac{1}{2}\sum_{\mu}\sum_{\nu} P_{\mu\nu}(H_{\mu\nu}^{core} + F_{\mu\nu}) \tag{2.40}$$

This formulation combines the one-electron core Hamiltonian (H^{core}), Fock matrix elements, and nuclear repulsion terms within the Hartree-Fock framework, while consistently maintaining the notation for Coulomb (J_{jk}) and exchange (K_{jk}) integrals throughout the derivation.

2.2 MOLECULAR ORBITALS

In this section we describe how the orbital bases used to construct the configuration spaces in this work are generated. Three classes of unoccupied orbitals play a central role in electron–molecule scattering calculations: the standard Virtual Orbitals (VOs), the Improved Virtual Orbitals (IVOs) [32], and the Modified Virtual Orbitals (MVOs) [33]. These orbitals differ in the electronic field under which they are produced, and therefore in their physical suitability for describing scattering functions, target excitations, and resonance phenomena.

A Hartree–Fock (HF) calculation of the ground state of an N-electron molecule yields a set of K spatial orbitals. Of these, $N/2$ are occupied, and the remaining $(K - N/2)$ orbitals constitute the standard VOs, which arise because the one-electron basis set is larger than the minimum needed to describe the occupied space. In electron–molecule scattering, VOs are appropriate for describing the continuum orbital in the static-exchange approximation, as they are orthogonal to the occupied orbitals and are generated in the mean field of the neutral target [34]. However, their adequacy deteriorates when excited configurations of the target are included, as in the static-exchange-plus-polarization (SEP) approximation.

According to Koopmans' theorem, the VOs produced by an N-electron HF calculation approximate orbitals of an $(N+1)$-electron system [35]. Thus, occupying a VO effectively mimics an $(N + 1)$-electron configuration rather than an excited configuration of the neutral molecule. For this reason, VOs do not provide a consistent description of neutral excited states and must be replaced when target polarization and excitation effects are important.

The IVOs [32, 34] were introduced to overcome this limitation. Instead of being generated in the N-electron field, they are constructed in the mean field of an $(N - 1)$-electron cation. Operationally, one removes an electron from the highest occupied molecular orbital (HOMO), freezes the remaining occupied orbitals, constructs the Fock operator of the resulting $+1$ cation, and diagonalizes it. The unoccupied eigenfunctions of this cationic Fock operator form the IVOs. When a single electron is added to one of these orbitals, the configuration corresponds, through Koopmans' theorem, to a singly excited state of the neutral molecule. Thus, IVOs offer a more physically meaningful basis for describing target excitations and the scattering orbital in SEP-like schemes. Spin-adapted (singlet or triplet) constructions may also be employed.

A further refinement is provided by the Modified Virtual Orbitals (MVOs) introduced by Bauschlicher and Taylor [33]. Their aim is to generate virtual orbitals that are more compact and localized than VOs, thereby improving the convergence of configuration-interaction expansions and enhancing the description of temporary

negative-ion states [33]. Conceptually, the procedure resembles that of the IVOs, but instead of removing a single electron, one removes n electrons (with n even) from the $n/2$ highest-energy occupied orbitals, maintaining the spatial and spin symmetry of the ground state. A Fock operator is then constructed for the resulting $+n$ cation, and its diagonalization yields the MVOs, which are virtual orbitals of an $(N-n)$-electron system.

An energy-based criterion is typically applied: only valence orbitals are removed, whereas core orbitals are retained in their HF form. The resulting orbitals are more compact and provide an improved description of short-range correlation and polarization effects, which are essential for the characterization of resonance states. The reference Slater determinant for the MVOs can be written as

$$|\Phi_{\mathrm{MVO}}\rangle = |X_1 X_2 \cdots X_n, X_0 \cdots X_{N-n}\rangle, \tag{2.1}$$

where $X_1, \ldots, X_n$ denote the orbitals from which electrons have been removed.

Among the three families of virtual orbitals discussed above, this dissertation places particular emphasis on the MVOs. Their compactness, enhanced localization, and ability to capture the short-range polarization responsible for temporary anion formation make them particularly suitable for the description of resonance states, the central topic of this work. Accordingly, the chapters that follow employ MVOs as the central orbital basis in the SEP treatment, where they are used to construct scattering functions and to analyze the structure and behavior of resonance states.

2.3 THE SCATTERING PROBLEM

The collision process can be described as a beam of particles (electrons) directed toward a gaseous target, where the incident particles are scattered upon interaction with the molecules. The scattered electrons are then detected by a detector positioned far from the target, which records the number of electrons scattered into a solid angle element $d\Omega$. The incident beam is assumed to be collimated and monoenergetic, i.e., it possesses a well-defined energy with only a narrow spread around this value. When such a beam interacts with the target gas, the molecules serve as independent scattering centers. Because the average intermolecular separation is much larger than the electron's de Broglie wavelength, interference between waves scattered by different molecules can be neglected. Furthermore, by considering the gas sufficiently dilute, multiple scattering events are suppressed, and the process may be treated as a sequence of independent single-molecule collisions. This simplified picture of the scattering geometry is schematically represented in Figure 2

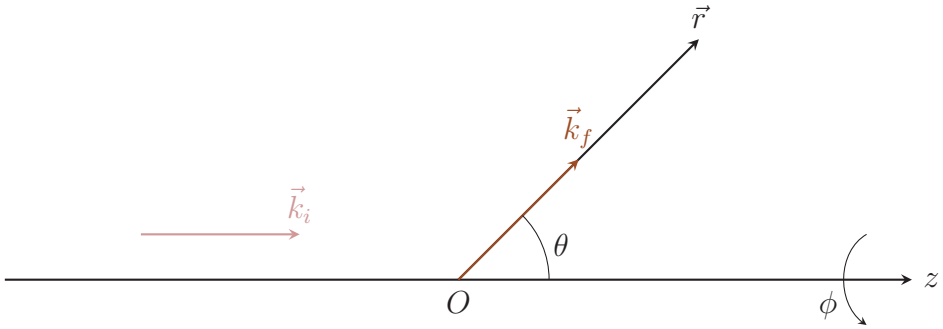

FIGURE 2 – Representation of the coordinates employed in the scattering calculations. Since the scattering is elastic, $|\vec{k}_i| = |\vec{k}_f| = k$. The incident vector $\vec{k}_i$ (in pink) coincides with the z-axis ($\vec{k}_i = k\hat{\boldsymbol{z}}$), whereas the scattered vector $\vec{k}_f$ (in orange) coincides with the position vector $\vec{r}$ ($\vec{k}_f = k\hat{\boldsymbol{r}}$).

The process can result in either elastic or inelastic scattering, depending on whether the target and the scattered electron retain or exchange energy. Scattering is said to be elastic when the scattered particle and the target remain with their energies unaltered. In the inelastic process, however, the electron transfers part of its energy to the molecule upon collision, which may lead the molecule to an excited state or even to dissociation. In this work, we will present the results of calculations for the elastic scattering of electrons by molecules.

2.3.1 Schwinger Variational Principle

In the problem of scattering by a potential, the time-independent Schrödinger equation in the coordinate basis $|\boldsymbol{r}\rangle$ is written as:

$$\left[-\frac{\nabla^2}{2} + V(\boldsymbol{r})\right] \Psi_{\boldsymbol{k}_{i,f}}(\boldsymbol{r}) = E\Psi_{\boldsymbol{k}_{i,f}}(\boldsymbol{r}), \tag{2.41}$$

where $\Psi_{\boldsymbol{k}_{i,f}}$ is the scattering wave function i and f denote the initial and final states of the scattering process, respectively), E is the total collision energy[2], and V is the scattering potential. Assuming the potential $V(\boldsymbol{r})$ must tend to zero faster than r^{-1} when $r \to \infty$, the scattering wave function must then satisfy the asymptotic condition [20], written as:

$$\left\langle \boldsymbol{r} \mid \Psi^{(+)}_{\boldsymbol{k}_i} \right\rangle = \Psi^{(+)}_{\boldsymbol{k}_i}(\boldsymbol{r}) \underset{|\boldsymbol{r}|\to\infty}{\longrightarrow} \frac{1}{(2\pi)^{\frac{3}{2}}} \left[e^{i\boldsymbol{k}_i\cdot\boldsymbol{r}} + f_{\boldsymbol{k}_f,\boldsymbol{k}_i} \frac{e^{ikr}}{r} \right], \tag{2.42}$$

[2] The possible final states are those that satisfy energy conservation:

$$E = E_i + \frac{k_i^2}{2} = E_f + \frac{k_f^2}{2},$$

where k is the magnitude of the particle's linear momentum, and E_i and E_f are the initial and final energies, respectively, of the target molecule.

where the first term is the plane wave, representing the free incident particle before any interaction with the target. The second term is an outgoing spherical wave, originating from the target, modulated by $f_{\boldsymbol{k}_f,\boldsymbol{k}_i}$, known as the scattering amplitude.

Using Dirac notation, equation (2.41) is written as (note that here we employ the relation $H = H_0 + V(\boldsymbol{r})$):

$$H \left|\Psi_{\boldsymbol{k}_{i,f}}\right\rangle = E \left|\Psi_{\boldsymbol{k}_{i,f}}\right\rangle \tag{2.43}$$

which is the non-homogeneous equation of the problem. The homogeneous equation for the energy eigenvalue E is written as:

$$H_0 \left|S_{\boldsymbol{k}_{i,f}}\right\rangle = E \left|S_{\boldsymbol{k}_{i,f}}\right\rangle \tag{2.44}$$

where $\left|S_{\boldsymbol{k}_{i,f}}\right\rangle$ is a plane wave and, in the coordinate representation, is given by:

$$\left\langle \boldsymbol{r} \mid S_{\boldsymbol{k}_{i,f}}\right\rangle = \frac{1}{(2\pi)^{\frac{3}{2}}} e^{i\boldsymbol{k}_{i,f}\cdot\boldsymbol{r}} \tag{2.45}$$

The general solution of equation (2.43) is:

$$\left|\Psi^{(\pm)}_{\boldsymbol{k}_{i,f}}\right\rangle = \left|S_{\boldsymbol{k}_{i,f}}\right\rangle + G_0^{(\pm)} V \left|\Psi^{(\pm)}_{\boldsymbol{k}_{i,f}}\right\rangle \tag{2.46}$$

which is called the Lippmann-Schwinger equation [36]. This equation replaces the Schrödinger equation, where $\left|\Psi^{(\pm)}_{\boldsymbol{k}_{i,f}}\right\rangle$ is the solution of the problem with interaction, and $G_0^{(\pm)}(\boldsymbol{r},\boldsymbol{r}')$ is the free-particle Green's function, which now carries the asymptotic condition. The Green's operator is given by:

$$G_0^{(\pm)} = \frac{1}{(E - H_0 \pm i\epsilon)} \tag{2.47}$$

The positive and negative signs correspond to the boundary conditions, for which there are two possible mathematical solutions. However, only the solution corresponding to the (+) sign has physical meaning, which corresponds to a plane wave plus an outgoing spherical wave. In this case, a particle is incident with momentum $\boldsymbol{k}_i$ and leaves the target region with momentum $\boldsymbol{k}_f$.

Projecting the Lippmann-Schwinger equation onto the coordinate basis $|\boldsymbol{r}\rangle$, we obtain:

$$\left\langle \boldsymbol{r}\middle|\Psi^{(\pm)}_{\boldsymbol{k}_{i,f}}\right\rangle = \left\langle \boldsymbol{r}\middle|S_{\boldsymbol{k}_{i,f}}\right\rangle + \left\langle \boldsymbol{r}\middle|G_0^{(\pm)} V\middle|\Psi^{(\pm)}_{\boldsymbol{k}_{i,f}}\right\rangle \tag{2.48}$$

We then arrive at:

$$\left\langle \boldsymbol{r} \mid \Psi^{(\pm)}_{\boldsymbol{k}_{i,f}} \right\rangle = \left\langle \boldsymbol{r} \mid S_{\boldsymbol{k}_{i,f}} \right\rangle + \int d\boldsymbol{r}' \langle \boldsymbol{r}| G^{(\pm)}_0 |\boldsymbol{r}'\rangle \langle \boldsymbol{r}'| V \left| \Psi^{(\pm)}_{\boldsymbol{k}_{i,f}} \right\rangle, \tag{2.49}$$

here, we used the completeness relation:

$$1 = \int d^3r' \, |\boldsymbol{r}'\rangle \langle \boldsymbol{r}'| \tag{2.50}$$

The free-particle Green's function operator is written as:

$$G^{(\pm)}_0 (\boldsymbol{r}, \boldsymbol{r}') = \langle \boldsymbol{r}| \left[\frac{1}{(E - H_0 \pm i\epsilon)} \right] |\boldsymbol{r}'\rangle \tag{2.51}$$

Also we can write the homogeneous equation in the plane wave basis as:

$$H_0 |\boldsymbol{k}\rangle = \frac{k^2}{2} |\boldsymbol{k}\rangle \tag{2.52}$$

We introduce the completeness relation for the plane wave basis, $1 = \int dk' \, |\boldsymbol{k}'\rangle \langle \boldsymbol{k}'|$, into the Green's function Equation (2.51) to obtain the following equation:

$$G^{(\pm)}_0 (\boldsymbol{r}, \boldsymbol{r}') = \langle \boldsymbol{r}| \left[\frac{1}{(E - H_0 \pm i\epsilon)} \right] \left\{ \int d\boldsymbol{k}' \, |\boldsymbol{k}'\rangle \langle \boldsymbol{k}'| \right\} |\boldsymbol{r}'\rangle \tag{2.53}$$

The solution of equation (2.53) can be found using equation (2.45) and the eigenvalue from (2.52) (where $E = \frac{k^2}{2}$ is the total collision energy). We then have:

$$G^{(\pm)}_0 (\boldsymbol{r}, \boldsymbol{r}') = \int d\boldsymbol{k}' \frac{\langle \boldsymbol{r} \mid \boldsymbol{k}' \rangle \langle \boldsymbol{k}' \mid \boldsymbol{r} \rangle}{\frac{k^2}{2} - \frac{k'^2}{2} \pm i\epsilon} \tag{2.54}$$

after some algebraic manipulations, we arrive at the following integral equation:

$$G^{(\pm)}_0 (\boldsymbol{r}, \boldsymbol{r}') = -\frac{1}{8\pi^3} \int d\boldsymbol{k}' \frac{e^{i\boldsymbol{k}' \cdot (\boldsymbol{r} - \boldsymbol{r}')}}{(k'^2 - k^2 \mp i\epsilon)} \tag{2.55}$$

which can be solved by the residue theorem [20]. The result is given by:

$$G^{(\pm)}_0 (|\boldsymbol{r} - \boldsymbol{r}'|) = -\frac{1}{4\pi} \frac{e^{\pm ik|\boldsymbol{r} - \boldsymbol{r}'|}}{|\boldsymbol{r} - \boldsymbol{r}'|} \tag{2.56}$$

Using equation (2.56) into equation (2.49), the Lippmann-Schwinger equation in the coordinate basis becomes:

$$\left\langle \boldsymbol{r} \mid \Psi^{(\pm)}_{\boldsymbol{k}_{i,f}} \right\rangle = \frac{e^{i\boldsymbol{k}_{i,f} \cdot \boldsymbol{r}}}{(2\pi)^{\frac{3}{2}}} - 2 \int d\boldsymbol{r}' \frac{1}{4\pi} \frac{e^{\pm ik|\boldsymbol{r} - \boldsymbol{r}'|}}{|\boldsymbol{r} - \boldsymbol{r}'|} V(\boldsymbol{r}') \left\langle \boldsymbol{r}' \mid \Psi^{(\pm)}_{\boldsymbol{k}_{i,f}} \right\rangle \tag{2.57}$$

The boundary condition for our scattering problem consists of an incident plane wave with wave vector $\boldsymbol{k}_i$ and outgoing spherical waves generated from the target's

interaction region. The vector $\boldsymbol{r}$ is directed towards the point where the function will be evaluated, i.e., where the detector is located, and the potential is short-ranged. In scattering, we are interested in studying the effect of this finite-range potential at a point outside its range, as observations are always made by a detector placed far from the scattering center. Therefore, we are interested in the behavior of $\left\langle \boldsymbol{r} \mid \Psi^{(\pm)}_{\boldsymbol{k}_{i,f}} \right\rangle$ when $|\boldsymbol{r}| \gg |\boldsymbol{r}'|$ (which is mathematically equivalent to $|\boldsymbol{r}| \to \infty$). With this approximation, we can write the term $|\boldsymbol{r} - \boldsymbol{r}'|$ as follows:

$$|\boldsymbol{r} - \boldsymbol{r}'| \underset{|\boldsymbol{r}|\to\infty}{\cong} r - \hat{r} \cdot \boldsymbol{r}', \tag{2.58}$$

applying relation (2.58) to the Green's function, we have:

$$\frac{e^{ik|\boldsymbol{r}-\boldsymbol{r}'|}}{|\boldsymbol{r} - \boldsymbol{r}'|} \underset{|\boldsymbol{r}|\to\infty}{\cong} \frac{e^{ikr}e^{-ik\hat{r}\cdot\boldsymbol{r}'}}{r}\left(1 + \frac{\hat{r}\cdot\boldsymbol{r}'}{r} + \ldots\right). \tag{2.59}$$

We consider only the first-order term in the expansion of equation (2.59), as it is clear that terms beyond this order are negligible. With this, $\left|\Psi^{(+)}_{\boldsymbol{k}_i}\right\rangle$ is written as:

$$\left\langle \boldsymbol{r} \mid \Psi^{(+)}_{\boldsymbol{k}_i} \right\rangle = \Psi^{(+)}_{\boldsymbol{k}_i}(\boldsymbol{r}) \underset{|\boldsymbol{r}|\to\infty}{=} \frac{e^{i\boldsymbol{k}_i\cdot\boldsymbol{r}}}{(2\pi)^{\frac{3}{2}}} - \frac{1}{2\pi}\left(\frac{e^{ikr}}{r}\right)\int d\boldsymbol{r}' e^{-i\boldsymbol{k}_f\cdot\boldsymbol{r}'} V(\boldsymbol{r}') \left\langle \boldsymbol{r}' \mid \Psi^{(+)}_{\boldsymbol{k}_i} \right\rangle. \tag{2.60}$$

Comparing equation (2.60) with (2.42), we can find an expression for the scattering amplitude, written as:

$$f_{\boldsymbol{k}_f,\boldsymbol{k}_i} = -(2\pi)^{1/2}\int d\boldsymbol{r}' e^{-i\boldsymbol{k}_f\cdot\boldsymbol{r}'} V(\boldsymbol{r}') \left\langle \boldsymbol{r}' \mid \Psi^{(+)}_{\boldsymbol{k}_i} \right\rangle \tag{2.61}$$

and after some algebraic manipulations, we obtain an expression for the scattering amplitude in bra-ket notation, written as:

$$f_{\boldsymbol{k}_f,\boldsymbol{k}_i} = -(2\pi)^2 \left\langle S_{\boldsymbol{k}_f} \right| V \left|\Psi^{(+)}_{\boldsymbol{k}_i}\right\rangle. \tag{2.62}$$

it is also possible, starting from the equation for $\left|\Psi^{(-)}_{\boldsymbol{k}_f}\right\rangle$ and $|S_{\boldsymbol{k}_i}\rangle$, to obtain a second expression for the scattering amplitude:

$$f_{\boldsymbol{k}_f,\boldsymbol{k}_i} = -(2\pi)^2 \left\langle \Psi^{(-)}_{\boldsymbol{k}_f} \right| V |S_{\boldsymbol{k}_i}\rangle. \tag{2.63}$$

The equation (2.62) relates an incident plane wave plus an outgoing spherical wave, and equation (2.63) relates an incoming spherical wave plus a scattered plane wave. Multiplying the Lippmann-Schwinger equation (equation 2.46) by the potential, we obtain:

$$V\left|\Psi^{(\pm)}_{\boldsymbol{k}_{i,f}}\right\rangle = V\left|S_{\boldsymbol{k}_{i,f}}\right\rangle + VG_0^{(\pm)}V\left|\Psi^{(\pm)}_{\boldsymbol{k}_{i,f}}\right\rangle, \tag{2.64}$$

isolating the term $V\left|S_{\boldsymbol{k}_{i,f}}\right\rangle$ in the equation above, we arrive at the relation:

$$V\left|S_{\boldsymbol{k}_{i,f}}\right\rangle = \left(V - VG_0^{(\pm)}V\right)\left|\Psi^{(\pm)}_{\boldsymbol{k}_{i,f}}\right\rangle \tag{2.65}$$

then, if we substitute equation (2.65) into equation (2.63), we obtain a third expression for the scattering amplitude, written as:

$$f_{\boldsymbol{k}_f,\boldsymbol{k}_i} = -(2\pi)^2\left\langle\Psi^{(-)}_{\boldsymbol{k}_f}\right|\left(V - VG_0^{(+)}V\right)\left|\Psi^{(+)}_{\boldsymbol{k}_i}\right\rangle. \tag{2.66}$$

Thus, we have three expressions for the scattering amplitude. If we add equations (2.62) and (2.63) and subtract equation (2.66), we obtain a functional for the scattering amplitude. This functional has the form:

$$[f] = -(2\pi)^2\left[\left\langle S_{\boldsymbol{k}_f}\right|V\left|\Psi^{(+)}_{\boldsymbol{k}_i}\right\rangle + \left\langle\Psi^{(-)}_{\boldsymbol{k}_f}\right|V\left|S_{\boldsymbol{k}_i}\right\rangle - \left\langle\Psi^{(-)}_{\boldsymbol{k}_f}\right|A^{(+)}\left|\Psi^{(+)}_{\boldsymbol{k}_i}\right\rangle\right], \tag{2.67}$$

which is the so-called bilinear form of the Schwinger variational principle, where the operator $A^{(+)}$ is written as $A^{(+)} = V - VG_0^{(+)}V$. If the functions used $\left|\Psi^{(+)}_{\boldsymbol{k}_i}\right\rangle$ and $\left\langle\Psi^{(-)}_{\boldsymbol{k}_f}\right|$ are exact, $[f]$ represents the exact scattering amplitude [20]. Making small variations on the ket and the bra, we obtain trial functions, written as:

$$\left|\Psi^{(+)}_{\boldsymbol{k}_i}\right\rangle = \left|\Psi^{(+)}_{\boldsymbol{k}_i}\right\rangle + \left|\delta\Psi^{(+)}_{\boldsymbol{k}_i}\right\rangle \tag{2.68}$$

and

$$\left\langle\Psi^{(-)}_{\boldsymbol{k}_f}\right| = \left\langle\Psi^{(-)}_{\boldsymbol{k}_f}\right| + \left\langle\delta\Psi^{(-)}_{\boldsymbol{k}_f}\right|. \tag{2.69}$$

Applying these variations into equation (2.67), we have for the ket:

$$\delta[f] = -(2\pi)^2\left\{\left\langle S_{\boldsymbol{k}_f}\right|V + \left\langle\Psi^{(-)}_{\boldsymbol{k}_f}\right|A^{(+)}\right\}\left|\delta\Psi^{(+)}_{\boldsymbol{k}_i}\right\rangle, \tag{2.70}$$

and for the bra:

$$\delta[f] = -(2\pi)^2\left\langle\delta\Psi^{(-)}_{\boldsymbol{k}_f}\right|\left\{V\left|S_{\boldsymbol{k}_i}\right\rangle - A^{(+)}\left|\Psi^{(+)}_{\boldsymbol{k}_i}\right\rangle\right\}. \tag{2.71}$$

When $\left|\Psi^{(+)}_{\boldsymbol{k}_i}\right\rangle\left(\left\langle\Psi^{(-)}_{\boldsymbol{k}_f}\right|\right)$ is a solution of the Lippmann-Schwinger equation and $A^{(+)\dagger} = A^{(-)}$, we have $\delta[f] = 0$ for any $\left|\delta\Psi^{(+)}_{\boldsymbol{k}_i}\right\rangle\left(\left\langle\delta\Psi^{(-)}_{\boldsymbol{k}_f}\right|\right)$. We now consider kets and bras in the form:

$$\left|\Psi_{\boldsymbol{k}_i}^{(+)}\right\rangle \rightarrow A\left|\Psi_{\boldsymbol{k}_i}^{(+)}\right\rangle \tag{2.72}$$

$$\left\langle\Psi_{\boldsymbol{k}_f}^{(-)}\right| \rightarrow \tilde{B}^*\left\langle\Psi_{\boldsymbol{k}_f}^{(-)}\right| \tag{2.73}$$

where A and B are variational parameters. Inserting these expressions into the variational principle and varying with respect to A and $\tilde{B}$, we obtain the resulting expression of the variational method, written as:

$$\left[f_{\boldsymbol{k}_f,\boldsymbol{k}_i}\right] = -(2\pi)^2 \frac{\left\langle\Psi_{\boldsymbol{k}_f}^{(-)}\right| V\left|S_{\boldsymbol{k}_i}\right\rangle\left\langle S_{\boldsymbol{k}_f}\right| V\left|\Psi_{\boldsymbol{k}_i}^{(+)}\right\rangle}{\left\langle\Psi_{\boldsymbol{k}_f}^{(-)}\right| A^{(+)}\left|\Psi_{\boldsymbol{k}_i}^{(+)}\right\rangle} \tag{2.74}$$

this is the fractional form of the scattering amplitude. Note that the scattering functions always appear multiplied by the interaction potential V, and as a consequence, we only need to describe these functions where V is relevant.

We can expand the scattering wave functions $\left(\left|\Psi_{\boldsymbol{k}_i}^{(+)}\right\rangle \text{ and } \left|\Psi_{\boldsymbol{k}_f}^{(-)}\right\rangle\right)$ in known basis functions $\{|\chi_m\rangle\}$:

$$\left|\Psi_{\boldsymbol{k}_i}^{(+)}\right\rangle = \sum_m a_m^{(+)}\left(\boldsymbol{k}_i\right)|\chi_m\rangle \tag{2.75}$$

and

$$\left\langle\Psi_{\boldsymbol{k}_f}^{(-)}\right| = \sum_n a_n^{(-)*}\left(\boldsymbol{k}_f\right)\langle\chi_n| \tag{2.76}$$

where $a_m^{(+)}\left(\boldsymbol{k}_i\right)$ and $a_n^{(-)}\left(\boldsymbol{k}_f\right)$ are the variational parameters. Using (2.75) and (2.76) into (2.67), we obtain:

$$\begin{aligned}[f] = -(2\pi)^2 \Bigg[&\sum_m \langle\ S_{\boldsymbol{k}_f}|V|\,\chi_m\rangle\, a_m^{(+)}\left(\boldsymbol{k}_i\right) + \sum_n a_n^{(-)*}\left(\boldsymbol{k}_f\right)\langle\chi_n|\,V\,|S_{\boldsymbol{k}_i}\rangle - \\ &- \sum_{m,n} a_n^{(-)*}\left(\boldsymbol{k}_f\right)\langle\chi_n|\left(V - VG_0^{(+)}V\right)|\chi_m\rangle\, a_m^{(+)}\left(\boldsymbol{k}_i\right)\Bigg]\end{aligned} \tag{2.77}$$

Applying the condition that the scattering amplitude must be stationary, differentiating with respect to the variational parameters and setting to zero, we obtain:

$$\frac{\partial[f]}{\partial a_m^{(+)}\left(\boldsymbol{k}_i\right)} = -(2\pi)^2\left[\left\langle S_{\boldsymbol{k}_f}\right| V\left|\chi_m\right\rangle - \sum_n a_n^{(-)*}\left(\boldsymbol{k}_f\right)\langle\chi_n|\left(V - VG_0^{(+)}V\right)|\chi_m\rangle\right] = 0 \tag{2.78}$$

and

$$\frac{\partial[f]}{\partial a_n^{(-)*}(\boldsymbol{k}_f)} = -(2\pi)^2 \left[\langle \chi_n | V | S_{\boldsymbol{k}_i} \rangle - \sum_m a_m^{(+)}(\boldsymbol{k}_i) \langle \chi_n | \left(V - V G_0^{(+)} V \right) | \chi_m \rangle \right] = 0 \quad (2.79)$$

Then, the coefficients $a_m^{(+)}$ and $a_n^{(-)*}$ [34] are respectively written as:

$$a_m^{(+)}(\boldsymbol{k}_i) = \sum_n \langle \chi_n | V | S_{\boldsymbol{k}_i} \rangle \left(d^{-1} \right)_{mn} \quad (2.80)$$

and

$$a_n^{(-)*}(\boldsymbol{k}_f) = \sum_m \langle S_{\boldsymbol{k}_f} | V | \chi_m \rangle \left(d^{-1} \right)_{mn} \quad (2.81)$$

The matrix elements d_{mn} are written as:

$$d_{mn} = \langle \chi_m | A^{(+)} | \chi_n \rangle \quad (2.82)$$

and the operator $A^{(+)}$ is written as:

$$A^{(+)} = V - V G_0^{(+)} V \quad (2.83)$$

Therefore, the scattering amplitude is given by:

$$f_{\boldsymbol{k}_f, \boldsymbol{k}_i} = -(2\pi)^2 \sum_{m,n} \langle S_{\boldsymbol{k}_f} | V | \chi_m \rangle \left(d^{-1} \right)_{mn} \langle \chi_n | V | S_{\boldsymbol{k}_i} \rangle , \quad (2.84)$$

which is the expression obtained through the Schwinger variational principle (SVP) [36].

Among the advantages of the SVP is the fact that the boundary conditions of the problem are already included in the Green's function. As a consequence, the $|\chi_m\rangle$ do not need to obey any boundary conditions. Furthermore, the scattering wave function always appears multiplied by the potential V, and since V is short-ranged, the χ_m can be represented by square-integrable (L^2) functions, that is, functions that describe the scattering problem only within the region of influence of the target.

2.4 THE SCHWINGER MULTICHANNEL METHOD

The Schwinger multichannel (SMC) method [21, 22] is an extension of the Schwinger variational principle [36] for the study of low-energy electron scattering by molecules of arbitrary geometry. This method allows for the inclusion of exchange, correlation, polarization, among other effects, in an ab-initio manner.

The collision Hamiltonian for an electron plus a molecule can be written as:

$$H_{N+1} = (H_N + T_{N+1}) + V = H_0 + V, \quad (2.85)$$

where H_N is the electronic Hamiltonian of the molecule in the Born-Oppenheimer approximation, T_{N+1} is the kinetic energy operator of the incident electron, and V is the interaction potential between the incident electron and the target molecule. The electronic Hamiltonian, the kinetic energy operator, and the potential are defined by:

$$H_N = \sum_{i=1}^{N} \left[-\frac{\nabla_i^2}{2} + \sum_{A=1}^{M} -\frac{Z_A}{|\boldsymbol{r}_i - \boldsymbol{r}_A|} \right] + \sum_{i=1}^{N} \sum_{j>1}^{N} \frac{1}{|\boldsymbol{r}_i - \boldsymbol{r}_j|} \tag{2.86}$$

$$T_{N+1} = -\frac{\nabla_{N+1}^2}{2} \tag{2.87}$$

and

$$V = \sum_{i=1}^{N} \frac{1}{|\boldsymbol{r}_{N+1} - \boldsymbol{r}_i|} + \sum_{A=1}^{M} -\frac{Z_A}{|\boldsymbol{r}_{N+1} - \boldsymbol{r}_A|}, \tag{2.88}$$

where $\boldsymbol{r}_{N+1}$ is the position vector of the continuum electron, and $\boldsymbol{r}_i$ and $\boldsymbol{r}_A$ are the coordinates of the molecule's electrons and nuclei.

The scattering wave function must satisfy the Schrödinger Equation

$$\hat{H}|\Psi\rangle = (E - H_{N+1})\,|\Psi\rangle \tag{2.89}$$

where E is the total collision energy. [3]

We know that the Lippmann-Schwinger equation is written as:

$$\left|\Psi_{\boldsymbol{k}_{i,f}}^{(\pm)}\right\rangle = \left|S_{\boldsymbol{k}_{i,f}}\right\rangle + G_0^{(\pm)} V \left|\Psi_{\boldsymbol{k}_i}^{(\pm)}\right\rangle \tag{2.90}$$

where $\left|\Psi_{\boldsymbol{k}_i}^{(\pm)}\right\rangle$ represents the scattering wave function of the $(N+1)$ electron system, $G_0^{(\pm)}$ is the free-particle Green's function, and $\left|S_{\boldsymbol{k}_{i,f}}\right\rangle$ is an eigenstate of the Hamiltonian H_0, being the product of the initial (final) target state ($\Phi_{i,f}$) and a plane wave. $G_0^{(\pm)}$ and $\left|S_{\boldsymbol{k}_{i,f}}\right\rangle$ are respectively written as:

$$G_0^{(\pm)} = \frac{1}{E - H_0 \pm i\varepsilon} \tag{2.91}$$

and

$$\left|S_{\boldsymbol{k}_{i,f}}\right\rangle = |\Phi_{i,f}\rangle \otimes \left|e^{i\boldsymbol{k}_{i,f}\cdot\boldsymbol{r}_{N+1}}\right\rangle \tag{2.92}$$

where $\boldsymbol{r}_{N+1}$ is the coordinate of the continuum electron.
If we multiply equation (2.90) by the potential V and rearrange the terms, we obtain:

[3] During the collision, the total energy must be conserved:

$$E = E_i + \frac{k_i^2}{2} = E_f + \frac{k_f^2}{2}.$$

$$A^{(\pm)} \left| \Psi^{(\pm)}_{\boldsymbol{k}_{i,f}} \right\rangle = V \left| S_{\boldsymbol{k}_{i,f}} \right\rangle . \tag{2.93}$$

where the operator $A^{(\pm)}$ has the form:

$$A^{(\pm)} = V - V G_0^{(\pm)} V \tag{2.94}$$

Thus, the scattering amplitude given in (2.84) is now written as:

$$f_{\boldsymbol{k}_f,\boldsymbol{k}_i} = -\frac{1}{2\pi} \sum_{m,n} \left\langle S_{\boldsymbol{k}_f} \right| V \left| \chi_m \right\rangle \left(d^{-1} \right)_{mn} \left\langle \chi_n \right| V \left| S_{\boldsymbol{k}_i} \right\rangle . \tag{2.95}$$

now, for the equations:

$$V \left| S_{\boldsymbol{k}_i} \right\rangle = A^{(+)} \left| \Psi^{(+)}_{\boldsymbol{k}_i} \right\rangle \tag{2.96}$$

and

$$V \left| S_{\vec{k}_f} \right\rangle = A^{(+)^\dagger} \left| \Psi^{(-)}_{\boldsymbol{k}_f} \right\rangle \tag{2.97}$$

to be equivalent [4] to equation (2.93), the following must be satisfied:

$$A^{(-)\dagger} = A^{(+)}, \tag{2.98}$$

which is the variational stability condition. This condition must be satisfied to apply the variational principle to the calculation of the scattering amplitude. The condition will be satisfied when the right-hand side of equation (2.90) is antisymmetric, as the wave function $\Psi_{\boldsymbol{k}_{i,f}}$ is antisymmetric. However, it is necessary to include the continuum eigenstates of the target in the Green's function [37]; thus, we will have the right and left sides of equation (2.90) antisymmetric.

To this end, let us expand the Green's function in the basis of eigenstates of H_0[5]:

$$G_0^{(\pm)} = \sum_N \int d^3k \frac{\left| \Phi_N \boldsymbol{k} \right\rangle \left\langle \Phi_N \boldsymbol{k} \right|}{E - E_N - \frac{k^2}{2} \pm i\varepsilon}, \tag{2.99}$$

the integral over $\boldsymbol{k}$ is performed over the momentum of the free particle. We can also use $E = E_N + \frac{k_N^2}{2}$, and rewrite equation (2.99) as:

$$G_0^{(\pm)} = \sum_N \int d^3k \frac{\left| \Phi_N \boldsymbol{k} \right\rangle \left\langle \Phi_N \boldsymbol{k} \right|}{\frac{k_N^2 - k^2}{2} \pm i\varepsilon}. \tag{2.100}$$

[4] We now have the multiplicative factor as $-\frac{1}{2\pi}$, because we consider the normalization constants $\left(\frac{1}{(2\pi)^{\frac{3}{2}}} \right)$ of two plane waves ($S_{\boldsymbol{k}_i}$ and $S_{\boldsymbol{k}_f}$) explicitly. Obs: where equation (2.97) is the Hermitian conjugate of:

$$\left\langle S_{\boldsymbol{k}_f} \right| V = \left\langle \Psi^{(-)}_{\boldsymbol{k}_f} \right| A^{(+)}.$$

In order to circumvent the difficulty arising from the Green's function, we introduce a projection operator P, which projects onto all open channels of the target, and can be written as

$$P = \sum_{l}^{\text{open}} \left|\Phi_l\left(\boldsymbol{r}_1, \boldsymbol{r}_2, \ldots, \boldsymbol{r}_N\right)\right\rangle \left\langle\Phi_l\left(\boldsymbol{r}_1, \boldsymbol{r}_2, \ldots, \boldsymbol{r}_N\right)\right|, \tag{2.101}$$

and according to the problem to be studied, these channels are chosen. In this dissertation, we will only deal with elastic scattering, so the only possible final state for the target is the ground state, so that equation (2.102) is written in the following form:

$$P = \left|\Phi_0\left(\boldsymbol{r}_1, \boldsymbol{r}_2, \ldots, \boldsymbol{r}_N\right)\right\rangle \left\langle\Phi_0\left(\boldsymbol{r}_1, \boldsymbol{r}_2, \ldots, \boldsymbol{r}_N\right)\right|. \tag{2.102}$$

In order to remove the continuum component from the Green's function, we apply the projection operator P to the Lippmann-Schwinger equation, so as to obtain:

$$P\left|\Psi_{\boldsymbol{k}_i}^{(+)}\right\rangle = \left|S_{\boldsymbol{k}_i}\right\rangle + G_P^{(+)} V \left|\Psi_{\boldsymbol{k}_i}^{(+)}\right\rangle, \tag{2.103}$$

being also, the Green's function projected into the space defined by P

$$PG_0^{(\pm)} = G_P^{(\pm)} = \sum_{l}^{\text{open}} \int d^3k \frac{\left|\Phi_l \boldsymbol{k}\right\rangle \left\langle\Phi_l \boldsymbol{k}\right|}{\frac{\left(k_l^2 - k^2\right)}{2} \pm i\varepsilon} \tag{2.104}$$

Multiplying equation (2.103) by V and performing some manipulations, we arrive at the following equation:

$$A^{(+)}\left|\Psi_{\boldsymbol{k}_i}^{(+)}\right\rangle = V\left|S_{\boldsymbol{k}_i}\right\rangle, \tag{2.105}$$

where we define $A^{(+)} = VP - VG_P^{(+)}V$. It is important to note that, in the way the operator $A^{(+)}$ is written, we lose the guarantee of variational stability for the scattering amplitude, because in general the operator VP is no longer Hermitian and, as a consequence, $A^{(-)\dagger} \neq A^{(+)}$.

To solve the problem described above, we will construct a new expression for the operator $A^{(+)}$, and for this, it is necessary to recover the information contained in the complementary space of the operator P. Thus, a space complementary to P is defined, given by the projector $(1 - aP)$, where a is a parameter that will be defined later. Let us initially separate the wave function into two components, one projected onto the open channels and another recovering the closed channels, having the form:

$$\left|\Psi_{\boldsymbol{k}_i}^{(+)}\right\rangle = aP\left|\Psi_{\boldsymbol{k}_i}^{(+)}\right\rangle + (1 - aP)\left|\Psi_{\boldsymbol{k}_i}^{(+)}\right\rangle \tag{2.106}$$

and require that $\left|\Psi_{\boldsymbol{k}_i}^{(+)}\right\rangle$ satisfies the Schrödinger equation:

$$\hat{H}\left|\Psi_{\boldsymbol{k}_i}^{(+)}\right\rangle = \hat{H}\left[aP\left|\Psi_{\boldsymbol{k}_i}^{(+)}\right\rangle + (1-aP)\left|\Psi_{\boldsymbol{k}_i}^{(+)}\right\rangle\right] = 0 \tag{2.107}$$

using equation (2.104) in equation (2.107), we obtain:

$$\hat{H}\left[a\left(|S_{\boldsymbol{k}_i}\rangle + G_P^{(+)}V\left|\Psi_{\boldsymbol{k}_i}^{(+)}\right\rangle\right) + (1-aP)\left|\Psi_{\boldsymbol{k}_i}^{(+)}\right\rangle\right] = 0 \tag{2.108}$$

Manipulating the equation above algebraically and using the relations below [38]:

$$[H_0, P] = 0 \tag{2.109}$$

and

$$\hat{H}P\left|\Psi_{\boldsymbol{k}_i}^{(+)}\right\rangle = \frac{1}{2}\left[\hat{H}_0 P + P\hat{H}_0\right]\left|\Psi_{\boldsymbol{k}_i}^{(+)}\right\rangle - VP\left|\Psi_{\boldsymbol{k}_i}^{(+)}\right\rangle, \tag{2.110}$$

where $\hat{H}_0 = E - H_0$, we arrive at the following equation:

$$A^{(+)}\left|\Psi_{\boldsymbol{k}_i}^{(+)}\right\rangle = V\left|S_{\boldsymbol{k}_i}\right\rangle, \tag{2.111}$$

where now:

$$A^{(+)} = \frac{1}{2}(PV + VP) - VG_P^{(+)}V + \frac{1}{a}\left[\hat{H} - \frac{a}{2}(\hat{H}P + P\hat{H})\right]. \tag{2.112}$$

From equations (2.112) and (2.111), we now see that the form of the operator $A^{(+)}$ satisfies the variational stability condition $A^{(-)\dagger} = A^{(+)}$ for all matrix elements involving functions from the L^2 space and for any value of a. However, when using functions that are not of the L^2 form, the stability condition is no longer satisfied. The problem is contained in the term:

$$\frac{1}{a}\left[\hat{H} - \frac{a}{2}(\hat{H}P + P\hat{H})\right]. \tag{2.113}$$

In this term, we have the kinetic energy operator T_{N+1}, which involves two scattering orbitals (continuum functions), and because of this, the operator $\hat{H}$ ceases to be Hermitian. Thus, the parameter a is determined from the condition that the operator described in equation (2.113) remains Hermitian. Therefore, we must impose that the matrix elements (only the terms that have $\hat{H}$ are being used, for the reason described earlier) written in the form:

$$\left\langle\Psi_n^{(-)}\right|\frac{1}{a}\left[\hat{H} - \frac{a}{2}(\hat{H}P + P\hat{H})\right]\left|\Psi_m^{(+)}\right\rangle \tag{2.114}$$

are null for functions that are not square-integrable (L^2). This will happen when the parameter a assumes the value $a = N + 1$, and thus, the variational stability condition is respected for all matrix elements.

We now need to obtain a new expression for the scattering amplitude. To this end, let us start from equation (2.67) and expand the wave function $\left(\left|\Psi^{(+)}_{\boldsymbol{k}_i}\right\rangle \text{ and } \left\langle\Psi^{(-)}_{\boldsymbol{k}_f}\right|\right)$ in a known set of basis functions $\{|\chi_m\rangle\}$:

$$\left|\Psi^{(+)}_{\boldsymbol{k}_i}\right\rangle = \sum_m a_m\left(\boldsymbol{k}_i\right)|\chi_m\rangle \tag{2.115}$$

and

$$\left\langle\Psi^{(-)}_{\boldsymbol{k}_f}\right| = \sum_n a^*_n\left(\boldsymbol{k}_f\right)\langle\chi_n| \tag{2.116}$$

Then, substituting the expansion in terms of the basis $|\chi_m\rangle$ into equation (2.67) and imposing the condition that the scattering amplitude is stationary, we obtain the expression for the scattering amplitude, which is written as:

$$f_{\boldsymbol{k}_f,\boldsymbol{k}_i} = -\frac{1}{2\pi}\sum_{m,n}\left\langle S_{\boldsymbol{k}_f}\right| V\left|\chi_m\right\rangle \left(d^{-1}\right)_{mn}\left\langle\chi_n\right| V\left|S_{\boldsymbol{k}_i}\right\rangle \tag{2.117}$$

the matrix elements d_{mn} are written as:

$$d_{mn} = \langle\chi_m| A^{(+)}|\chi_n\rangle \tag{2.118}$$

and the operator $A^{(+)}$ is now written as:

$$A^{(+)} = \frac{1}{2}(PV + VP) - VG^{(+)}_P V + \frac{1}{N+1}\left[\hat{H} - \frac{N+1}{2}(\hat{H}P + P\hat{H})\right] \tag{2.119}$$

.

2.4.1 Frame Transformation

We have expressed the scattering amplitude in the molecular frame[5] $\left(f^b\right)$. Working in this frame is advantageous because it exploits the intrinsic symmetries of the molecule, making the formulation more manageable and reducing the computational effort required. However, when comparing our theoretical results with experimental measurements, it is essential to express the scattering amplitude in the laboratory frame $\left(f^L\right)$.

In the laboratory frame, the z-axis is aligned with the incident electron momentum $\boldsymbol{k}_i$, which matches the geometry of the experiment. To connect both frames, we perform a rotation of the molecular axes (x, y, z) into the laboratory axes (x', y', z')

[5] We will use b for (body-frame) to indicate the molecular frame and L to represent the laboratory frame.

using Euler angles. This change of reference frame is implemented by expanding the scattering amplitude in spherical harmonics, which naturally accommodate rotations:

$$f^B\left(\boldsymbol{k}_i, \boldsymbol{k}_f\right) = \sum_{l=0}^{l_{\max}} \sum_{m=-l}^{l} f_{lm}\left(\boldsymbol{k}_i, k_f\right) Y_l^m\left(\hat{k_f}\right), \tag{2.120}$$

where the coefficients $f_{lm}\left(\boldsymbol{k}_i, k_f\right)$ are written as:

$$f_{lm}\left(\boldsymbol{k}_i, k_f\right) = \int d\hat{k_f} Y_l^{m*}\left(\hat{k_f}\right) f^b\left(\boldsymbol{k}_i, \boldsymbol{k}_f\right) \tag{2.121}$$

We can now see, in equation (2.121), that the scattering amplitude is written in terms of the spherical harmonics Y_l^m. Therefore, to obtain the scattering amplitude in the laboratory frame, it is necessary to perform a rotation on the spherical harmonics, where we will use the Wigner rotation matrices [39] $D_{m',m}(\alpha, \beta, \gamma)$, as shown

$$Y_l^{m'}\left(\hat{k_f'}\right) = \sum_{m=-l}^{l} D_{m',m}\left(\phi_i, \theta_i, 0\right) Y_l^m\left(\hat{k_f}\right) \tag{2.122}$$

where α, β, γ are the Euler angles. Here we will use $\alpha = \phi_i, \beta = \theta_i$ and $\gamma = 0$, as shown in Figure 3

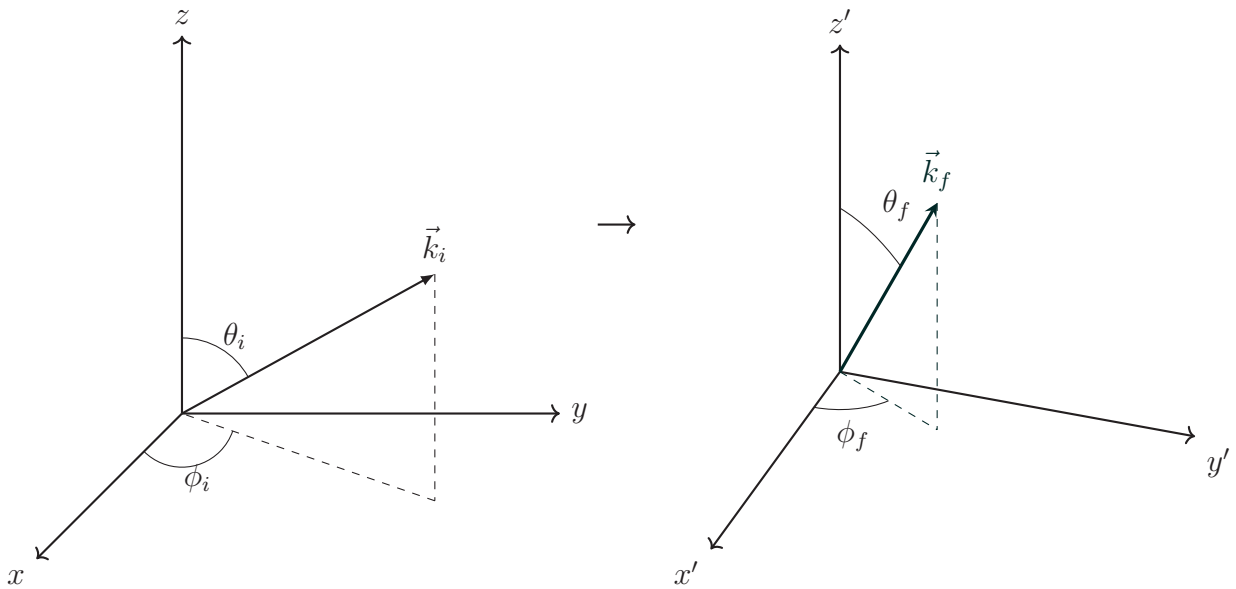

FIGURE 3 – Graphical representation of an arbitrary Euler rotation, where the angles before the rotation are θ_i and ϕ_i, and after the rotation are θ_f and ϕ_f. Note that the vector $\vec{k}_i$ has also been rotated into $\vec{k}_f$.

Thus, the scattering amplitude written in the laboratory frame is:

$$f^L\left(\boldsymbol{k}_f, \boldsymbol{k}_i\right) = \sum_{l=0}^{l_{\max}} \sum_{m'=-l}^{l} \sum_{m=-l}^{l} f_{lm}^B\left(\boldsymbol{k}_i, k_f\right) D_{mm'}\left(\phi_i, \theta_i, 0\right) Y_l^m\left(\hat{\boldsymbol{k}}_f\right). \tag{2.123}$$

Having the scattering amplitude f^L, it is possible to calculate the differential cross section in the laboratory frame:

$$\frac{d\sigma}{d\Omega}\left(\theta_f, \phi_f, k_f, k_i\right) = \frac{k_f}{4\pi k_i} \int d\hat{k}_i \left| f^L\left(\boldsymbol{k}_f, \boldsymbol{k}_i\right)\right|^2 \tag{2.124}$$

where we average over all incidence directions $\hat{k}_i$, which is equivalent to keeping the molecule fixed and varying the directions of the electron beam. This average is done to account for the fact that in a scattering experiment, the gas molecules are randomly oriented.

The cross section will be obtained by integrating over the azimuthal angle ϕ_f; we also perform an average over the spins of the initial state and a sum over the spins of the final state. Integrating equation (2.124), we obtain the integral cross section:

$$\sigma = \int_0^\pi d\theta_f \sin\left(\theta_f\right) \frac{d\sigma}{d\Omega} \tag{2.125}$$

and we can also obtain the momentum transfer cross section:

$$\sigma_{mt} = \int_0^\pi d\theta_f \sin\left(\theta_f\right)\left[1 - \cos\left(\theta_f\right)\right] \frac{d\sigma}{d\Omega}. \tag{2.126}$$

In this work, the calculations performed are for elastic scattering, where $k_i = k_f$; this removes the dependence on k_i and k_f in the differential cross section.

2.5 STATIC-EXCHANGE AND STATIC-EXCHANGE PLUS POLARIZATION APPROXIMATIONS

Having established the method, we now examine the basis set $|\chi_m\rangle$ employed in the scattering calculations. This set, referred to as the $(N+1)$-electron configuration space, consists of individual configurations $|\chi_m\rangle$. The configuration space defines the level of approximation within an SMC scattering calculation: a larger configuration space provides greater variational flexibility of the wave function and, consequently, a more accurate description of the scattering process, albeit at increased computational expense. Each configuration is constructed as an antisymmetrized product of a target state and a scattering orbital, the latter representing the incident electron. In practice, the configuration space is treated at two principal levels of approximation the static-exchange (SE) approximation and the static-exchange-plus-polarization (SEP) approximation.

2.5.1 Static Exchange

The effects taken into account in the static-exchange approximation are the Coulomb effect, which contributes an attractive static potential (between the incident

electron and the molecule's electrons and nuclei), and the exchange effect (between the incident electron and a molecular electron, which arises from the antisymmetric wave function to respect the principle of indistinguishability of the $N+1$ electrons).

In this approximation, the configuration space $|\chi_m\rangle$ is generated as follows:

$$|\chi_m\rangle = \mathcal{A}_{N+1} |\Phi_0\rangle \otimes |\phi_m\rangle \,, \tag{2.127}$$

where $|\Phi_0\rangle$ corresponds to the ground state of the molecule ($|\Phi_0\rangle$ is obtained via the Hartree-Fock method), $|\phi_m\rangle$ is a scattering orbital, and $\mathcal{A}_{N+1}$ is the antisymmetrizer for $N+1$ particles, which is written as:

$$\mathcal{A}_{N+1} = \frac{1}{\sqrt{(N+1)!}} \sum_{q=1}^{(N+1)} \epsilon_q Q, \tag{2.128}$$

here ϵ_q is the permutation sign and Q is the permutation operator. The total spin of the configurations becomes $s = \frac{1}{2}$ (doublet), since we couple the spin of the closed-shell molecule ($s = 0$, singlet) with the spin of the continuum electron ($s = \frac{1}{2}$). In this approximation, only the ground state of the molecule is considered for the description of the target, as the distortion of the target's electron cloud due to the presence of the incident electron is not taken into account.

That is, the molecular electronic cloud remains "frozen"during and after the incidence of the electron. This level of approximation is only valid for energies typically higher than 10 eV, because in this energy regime, the molecule's electrons do not have time to rearrange under the presence of the continuum electron (incident electron). The continuum electron passes through the target region so quickly that the effects of the distortion of the molecular electron density can be neglected.

On the other hand, at low energies, this approximation fails to adequately describe the scattering process because the incident electron moves sufficiently slowly that the distortion of the target's electron cloud, induced by the electric field of the scattering electron, becomes crucial for a proper description of the interaction.

2.5.2 Static Exchange Plus Polarization

In the static-exchange-plus-polarization (SEP) approximation, in addition to the Coulomb and exchange effects, we also account for the polarization of the target induced by the presence of the incident electron. The configuration space $|\chi_{im}\rangle$ in the SEP approximation is constructed as

$$|\chi_{im}\rangle = A_{N+1} |\Phi_i\rangle \otimes |\phi_m\rangle, \tag{2.129}$$

where $|\Phi_i\rangle$ denotes a virtual excitation of the target, $|\phi_m\rangle$ is a scattering orbital, and A_{N+1} is the antisymmetrizer.

Within this configuration space, the target polarization allows for singlet and triplet couplings in the target, leading to doublet configurations for the total system. The polarization effect of the target arises from the Coulomb repulsion between the incident electron and the target electrons. As the continuum electron approaches the target, it repels the molecular electrons, inducing a dipole moment through the distortion of the target's electronic cloud. This distortion is incorporated by including virtual excitations of the target, thereby increasing the flexibility of the wave function.

The states $|\Phi_i\rangle$ are generated from single virtual excitations of the target, in which an electron is promoted from an occupied orbital (hole orbital) to a previously unoccupied orbital (particle orbital). In this case, the excited states of the target may possess either singlet or triplet total spin, as noted above.

The antisymmetrized product of such an excited state with a scattering orbital defines a configuration, characterized by the set: hole orbital + particle orbital + singlet or triplet coupling + scattering orbital. The hole and particle orbitals used to construct these excited states differ from the virtual orbitals of the target, as the latter do not provide an adequate description of excited states.

2.6 PSEUDOPOTENTIALS

When heavy atoms are involved, scattering studies become computationally prohibitive, since describing a large number of electrons requires an expanded set of atomic basis functions. The major contribution to the computational cost comes from the evaluation of two-electron integrals, which must be computed for all possible combinations of basis functions. Core electrons, however, remain tightly bound to the nucleus and are energetically inaccessible at low incident electron energies; therefore, their contribution to low-energy scattering processes is negligible.

In contrast, valence electrons are crucial in low-energy electron scattering, as they are accessible at such energy scales and are directly responsible for molecular properties such as ionization potentials, dissociation energies, and chemical bonding. For this reason, the use of pseudopotentials to represent the core electrons constitutes a suitable approximation in low-energy scattering, where their contribution is negligible. The spatial orbitals explicitly describe only the valence electrons, significantly reducing the computational cost and enabling the treatment of systems containing heavier nuclei.

The implementation of pseudopotentials within the Hartree–Fock and Schwinger multichannel (SMC) frameworks was first carried out by Bettega *et al.* [40]. In this formulation, the SMC method is referred to as the Schwinger multichannel method

with pseudopotentials (SMCPP). In the present work, we employed pseudopotentials generated by Bachelet, Hamann, and Schlüter (BHS) [41].

The BHS pseudopotentials have the following form:

$$\hat{V}_{PP} = \hat{V}_{\text{core}} + \hat{V}_{\text{ion}} \,, \tag{2.130}$$

with V_{core} and V_{ion} given by:

$$\hat{V}_{\text{core}} = -\frac{Z_v}{r} \sum_{i=1}^{2} c_i \,\text{erf}\left[(\rho_i)^{1/2}\, r\right], \tag{2.131}$$

and

$$\hat{V}_{ion} = \sum_{n=0}^{1} \sum_{j=1}^{3} \sum_{l=0}^{2} A_{njl} r^{2n} e^{-\sigma_{jl} r^2} \sum_{m=-l}^{l} |lm\rangle\langle lm|, \tag{2.132}$$

where Z_v corresponds to the valence charge, erf is the Gauss error function and the parameters $A_{njl}, \sigma_{jl}, c_i$, and ρ_i are listed in [33]. For the implementation of the pseudopotentials, it is necessary to replace the nuclear potential $-\frac{Z}{r}$ with the pseudopotential V_{PP}. Then, in the Hartree-Fock method we have:

$$V_{\mu\nu}^{nuc} = \int d\boldsymbol{r} \phi_\mu \left[-\frac{Z_C}{r}\right] \phi_\nu \tag{2.133}$$

which are replaced by:

$$V_{\mu\nu}^{PP} = \int d\boldsymbol{r} \phi_\mu \hat{V}_{PP} \phi_\nu \tag{2.134}$$

where ϕ_ν represents the spacial orbital. In the SMC method, the integrals involving the atomic orbital, plane wave, and nuclear potential are:

$$V_{\boldsymbol{k}\nu}^{nucl} = \int d\boldsymbol{r} e^{-i\boldsymbol{k}.\boldsymbol{r}} \left[-\frac{Z_C}{r}\right] \phi_\nu \tag{2.135}$$

and are replaced by:

$$V_{\boldsymbol{k}\nu}^{PP} = \int d\boldsymbol{r} e^{-i\boldsymbol{k}\cdot\boldsymbol{r}} \hat{V}_{PP} \phi_\nu \tag{2.136}$$

All integrals involving V_{PP} continue to be solved analytically. The use of BHS pseudopotentials requires the use of an adequate set of basis functions to represent the valence electrons. We find how these basis functions are generated in reference [40].

2.7 BORN-CLOSURE

The Schwinger Multichannel (SMC) method provides an enhanced description of the electron-molecule interaction in the target's vicinity through the use of square-integrable (L^2) basis functions. For non-polar molecules, this approach is highly effective, as the dominant interactions are short-ranged. However, a significant limitation arises

when applying the SMC method to polar targets. The presence of a permanent electric dipole moment introduces a long-range potential that exerts a force on the incident electron even at large distances. The L^2 basis functions, due to their rapid decay, fail to accurately represent this slowly varying dipole potential in regions far from the molecule [20].

The neglect of this long-range interaction has pronounced consequences on calculated scattering observables. It particularly affects the low-energy regime, where it leads to an underestimation of the integral cross section, and the small-angle (forward) scattering region, where it fails to reproduce a characteristic sharp rise in the differential cross section.

To address this deficiency, we use the Born-closure procedure. This technique incorporates the long-range dipole effects by combining the SMC wave function with the first Born approximation. The procedure yields a corrected scattering amplitude that includes the contribution from the molecular dipole potential, which is given by:

$$f^{FBA}\left(\boldsymbol{k}_i, \boldsymbol{k}_f\right) = 2i\frac{\boldsymbol{D}\cdot\left(\boldsymbol{k}_i - \boldsymbol{k}_f\right)}{\left|\boldsymbol{k}_i - \boldsymbol{k}_f\right|^2}. \tag{2.137}$$

the index FBA comes from First Born Approximation, and $\boldsymbol{D}$ is the dipole moment of the molecule. This new amplitude will be expanded in spherical harmonics to define the expansion coefficients f_{lm}^{FBA}, just as the amplitude obtained via SMC will also be expanded to generate the coefficients f_{lm}^{SMC}. With these coefficients, we have a new scattering amplitude:

$$\begin{aligned} f\left(\boldsymbol{k}_i, \boldsymbol{k}_f\right) = \sum_{l=0}^{l_{SMC}} \sum_{m=-l}^{+l} f_{lm}^{SMC}\left(\boldsymbol{k}_i, k_f\right) Y_{lm}\left(\hat{k_f}\right) + f^{FBA}\left(\boldsymbol{k}_i, \boldsymbol{k}_f\right) - \\ - \sum_{l=0}^{l_{SMC}} \sum_{m=-l}^{+l} f_{lm}^{FBA}\left(\boldsymbol{k}_i, k_f\right) Y_{lm}\left(\hat{k_f}\right) \end{aligned} \tag{2.138}$$

where f_{lm} are expansion coefficients. As we can see, the amplitude in equation (2.138) considers both calculations, the amplitude via SMC and the amplitude via FBA. For partial waves with small angular momentum ($l < l_{SMC}$), the description by f_{SMC} is adequate, and for larger partial waves ($l > l_{SMC}$), the description via f_{FBA} is adequate. The value l_{SMC} is chosen so that the differential cross sections calculated with and without the dipole moment are similar above $20°$, where the dipole effect is small. The dipole effect has no influence on resonances; in a system where the main interest is only to characterize and identify resonances, this effect can be disregarded.

We mentioned above that in the scattering by a long-range potential we have a greater contribution at low scattering angles and also requires higher partial waves (l's) in the cross-section calculation in this case. The explanation for this comes from the semiclassical theory of scattering, and we will use elastic scattering by a rigid sphere as an example, as we can see in Figure 4.

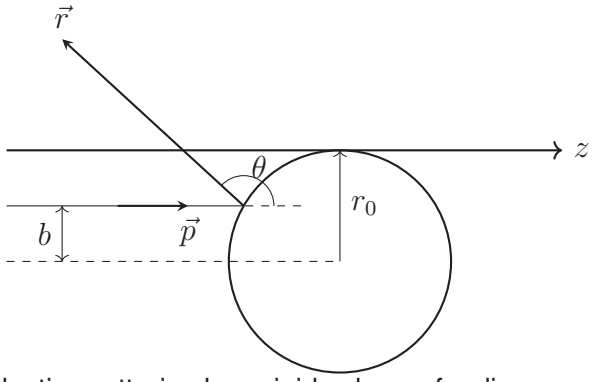

FIGURE 4 – Classical elastic scattering by a rigid sphere of radius r_0, where a particle is incident with impact parameter b and scatters at an angle θ. Note that b and θ are inversely related, such that in the limit $b = r_0 \Rightarrow \theta = 0$.

The quantity b is called the impact parameter, θ is the scattering angle, and R is the radius of the sphere. The particle strikes the sphere parallel to an axis passing through the center of mass at a distance b from it. The smaller the scattering angle θ, the larger the impact parameter b.

In magnitude, the angular momentum L can be written as:

$$L = rp\sin\gamma, \tag{2.139}$$

where r is the magnitude of the position vector, p is the magnitude of the linear momentum, and γ is the angle between them. Using trigonometry, we can rewrite L in terms of the impact parameter b:

$$L = bp, \tag{2.140}$$

isolating b in the equation above, we have:

$$b = \frac{L}{p}. \tag{2.141}$$

We can rewrite equation (2.141) in terms of the quantization rules for angular momentum $(\sqrt{l(l+1)}\hbar)$ and linear momentum $(k\hbar)$, so that we obtain:

$$b = \frac{\sqrt{l(l+1)}\hbar}{k\hbar} \sim \frac{l}{k}, \tag{2.142}$$

and finally we arrive at

$$l \sim bk. \tag{2.143}$$

Analyzing equation (2.143), we note that l increases as b increases, that is, in terms of potential, the greater the range of the potential, the higher the partial wave l needed to describe the scattering correctly.

2.8 RESONANCES

A resonance can occur during the process of electron scattering by a molecule. One of the objectives of studying electron scattering by molecules consists of identifying and characterizing these resonances. The resonance essentially consists of the temporary capture of the incident electron in the region of the target molecule [3] and can be classified according to the mechanism of electron trapping in the molecule as a shape resonance, core-excited resonance, or Feshbach resonance.

The shape resonance is so called because it is the shape of the potential energy that traps the electron, where the incident electron is captured by an empty orbital of the molecule. Figure 5 is a simple illustration of the shape resonance process.

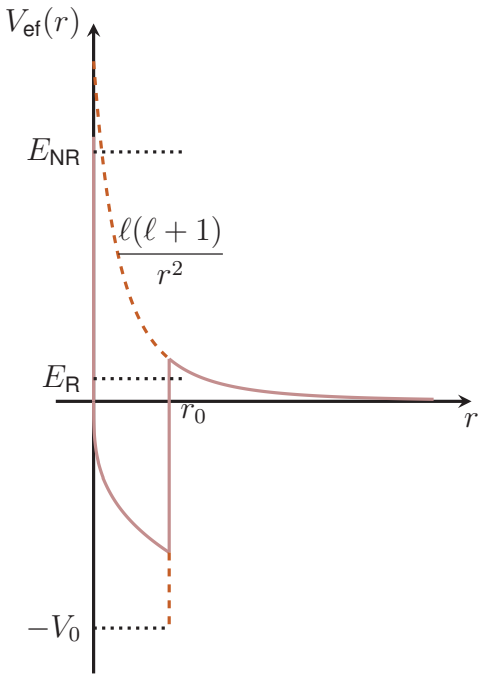

FIGURE 5 – A simple potential, yet capable of supporting a shape resonance, where E_{R} is the resonance energy and E_{NR} is a non-resonant energy.

The effective potential $V_{efe} = V_0 + (\ell(\ell+1))/r^2$ is given by the sum of the attractive potential plus the centrifugal barrier term, or in other words, the effective potential has an attractive well, followed by a repulsive barrier at large distances. The continuum electron with an energy E_{NR} is only scattered and feels the effective potential V_{efe} without being trapped. However, the electron with energy E_R can tunnel and form a temporary bound state in the ”effective well” before returning to the continuum via tunneling. Then we say that a shape resonance is formed.

In the other types of resonance, core-excited and Feshbach, the trapping of the electron also occurs by one of the empty orbitals of the molecule, but accompanied by an excitation of the target molecule. For the excited state, in this case called the parent

state, with energy below the resonant state, we have a core-excited resonance. For the parent state with energy above the resonant state, we have a Feshbach resonance.

Resonances are identified in elastic cross sections through pronounced structures. The energy at which the structure is centered corresponds to the resonance energy (E_R). This structure has a certain width, which is related to the lifetime of the resonance. From the Heisenberg uncertainty relation, we can obtain the relation for the resonance lifetime:

$$\Delta E \Delta t \simeq \hbar. \tag{2.144}$$

here ΔE corresponds to the width of the resonance Γ, Δt corresponds to the lifetime of the resonance τ, and $\hbar$ is Planck's constant divided by 2π.

Thus, from the uncertainty relation:

$$\Gamma\tau \simeq \hbar \quad \Rightarrow \quad \tau \simeq \frac{\hbar}{\Gamma} \tag{2.145}$$

at relatively lower energies, the resonance peaks become narrower and more intense, indicating a relatively longer lifetime of the temporary anion, consistent with the inverse relationship between resonance width and lifetime [20].

CHAPTER 3

C-CYANOMETHANIMINE

Molecules featuring C-N bonds, particularly hydrogen cyanide (HCN), are fundamental building blocks in prebiotic chemistry, serving as direct precursors to amino acids and nucleobases. The dimerization of HCN represents a crucial step in this chemical evolution, leading to the formation of C-cyanomethanimine (HNCHCN), a direct precursor to adenine [42].

C-cyanomethanimine is an organic molecule of significant astrochemical interest, characterized by an imino group (H-N=) and a nitrile group (CN) bonded to a carbon skeleton. It exhibits structural isomerism, existing in three primary forms as shown in Figure 5: the geometric Z and E isomers, which differ in their spatial orientation around the central C=N double bond due to restricted π-bond rotation, and the N-isomer, a higher-energy tautomer involving hydrogen migration and a distinct bonding connectivity [26]. [6]

The profound astrophysical importance of this molecule has motivated extensive theoretical investigations aimed at characterizing its properties. A landmark study provided the essential high-accuracy quantum chemical foundation [26], establishing definitive benchmark values. Using a sophisticated coupled-cluster-based composite scheme, the Z-isomer was confirmed as the global minimum, with the E- and N-isomers lying higher in energy by 0.0136 eV and 0.2422 eV, respectively. In addition, a high isomerization barrier (25 kcal/mol) between the Z and E forms was identified, confirming kinetic stability and indicating that interconversion is highly improbable under the extremely low temperatures of the interstellar medium (ISM). The same work also demonstrated the importance of including anharmonic corrections for accurate spectroscopic predictions, successfully reassigning a previously unclassified experimental IR peak at 3180 cm^{-1} to an overtone of the C=N stretching mode. These precise theoretical predictions paved the way for astronomical discovery. The first detection of cyanomethanimine in the ISM was reported by Zaleski [27], who identified rotational transition lines of the E-isomer in the prolific star-forming region Sagittarius B2(N) using data from the Green Bank Telescope PRIMOS survey. This detection was made possible

[6] The Z and E nomenclature, derived from the German zusammen (together) and entgegen (opposite), is assigned based on the Cahn-Ingold-Prelog [43] rules, indicating whether the highest-priority substituents reside on the same or opposite sides of the double bond, respectively.

by matching observed emission lines with the high-accuracy theoretical rotational spectrum. The study concluded that the E-isomer's formation likely occurs via radical-radical recombination on icy dust grains, followed by non-thermal desorption into the gas phase, as purely gas-phase routes were deemed insufficient.

The astrochemical understanding of cyanomethanimine was significantly advanced by Rivilla et al. [28], who used the Atacama Large Millimeter/submillimeter Array (ALMA) to achieve the first detection of the Z-isomer toward the Galactic Center source $G+0.693-0.027$. In that study, the abundances of both isomers were quantified, showing that the Z-isomer is five times more abundant than the E-isomer, a ratio consistent with thermodynamic equilibrium based on their calculated energy difference. These results indicate that grain-surface formation pathways favor the most stable product and establish the Z-isomer as the dominant and most astrophysically relevant form of the molecule.

Further progress was made with the recent detection of the highest-energy isomer, the N-isomer (H_2CNCN), in the same source [29]. Its derived abundance is more than an order of magnitude lower than that of the C-cyanomethanimine isomers, yielding a C/N abundance ratio of 31.8. This observed ratio contradicts the Minimum Energy Principle and instead points to kinetic control, with the gas-phase reaction between methanimine (CH_2NH) and the cyanogen radical (CN) identified as the main formation pathway for all three isomers. The high total abundance of cyanomethanimine in this region supports its role as a key intermediate in prebiotic chemistry, while the detection of H_2CNCN specifically enhances its prebiotic relevance, as it contains the NCN backbone present in purine nucleobases such as adenine.

In conclusion, the study of C-cyanomethanimine exemplifies the powerful synergy between theoretical chemistry and observational astronomy. The accurate characterization of its isomeric stability and spectroscopic properties enabled its astronomical detection and abundance estimation within interstellar molecular clouds, reinforcing its relevance in prebiotic chemical pathways. The Z-isomer, identified as the global minimum on the potential energy surface and observed to be the most abundant form under typical interstellar conditions, was therefore selected for the present electron-scattering calculations. The resulting cross sections provide essential quantitative data for modeling energy-transfer processes and reactivity in electron-dominated astrophysical environments.

3.1 COMPUTATIONAL DETAILS

We performed electron scattering calculations using the ground-state optimized geometry for each isomer. All geometry optimizations and energy calculations were conducted using the GAMESS package [44]. The molecular structures of the Z, E, and

N isomers, visualized using MacMolPlt [45], are presented in figure 6.

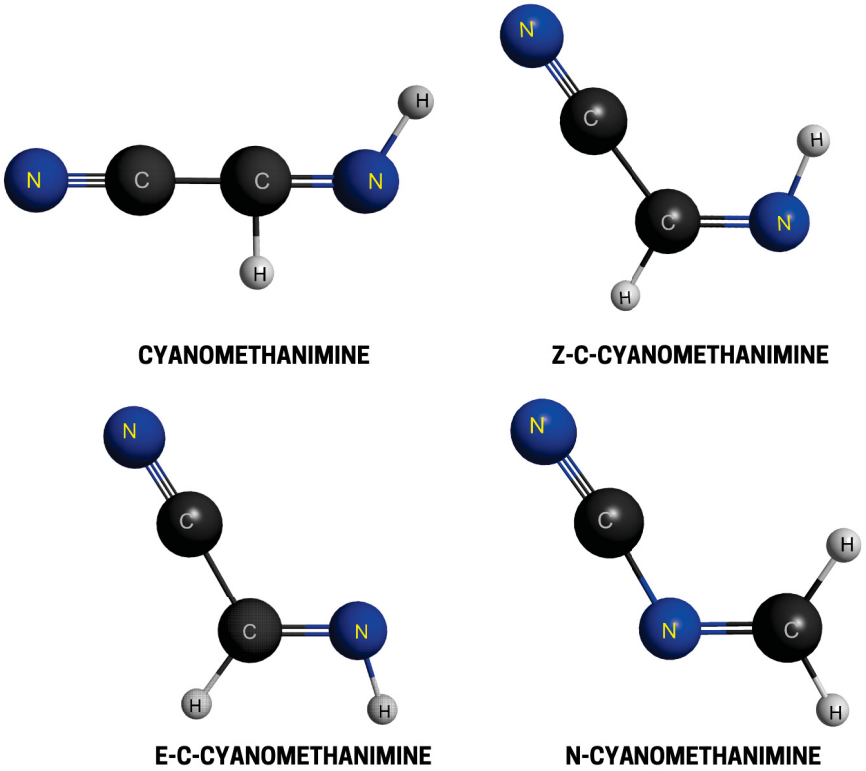

FIGURE 6 – Ball-and-stick representations of the generic form and the Z, E, and N isomers of C-cyanomethanimine. Generated with MacMolPlt.

The electronic structure of the neutral and anionic states of the Z, E, and N isomers werw characterized using Density Functional Theory (DFT). The calculations employed the CAM-B3LYP functional with an unrestricted Hartree-Fock (UHF) reference and the aug-cc-pVDZ basis set. For the subsequent electron scattering calculations, the molecular potential was described within the Hartree-Fock approximation. The core electrons of carbon and nitrogen were replaced with BHS pseudopotentials, and the valence electrons were described using a customized Gaussian basis set. This basis set, tailored for compatibility with the pseudopotentials, consists of 6 *s*-type, 5 *p*-type, and 3 *d*-type Gaussian functions per atom. All exponents of the Cartesian Gaussian functions used are listed in Table 2. The procedure for generating these functions followed the established methodology of Ref. [46].

TABLE 2 – Basis set exponents and contraction coefficients.

Type	Carbon Exponents	Nitrogen Exponents	Hydrogen	
			Exponent	Contraction
s	12.49628	17.56987	13.3515	0.130844
s	2.470286	3.423613	2.01330	0.921539
s	0.614028	0.884301	0.45380	1.000000
s	0.184028	0.259045	0.12330	1.000000
s	0.039982	0.053066	–	–
s	0.009996	0.022991	–	–
p	5.228869	7.050692	0.75000	1.000000
p	1.592058	1.910543	–	–
p	0.568612	0.579261	–	–
p	0.210326	0.165395	–	–
p	0.072250	0.037192	–	–
d	1.794795	0.975269	–	–
d	0.420257	0.253058	–	–
d	0.101114	0.078904	–	–

The C-cyanomethanimine molecule (HNCHCN) belongs to the point group C_s, an Abelian group whose classification is dictated by the presence of a single mirror plane as its only symmetry element. This symmetry gives rise to irreducible representations A′ and A″. To estimate the resonances positions, we employed two complementary methods:

An empirical scaling relation [47], which correlates the resonance energy (Virtual Attachment Energy, VAE) with the energy of the unoccupied orbital (Virtual Orbital Energy, VOE) via Koopmans' theorem, was employed: $VAE = 0.64795 \times VOE - 1.4298$. Following the procedure described in Ref. [47], the molecular geometries were optimized at the MP2/6-31G(1*d*) level, and the VOEs were obtained from Hartree–Fock calculations with the same 6-31G(1*d*) basis set. The 6-31G(1*d*) basis set was chosen based on convergence tests and to ensure consistency with the scaling-law calculations.Tables 3 and 4 present the optimized geometrical coordinates for each isomer, obtained at the MP2/HF/6-31G(1*d*) level of theory within the $\mathrm{C_s}$ point group.

TABLE 3 – Cartesian coordinates (x, y, z) of the atoms from C-Cyanomethanimine Isomers in $\mathring{\mathrm{A}}$.

Isomer	Atom	x	y	z
Z-C	C	-0.1929	-0.2475	0.0000
	C	0.8150	-1.3073	0.0000
	N	0.0398	1.0387	0.0000
	N	1.6765	-2.1487	0.0000
	H	1.0464	1.2801	0.0000
	H	-1.2333	-0.5676	0.0000
E-C	C	-0.2485	-0.2518	0.0000
	C	0.8199	-1.2398	0.0000
	N	0.0433	1.0208	0.0000
	N	1.6765	-2.0841	0.0000
	H	-0.8036	1.6121	0.0000
	H	-1.2649	-0.6595	0.0000
N	C	-0.2538	-0.2389	0.0000
	N	-0.3448	1.0652	0.0000
	C	0.7818	1.8622	0.0000
	N	1.6486	2.7018	0.0000
	H	-1.1825	-0.8026	0.0000
	H	0.6889	-0.7936	0.0000

TABLE 4 – Chemical bonds and bond angles for the isomers of C-cyanomethanimine. Bond lengths in $\mathring{\mathrm{A}}$ and angles in degrees.

Isomer	Bonding Atoms	Length	Angle	Value
Z-C	C≡N	1.204	H–N=C	113.75
	C–C	1.463	N=C–H	117.36
	C=N	1.307	N=C–C	126.18
	N–H	1.035	C–C≡N	177.89
	C–H	1.089	–	–
E-C	C≡N	1.203	H–N=C	112.00
	C–C	1.455	N=C–H	124.78
	C=N	1.306	N=C–C	119.84
	N–H	1.033	C–C≡N	178.17
	C–H	1.095	–	–
N	C≡N	1.208	H–C–H	118.27
	C–N	1.380	H–C=N	117.26
	N=C	1.307	N=C–H	124.47
	C–H	1.094	C=N–C	121.29
	H–C	1.086	N–C≡N	188.81

In parallel, the scattering calculations were performed on the molecular geometries previously optimized at the RHF/aug-cc-pVDZ level, Table 5 shows the coordinates optimized in this level. The scattering wavefunction was expanded in the larger 6s5p3d basis set, which was also used for the diagonalization of the H_{N+1} collision Hamiltonian, ensuring a consistent description between the electronic structure and scattering representations. This procedure yielded independent confirmation of the resonance positions and their corresponding orbitals.

TABLE 5 – Cartesian coordinates (x, y, z) of the atoms from C-cyanomethanimine isomers in Bohr.

Isomer	Atom	x	y	z
Z-C	C	-0.3764	-0.4402	0.0000
	C	1.5577	-2.4065	0.0000
	N	0.0766	1.9592	0.0000
	N	3.1537	-3.9889	0.0000
	H	1.9972	2.2762	0.0000
	H	-2.3429	-1.0894	0.0000
E-C	C	-0.4567	-0.4474	0.0000
	C	1.5616	-2.3198	0.0000
	N	0.1113	1.9265	0.0000
	N	3.1238	-3.9324	0.0000
	H	-1.5326	2.9651	0.0000
	H	-2.3868	-1.2199	0.0000
N-C	C	-0.4697	-0.3858	0.0000
	N	-0.7412	2.0467	0.0000
	C	1.4075	3.4688	0.0000
	N	3.1430	4.9023	0.0000
	H	-2.1906	-1.5309	0.0000
	H	1.3800	-1.3314	0.0000

For the SEP approximation, we employed the MVO scheme with symmetry-specific configurations. For the A′ symmetry, a total of 168 contracted functions were used, with 10 occupied orbitals, 5 hole orbitals, and 65 particle and scattering orbitals. The number of resulting configurations for this symmetry was 10,941 for both the Z- and E-isomers, and 10,897 for the N-isomer.For the A″ symmetry, the basis consisted of 168 contracted functions, with 10 occupied orbitals, 10 hole orbitals, 158 particle orbitals, and 2 scattering orbitals. In this case, the number of configurations was 2,044 for all three isomers (Z, E, and N).

It is important to note that the use of different polarization levels for each symmetry arises from methodological constraints: for the A″ symmetry, overcorrelation of the resonance must be avoided, and therefore the number of configurations must remain restricted. This issue does not occur for the A′ symmetry, allowing a larger and more flexible configuration space.

CHAPTER 4

RESULTS AND DISCUSSION

This chapter presents the main results on the electron-driven dynamics of C-cyanomethanimine. We begin by detailing the results of our electronic structure calculations performed using Density Functional Theory (DFT), establishing the geometric and energetic parameters of the isomers of the molecule and validating our approach through a direct comparison with the high-level benchmarks established by Puzzarini. Subsequently, we present the integral, differential, and momentum transfer cross-sections for elastic electron scattering, calculated within the Static-Exchange (SE) and Static-Exchange-Plus-Polarization (SEP) approximations.

The Born-closure approximation is applied to correct the scattering amplitude for the long-range electron-dipole interaction, producing cross-sections valid across all scattering angles. The convergence of key Hartree-Fock properties, essential for constructing the scattering potential, is thoroughly discussed. Additionally, the Maxwell-Boltzmann distribution is employed to calculate the equilibrium fractional populations of the C-cyanomethanimine isomers, unequivocally establishing the Z-isomer as the primary species in a thermal gas.

4.1 ELECTRONIC STRUCTURE

Figure 7 illustrates the ball and stick model of the molecular structures and orbital representations of each isomer. On the top, the molecular structures are shown with labeled and highlighted atoms for clarity. On the bottom, virtual orbitals, including the LUMO, LUMO+1 and LUMO+4 (LUMO+3 for the N-isomer), are visualized as contour plots depicting the electron density distribution.

These representations reveal differences in electronic distribution among the isomers, with each exhibiting distinct orbital shapes and resonance behaviors. In all cases, the visualized orbitals correspond to antibonding π^* orbitals, characterized by nodal planes perpendicular to the molecular framework. Such orbitals play a central role in electron attachment and excitation processes, as they correspond to the virtual antibonding π^* orbitals that, when temporarily occupied by the incoming electron, give rise to the resonant states observed in scattering calculations.

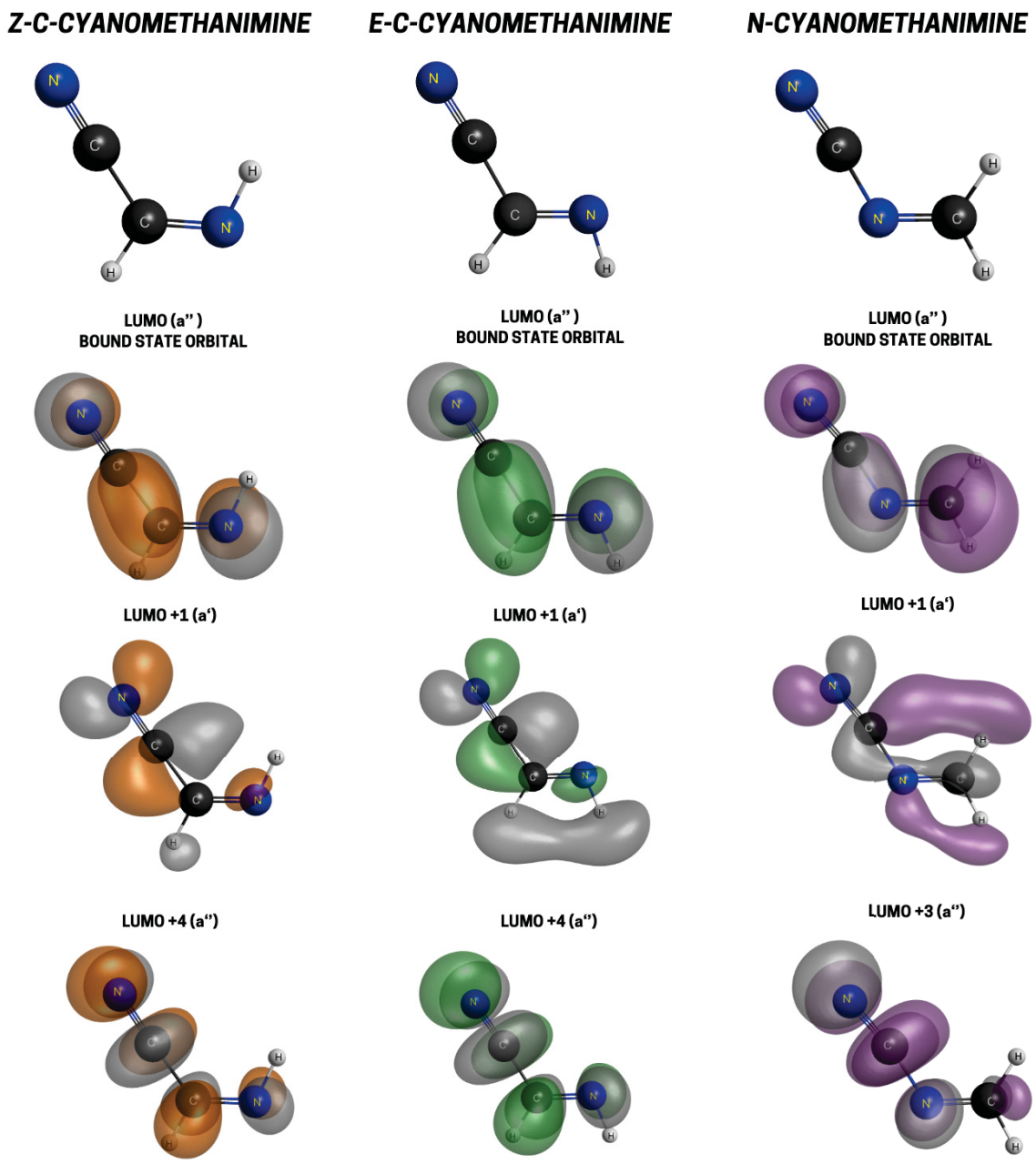

FIGURE 7 – Virtual orbitals obtained by symmetry from the empirical scaling relation [47] for the C-cyanomethanimine isomers, computed at the Hartree–Fock level.

In addition to the orbital representations for each resonance, a table of Vertical Attachment Energies (VAEs) provides a detailed comparison of the electronic properties of the isomers (Table 6). The VAEs, calculated in electron volts (eV), correspond to the π_1^*, π_2^*, and π_3^* resonances and reveal clear differences in the resonance spectrum among the isomers.

The VAE values reported here were obtained using the empirical linear relation proposed by Vazart et al [48].

$$\mathrm{VAE} = 0.64795 \times \mathrm{VOE} - 1.4298, \tag{4.1}$$

which allows the conversion from the Vertical Orbital Energies (VOEs) to the corresponding attachment energies. The negative VAE value obtained for the π_1^* resonance suggests that this very low attachment energy may indicate the formation of a bound or quasi-bound temporary anion state for the molecule.

TABLE 6 – Vertical attachment energies (in eV).

Resonance	Z	E	N
$\pi_1^*(a'')$	-0.37	-0.28	-0.34
$\pi_2^*(a')$	1.27	1.31	1.80
$\pi_3^*(a'')$	3.35	3.42	3.31

Specifically, the Z-cyanomethanimine exhibits the lowest VAE for the π_1^* resonance (-0.37 eV), indicating that electron attachment is most favorable in this state. For the π_2^* resonance, the N-isomer presents the highest VAE (1.80 eV), suggesting a less favorable attachment process. In contrast, for the π_3^* resonance, the VAE values are similar among the three isomers, with the N-isomer showing a slightly lower energy (3.31 eV). Overall, these results indicate that the Z-isomer tends to favor electron attachment at lower energies, while the N-isomer requires higher excitation for some of its virtual π^* states.

The permanent dipole moments of the Z, E, and N isomers are 1.628 D, 4.645 D, and 5.324 D, respectively. These results reveal substantial variations in polarity among the isomers. Although the Z and E isomers display similar geometries, their dipole moments differ considerably. This difference arises from the relative orientation of the CN and NH bond dipoles: in the Z isomer, these vectors partially cancel each other, resulting in a lower net dipole moment, whereas in the E isomer they are oriented more additively, leading to a stronger overall dipole.

The N isomer shows the highest dipole moment, consistent with its distinct atomic arrangement and enhanced charge separation. Altogether, these quantitative results complement the orbital visualizations, offering a deeper understanding of the electronic differences among the isomers.

4.2 DENSITY FUNCTIONAL CALCULATIONS

This section aims to analyze the neutral and anionic forms of the isomers to determine their relative stability. For the neutral state (Table 7), the Z isomer was identified as the most stable, with the lowest corrected energy (-186.7599 Hartree), followed closely by the E isomer. The N isomer was the least stable. Zero-point energy corrections were included to ensure a proper account of vibrational contributions to stability.

TABLE 7 – Calculated DFT energies for the neutral ground state of each isomer in Hartree.

Isomers	Total Energies	Zero Point Energy	$E_{DFT} = E_T + E_0$
Z-C	-186.7999	0.0400	-186.7599
E-C	-186.7993	0.0399	-186.7594
N	-186.7905	0.0349	-186.7556

For the anionic state (Table 8), the Z and N isomers exhibit nearly identical corrected energies, suggesting similar stability, while the E isomer is slightly less stable. This behavior inverts the relative order observed for the neutral species, emphasizing that the additional electron affects each isomer differently depending on its electronic distribution.

TABLE 8 – Calculated DFT energies for the anionic form of each isomer in Hartree.

Isomers	Total Energies	Zero Point Energy	$E_{DFT} = E_T + E_0$
Z-C	-186.8111	0.0373	-186.7738
E-C	-186.8085	0.0369	-186.7716
N	-186.8087	0.0358	-186.7729

The energy differences ($\Delta E = E_{\text{neutral}} - E_{\text{anion}}$) between the neutral and anionic forms were calculated to further assess stability. The ΔE values for the Z, E, and N isomers were 0.37992, 0.33141, and 0.59578 eV, respectively. The energy separations among the neutral isomers were also computed in kcal/mol to facilitate comparison with the results of Puzzarini [26]. These values correspond to 5.53 kcal/mol between the N and E isomers and 0.29 kcal/mol between the Z and E isomers, obtained directly from the total energy differences (in Hartree) using the conversion factor 1 Hartree = 627.51 kcal/mol.

The small energy gap between the Z and E isomers confirms their very similar stability, while the significantly higher energy of the N isomer indicates that it is much less stable in both electronic states. The empirical scaling-law analysis performed in this work also supports the greater stability of the Z form, reinforcing the internal consistency of our results.

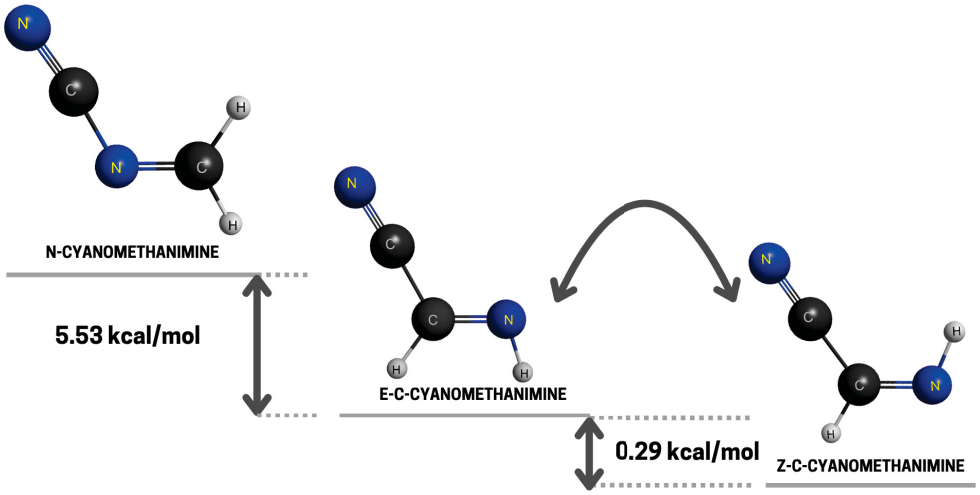

FIGURE 8 – Schematic representation of the molecular structures of the C-cyanomethanimine isomers and their respective energy differences for the neutral-to-anion transition.

These findings are in good agreement with those of Puzzarini et al., who reported energy differences of 6.72 kcal/mol for the N–E transition and 0.47 kcal/mol for the E–Z transition. The small discrepancies observed here likely arise from differences in the functional and basis set employed. Overall, the stability order is consistently established as Z $>$ E $>$ N for the neutral species, whereas for the anionic forms the order becomes Z $\approx$ N $>$ E. A schematic representation of the molecular structures and the corresponding energy differences (in kcal/mol) is shown in Figure 8, illustrating the close agreement between our calculations and the reference data.

4.3 CROSS SECTIONS

Building on the established ground-state geometries and stabilities of the cyanomethanimine isomers, we now examine their interaction with low-energy electrons. This section presents the integral cross sections (ICS) computed within the Static-Exchange (SE) and Static-Exchange-Plus-Polarization (SEP) approximations. The comparison between SE and SEP results highlights the crucial role of polarization effects in accurately describing the scattering process and in characterizing the formation of temporary negative ion states

4.3.1 Static-Exchange

The following analysis is based on the static–exchange approximation cross-section plots for the three isomers of C-cyanomethanimine. The graphs show the probability of an elastic electron–molecule collision (the cross section) as a function of the incident electron energy. The most prominent features are the sharp peaks corresponding to shape resonances, in which the incoming electron is temporarily captured by the molecular potential, in particular, by the localized unoccupied molecular

orbital that gives rise to the resonance state. The energy position of each peak indicates the resonance energy, while its width is inversely related to the lifetime of the transient negative ion.

For the Z-isomer, shown in Figure 9, the cross-section is characterized by a very sharp and intense peak in the A'' symmetry at approximately 1.16 eV. The large cross-section value, exceeding 150 a_0^2, indicates a high probability of electron capture at this specific energy. The narrowness of the peak suggests that the resulting temporary negative ion is relatively long-lived. Another broad feature in the same symmetry appears at 6.65 eV. These structures correspond to the π_1^* and π_3^* shape resonances of the Z-isomer.

A second, broad peak is also visible in the A' symmetry around 4.01 eV, though it is less intense and corresponds to the π_2^* shape resonance. It is worth noting that the small feature in the A' observed between 0.1 and 0.5eV is likely due to basis set deficiencies and is expected to be corrected upon inclusion of higher-level approximations, such as the SEP and Born closure correction.

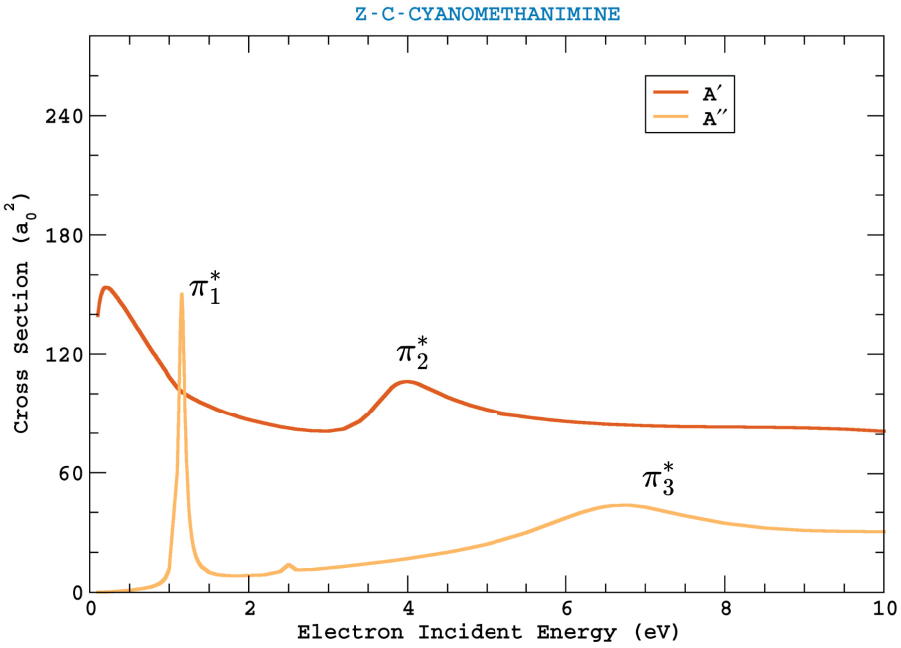

FIGURE 9 – Static Exchange Approximation Cross Section for Z-C-cyanomethanimine.

For the E-isomer, shown in Figure 10, a pronounced peak in the A'' symmetry appears at about 1.21 eV. This feature corresponds to the π_1^* shape resonance; compared with the Z-isomer, the π_1^* peak in the E-isomer is smaller in intensity, even though its resonance width is slightly narrower (0.55 eV against 0.61 eV for Z). A second A'' peak, attributed to the π_3^* shape resonance, is found at 6.74 eV; this resonance is broad and of relatively low intensity (just above 40 a_0^2), which points to a lower electron-capture probability and a short lived character.

The A' symmetry shows a small and broad feature near 4.20 eV. The dominant resonance in this isomer is the π_2^* state, which displays the highest cross section. Its width (1.41 eV) is larger than that of the corresponding π_2^* resonance in the Z isomer (1.09 eV), but still narrower than the π_3^* resonance of the E isomer (1.48 eV). In contrast, the π_3^* resonance in the Z isomer is considerably broader (1.92 eV).

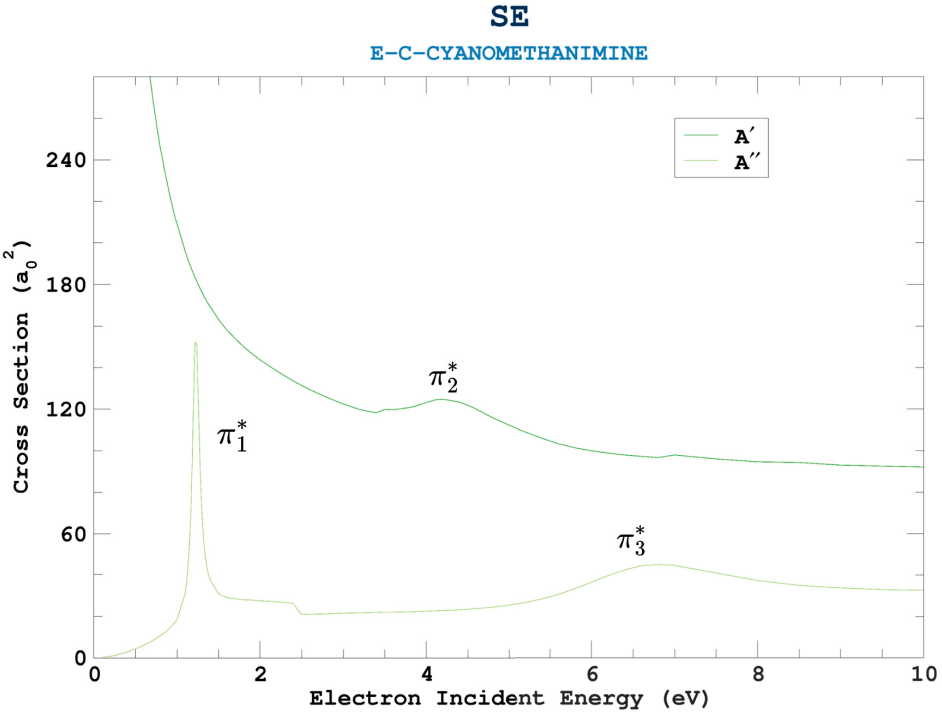

FIGURE 10 – Static Exchange Approximation Cross Section for E-C-cyanomethanimine.

The cross section for the N isomer (Figure 11) exhibits the most dramatic resonant behavior among the three species. A very sharp and intense peak in the A' symmetry appears at the remarkably low energy of about 1.09 eV, with a maximum cross section below 320 a_0^2. At first sight, this feature might be interpreted as an exceptionally strong resonance. It does correspond to a genuine shape resonance in the π_2^* orbital; however, its relatively narrow width (0.42 eV) reflects a well-defined temporary anion. In addition, the large dipole moment of this isomer (5.324 D) significantly enhances the background scattering, contributing to the overall intensity of the peak.

The interplay between these two effects accounts for both the resonance peak and the marked increase of the cross section as the incident energy decreases. A smaller but considerably broader feature is visible in the A'' symmetry around 0.87 eV, associated with the π_1^* orbital, which displays a width of 1.30 eV. The π_3^* shape resonance appears at higher energy, around 6.99 eV, and is the broadest among the three, with a width of 1.68 eV.

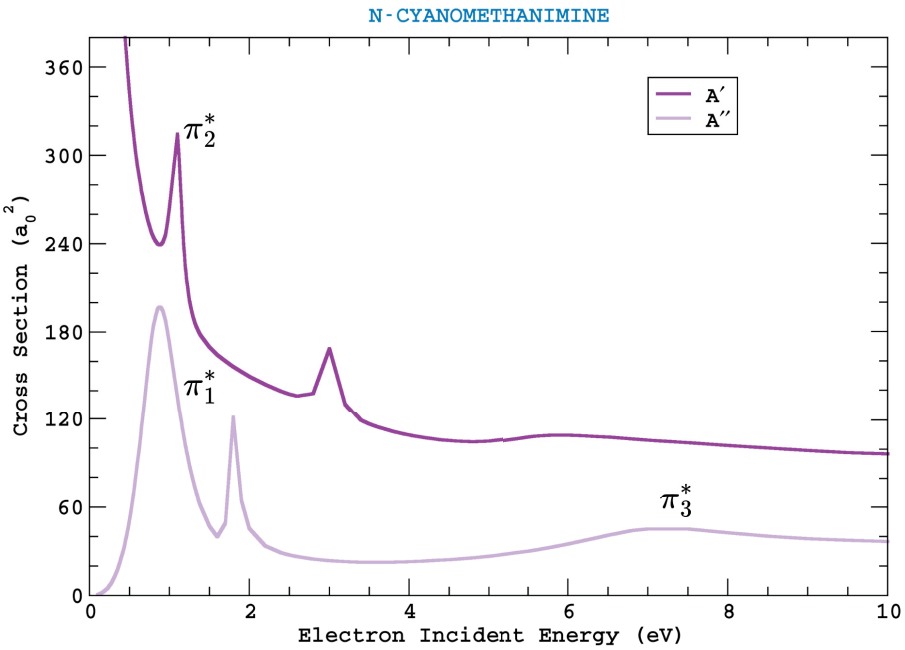

FIGURE 11 – Static Exchange Approximation Cross Section for N-C-cyanomethanimine.

A general comment can also be made regarding the presence of additional sharp structures across all three graphs. For the Z-isomer, a small peak appears around 2.5 eV in the A'' symmetry; for the E-isomer, features are visible around 3.5 eV and 7.0 eV in the A' symmetry and near 9.5 eV in the A'' symmetry.For the N-isomer, noticeable features appear at around 3.0 eV (A' symmetry) and 1.8 eV (A'' symmetry). These features are identified as spurious structures resulting from linear dependencies in the basis sets used for the C-cyanomethanimine calculations. They do not correspond to physically meaningful resonances, as confirmed by the convergence tests performed within the SMC framework. The physically relevant resonances are those explicitly assigned to the π^* orbitals in the discussion above.

Taken together, the individual analyses show that while all three isomers exhibit resonant behavior, the Z-isomer presents the clearest and most structured pattern of low-energy features in its cross section. Although the N-isomer hosts the narrowest low-energy resonance, indicating the longest-lived temporary anion, the Z-isomer displays the most distinct sequence of well-defined shape resonances across the energy range. Its geometry creates a particularly favorable environment for temporary electron capture, in line with its greater thermodynamic stability compared to the other C-cyanomethanimine isomers. This observation is consistent with the electronic structure and DFT results reported in the previous section.

In conclusion, the cross-section graphs reveal a distinct resonance spectrum for each isomer. The Z-isomer provides the most clearly resolved pattern of shape resonances, the N-isomer supports the longest-lived low-energy resonance, and the

E-isomer displays broader features consistent with shorter-lived anionic states. These differences in resonance energies and lifetimes directly reflect the unique electronic and geometric structures of each isomer.

4.3.2 Stactic Exchange Plus Polarization

This approximation also includes the interaction between the incoming electron and the target molecule's static electric field, incorporating exchange effects via the Pauli exclusion principle. The more advanced treatment also accounts for the target's dynamic response: the incoming electron induces a temporary polarization of the molecular electron cloud, producing an additional attractive potential. This polarization lowers the energies of temporary negative ion states and shifts resonance peaks to lower incident energies.

Figures 12, 13 and 14 compare the SE (static-exchange) and SEP (static-exchange plus polarization) results for each isomer, highlighting the role of the polarization potential and the influence of the molecular dipole moment.

For the Z isomer, as shown in Figure 12, the inclusion of the SEP approximation induces substantial shifts in the resonant states. The π_2^* and π_3^* resonances undergo pronounced red shifts, moving from 4.00 eV to 1.60 eV and from 6.65 eV to 3.81 eV, respectively. Their widths also decrease significantly: the π_2^* resonance narrows from 1.09 eV to 0.93 eV, while the π_3^* resonance contracts from 1.92 eV to 1.25 eV. These reductions reflect the stabilizing effect of including polarization, which suppresses the decay channels of the temporary anion.

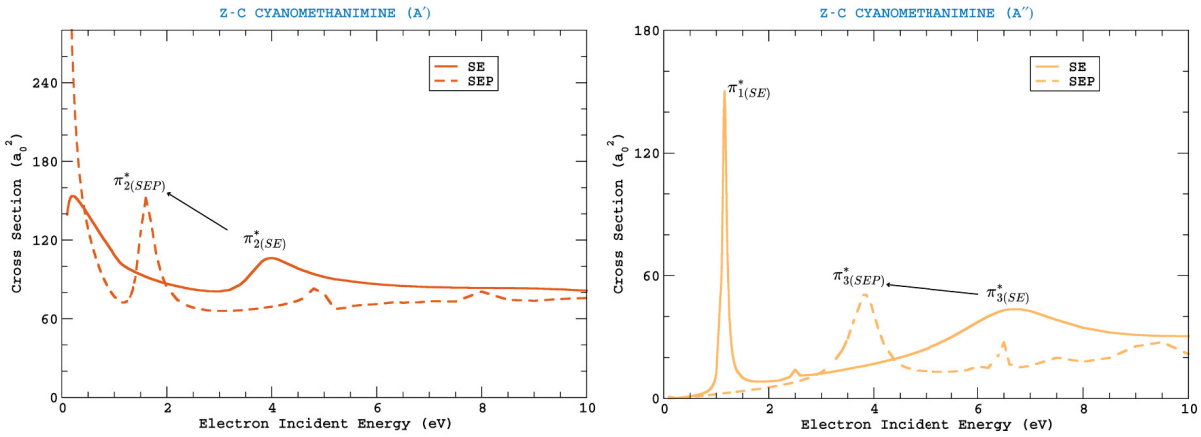

FIGURE 12 – Comparison of Static-Exchange and Static-Exchange-Plus-Polarization Cross Sections for the Symmetries of Z-C-Cyanomethanimine.

Meanwhile, the π_1^* resonance (1.59 eV in the SE approximation) is shifted below threshold upon the inclusion of polarization, transforming into a bound state and thus disappearing from the scattering spectrum. The broad SE feature observed between 0.1–0.5eV does not correspond to a real bound state. Instead, it vanishes upon the

application of more rigorous correlation treatments within the SEP framework, revealing its nonphysical character.[7]

Figure 13 shows a similar pattern for the E-isomer: the π_2^* resonance shifts from 4.20 eV (SE) to 1.88 eV (SEP), while the π_3^* resonance decreases from 6.74 eV to 3.69 eV. Their widths are also notably reduced upon inclusion of polarization. The π_2^* width contracts from 1.13 eV to 0.49 eV, indicating a substantially more stable temporary anion, whereas the π_3^* resonance narrows from 1.48 eV to 1.17 eV. These reductions reflect the expected stabilizing effect of the polarization term on the anionic states.

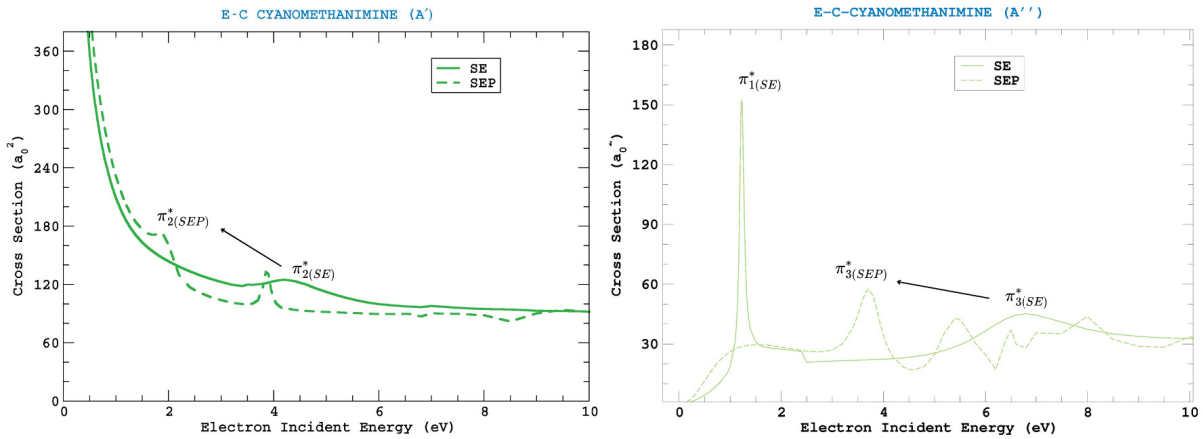

FIGURE 13 – Comparison of Static-Exchange and Static-Exchange-Plus-Polarization Cross Sections for the Symmetries of E-C-Cyanomethanimine.

As in the Z isomer, the π_1^* resonance shifts from 1.21 eV in the SE approximation to below threshold in the SEP model, confirming its bound-state character and causing it to vanish from the scattering spectrum.

Finally, for the N-isomer, shown in Figure 14, significant but less stable changes are observed, likely due to its larger dipole moment. Nevertheless, the overall behavior remains consistent with the bound states and resonance shifts found in the other isomers. The π_2^* resonance shifts from 1.09 eV (SE) to 2.79 eV (SEP), while the π_3^* resonance decreases from 6.99 eV to 3.91 eV. Their widths also change upon inclusion of polarization: the π_2^* resonance broadens from 0.42 eV to 1.18 eV, indicating a less stable temporary anion, whereas the π_3^* resonance narrows moderately from 1.68 eV to 1.35 eV.

The π_1^* resonance, located at 0.87 eV in the SE approximation, also shifts below threshold in the SEP model, confirming its bound-state nature and causing it to disappear from the scattering spectrum.

[7] Other unmarked sharp features are spurious artifacts, as discussed in the main text.

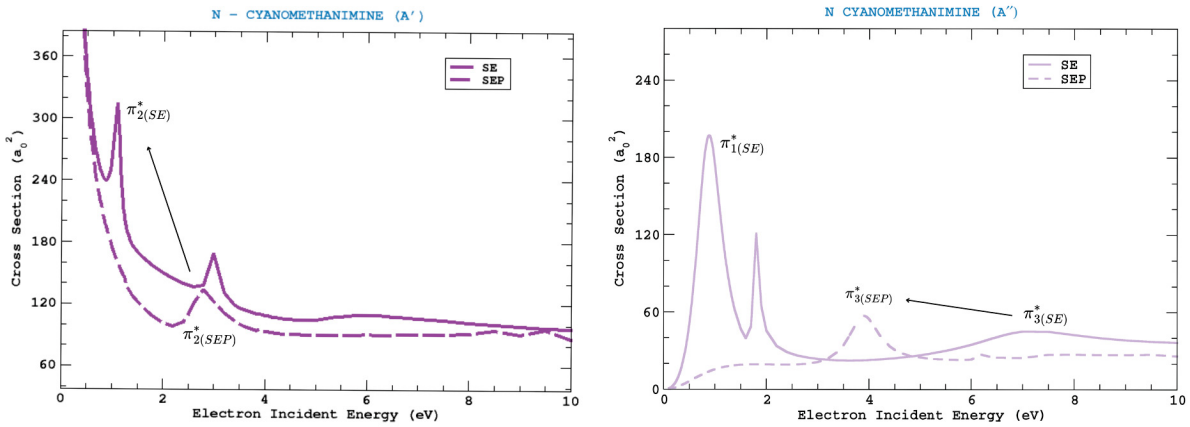

FIGURE 14 – Comparison of Static-Exchange and Static-Exchange-Plus-Polarization Cross Sections for the Symmetries of N-Cyanomethanimine.

In summary, the inclusion of the SEP approximation produces systematic and physically consistent modifications in the resonance spectra of the three C-cyanomethanimine isomers. For both the Z- and E-isomers, polarization leads to pronounced red shifts and a general narrowing of the resonances, reflecting the enhanced stabilization of the temporary anionic states. In contrast, the N-isomer exhibits a more complex response: its π_2^* resonance becomes significantly broader, while the π_3^* state narrows only moderately, a behavior that can be attributed to its large dipole moment and the resulting stronger coupling with the polarization potential. Despite these differences, all three isomers show the same qualitative trend in which the lowest-lying π_1^* resonance is driven below threshold, confirming its bound-state character in the SEP description.

4.3.3 Resonance Widths and Visual Analysis of the Cross Sections

As discussed in the theory subsection on resonances, the width of each resonance in the cross sections provides direct information about the lifetime of the temporary anion. The uncertainty relation $\Gamma\tau \simeq \hbar$ (Equation 2.145) states that narrower resonances correspond to longer-lived anionic states. For the π_1^*, π_2^*, and π_3^* resonances identified in the cross sections, the widths obtained within the static-exchange (SE) approximation are listed below.

TABLE 9 – Resonance widths (in eV) in the static-exchange approximation.

Resonance	Z	E	N
$\pi_1^*(a'')$	0.61	0.55	1.30
$\pi_2^*(a')$	1.09	1.13	0.42
$\pi_3^*(a'')$	1.92	1.48	1.68

Analysis of Table 9 shows that, for the π_1^* and π_2^* resonances, the temporary anion has the longest lifetime in the Z isomer, followed closely by the E isomer, while the N isomer presents the shortest lifetimes due to its larger widths. For the π_3^* resonance,

however, the trend differs: the E isomer displays the narrowest structure (1.48 eV), followed by the N isomer (1.68 eV), whereas the Z isomer shows the broadest peak (1.92 eV), corresponding to the shortest-lived π_3^* temporary anion.

To visualize these behaviors, Figure 15 displays the cross sections for the three isomers in the SE approximation.

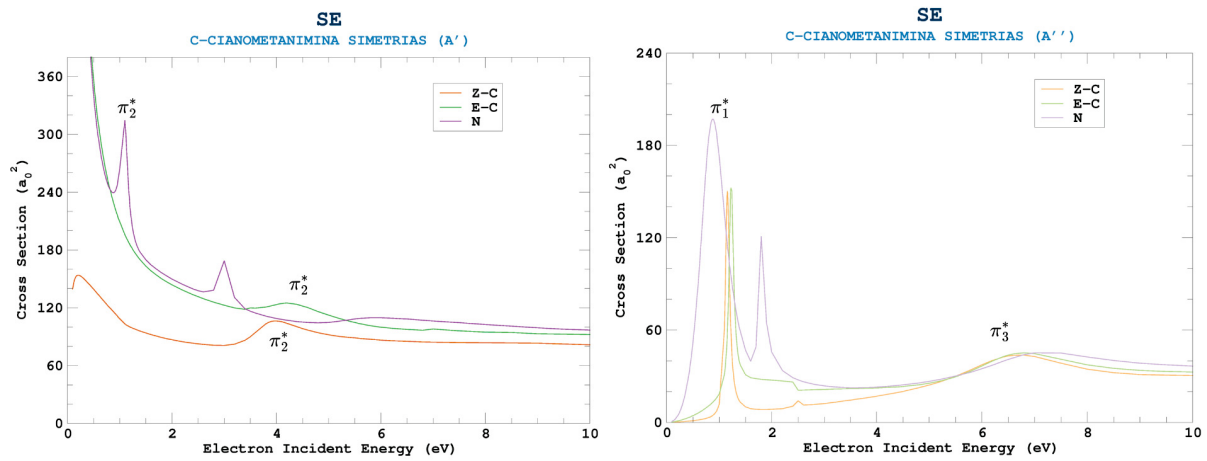

FIGURE 15 – Comparison of the Static Exchange (SE) Approximation Cross Sections for C-cyanomethanimine isomers in the a' and a'' symmetries.

A visual inspection of these spectra highlights the resonance structures discussed above. In the a' symmetry (left panel), associated with the π_2^* resonance, the Z and E isomers display broader peaks near 4 eV, consistent with their larger widths (1.09 and 1.13 eV), while the N isomer shows a noticeably sharper and more pronounced peak, reflecting its narrower width of 0.42 eV.

In the a'' symmetry (right panel), containing the π_1^* and π_3^* resonances, the Z and E isomers exhibit relatively narrow and visible π_1^* peaks at low energies, whereas the N isomer shows a much broader structure, aligned with its substantially larger width (1.30 eV). Around 6–7 eV, corresponding to the π_3^* resonance, the E isomer presents the narrowest feature (1.48 eV), followed by the N isomer (1.68 eV), while the Z isomer exhibits the broadest peak (1.92 eV).

When polarization effects are incorporated, the resonance widths obtained in the static-exchange plus polarization (SEP) approximation are shown below.

TABLE 10 – Resonance widths (in eV) in the static-exchange plus polarization approximation.

Resonance	Z	E	N
$\pi_1^*(a'')$	—	—	—
$\pi_2^*(a')$	0.93	0.49	1.18
$\pi_3^*(a'')$	1.25	1.17	1.35

Figure 16 illustrates the SEP cross sections and allows a direct comparison with the SE results.

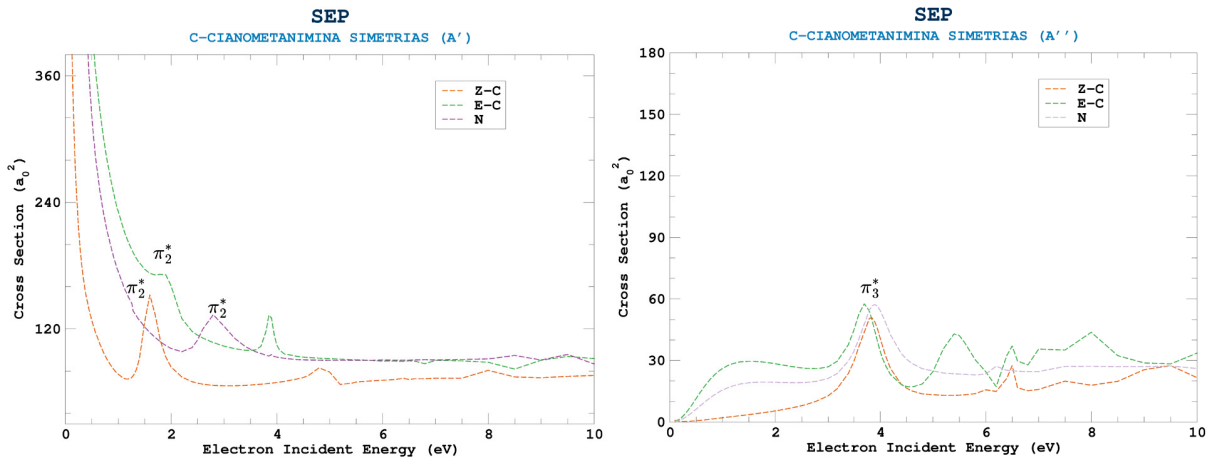

FIGURE 16 – Comparison of the Static Exchange plus Polarization (SEP) Approximation Cross Sections for the C-cyanomethanimine isomers in the a' and a'' symmetries.

In the a' symmetry (left), corresponding to the π_2^* resonance, the Z and E isomers show significantly narrower peaks after inclusion of polarization, consistent with their reduced widths (0.93 and 0.49 eV, respectively). The N isomer, however, displays a broader and less intense peak, aligned with its larger width (1.18 eV), indicating a comparatively shorter lifetime.

In the a'' symmetry (right), associated with the π_3^* resonance, all three isomers exhibit moderate narrowing relative to SE. The E isomer shows the smallest width (1.17 eV), followed closely by Z (1.25 eV), while the N isomer retains the broadest resonance (1.35 eV). The persistence of these relative trends between SE and SEP highlights the stability of the underlying physical picture.

Overall, the consistency between the visual inspection of the cross-section spectra and the numerical widths extracted in both approximations demonstrates the reliability of the results and reinforces the observed trends in the lifetimes of temporary anions formed through electron capture in the three isomers of C-cyanomethanimine.

4.3.4 Hamiltonian Diagonalization and Resonance Analysis

To accurately capture the target response and polarization effects critical for low-energy electron scattering, we employed a pseudostate calculation, diagonalizing the H_{N+1} collision Hamiltonian within the SEP configuration state functions of the A'' symmetry. This approach discretizes the continuum, providing a spectrum of eigenvalues (ε) that approximate both bound and continuum states of the temporary negative ion.

TABLE 11 – Comparison of Vertical Attachment Energies (VAE), stabilization (SEP) energies, and pseudostate eigenvalues (ε) from the diagonalization of the (H_{N+1}) scattering Hamiltonian (in eV) for each isomer.

	Z			**E**			**N**		
Resonance	VAE	SEP	ε	VAE	SEP	ε	VAE	SEP	ε
$\pi_1^*(a'')$	-0.37	—	-1.06	-0.28	—	-0.98	-0.34	—	-0.94
$\pi_2^*(a')$	1.27	1.60	1.66	1.31	1.88	1.86	1.80	2.80	2.63
$\pi_3^*(a'')$	3.35	3.81	3.73	3.42	3.69	3.82	3.31	3.91	3.82

The calculated eigenvalues for the lowest π^* orbitals of the Z-, E-, and N-isomers of cyanomethanimine reveal distinct energetic profiles, reflecting differences in their electronic structures (Table 11), which are visually apparent in the calculated molecular orbital representations (see accompanying Figure 17).

The orbitals displayed in Figure 17 are the Dyson orbitals, in practice, pseudo-states obtained from the diagonalization of the $(N+1)$-electron Hamiltonian. These orbitals are built as linear combinations of the scattering basis functions according to

$$|\phi_j\rangle \;=\; \sum_{\mu=1}^{n_{\rm sc}} \langle \chi_{0\mu} \mid \Psi_j^{N+1} \rangle \; |\varphi_\mu\rangle, \tag{4.2}$$

where $n_{\rm sc}$ runs over all configuration state functions (CSFs) that belong to the scattering space, $|\varphi_\mu\rangle$ denotes the scattering orbital used in the construction, and $|\Psi_j^{N+1}\rangle$ is the j-th eigenvector of the $(N+1)$-electron Hamiltonian H_{N+1}. In this representation, the coefficients $\langle \chi_{0\mu} \mid \Psi_j^{N+1} \rangle$ project the $(N+1)$-electron eigenstate onto the scattering CSF basis, producing the Dyson-like pseudo orbital $|\phi_j\rangle$ that effectively describes the electronic character of the resonant (temporary anion) state.

For the $\pi_1^*(a'')$ orbital, all three isomers support bound states, indicating the formation of stable transient anions. In contrast, the $\pi_2^*(a')$ resonance for the N-isomer appears at a much higher energy ($\varepsilon = 2.63$ eV) compared to the Z- and E-isomers (1.66 and 1.86 eV, respectively).

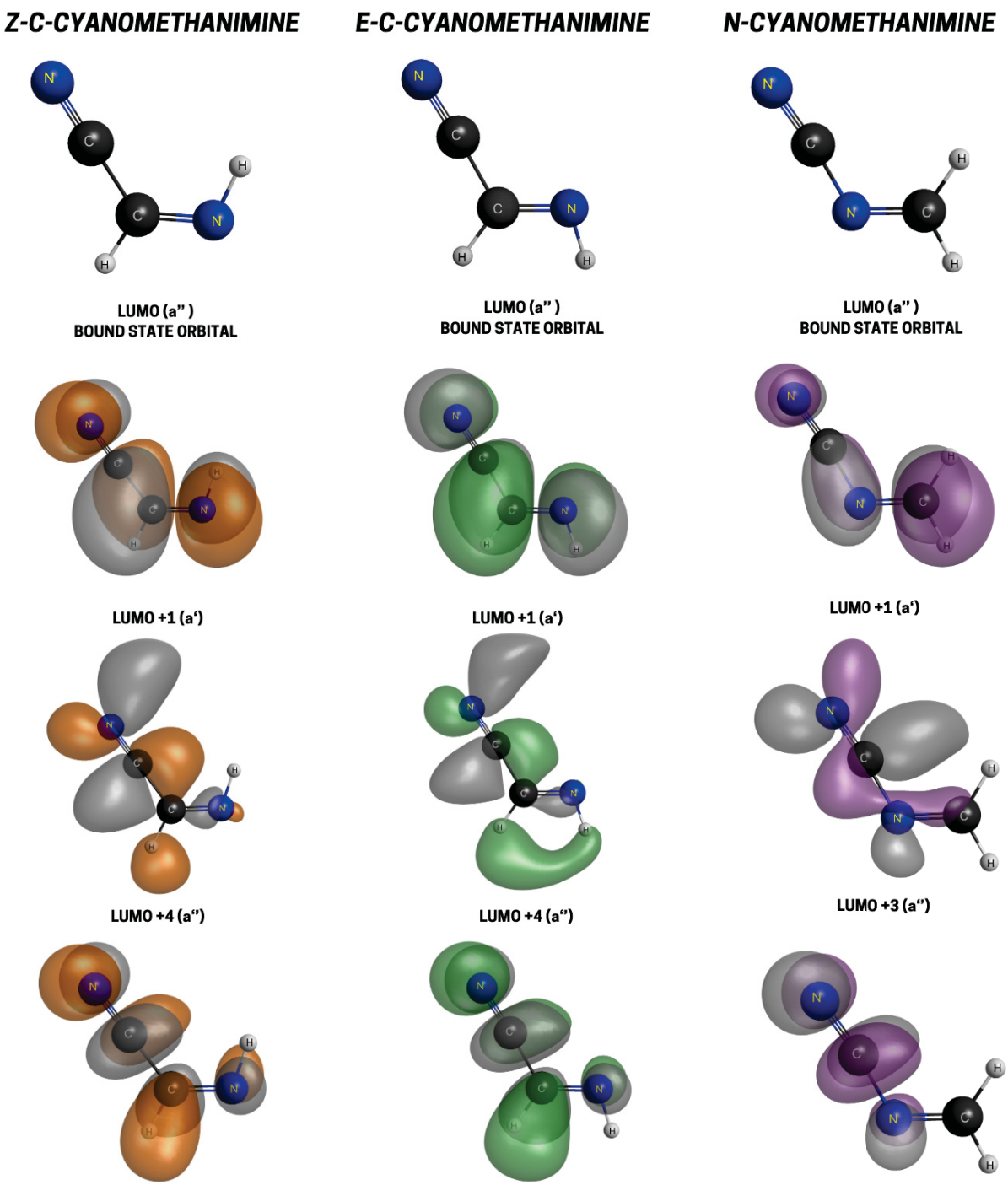

FIGURE 17 – Pseudostate virtual orbital morphology for C-cyanomethanimine isomers.

A comparison between the empirical scaling relation (VAE), the SEP resonance positions, and the eigenvalues from the diagonalization of the collision Hamiltonian (ε) shows excellent consistency across all three isomers: Z-C, E-C, and N (Table 11). Despite their geometric differences, the virtual orbitals obtained at the Hartree–Fock level (Fig.7) display the same qualitative ordering for all isomers: the unoccupied π_1^*, π_2^*, and π_3^* orbitals that give rise to the resonant states. In each case, the scaling relation correctly predicts this ordering, placing π_1^* below threshold (negative VAE), while π_2^* and

π_3^* appear as low-lying continuum resonances.

When polarization effects are included in the scattering calculation (SEP), the π_1^* resonance becomes bound in all three molecular configurations, again matching the negative eigenvalues obtained from the diagonalization of the collision Hamiltonian. Although the magnitude of the binding varies slightly between the Z, E, and N isomers, reflecting their distinct geometries and dipole moments, the qualitative behavior is the same. The π_2^* and π_3^* resonances remain in the continuum for the three isomers, but are consistently shifted to lower energy relative to the SE approximation, with SEP and pseudostate energies showing excellent agreement (Fig.17). The degree of stabilization is similar across Z, E, and N forms, indicating that the polarization response of the target is comparable for the three structural arrangements.

The combined analysis therefore demonstrates not only that the HF virtual orbitals can be directly associated with the observed shape resonances, but also that the three isomers of cyanomethanimine exhibit the same orbital ordering, symmetry patterns, and nodal structures, as seen in Fig.7. The most notable differences between isomers arise in the numerical values of the resonance energies, which reflect subtle variations in molecular geometry and charge distribution. Nonetheless, the physical picture, bound π_1^* and two short-lived π^* resonances in the continuum, is fully consistent across Z, E, and N isomers, and is confirmed simultaneously by the empirical scaling, SEP calculations, and Hamiltonian diagonalization.

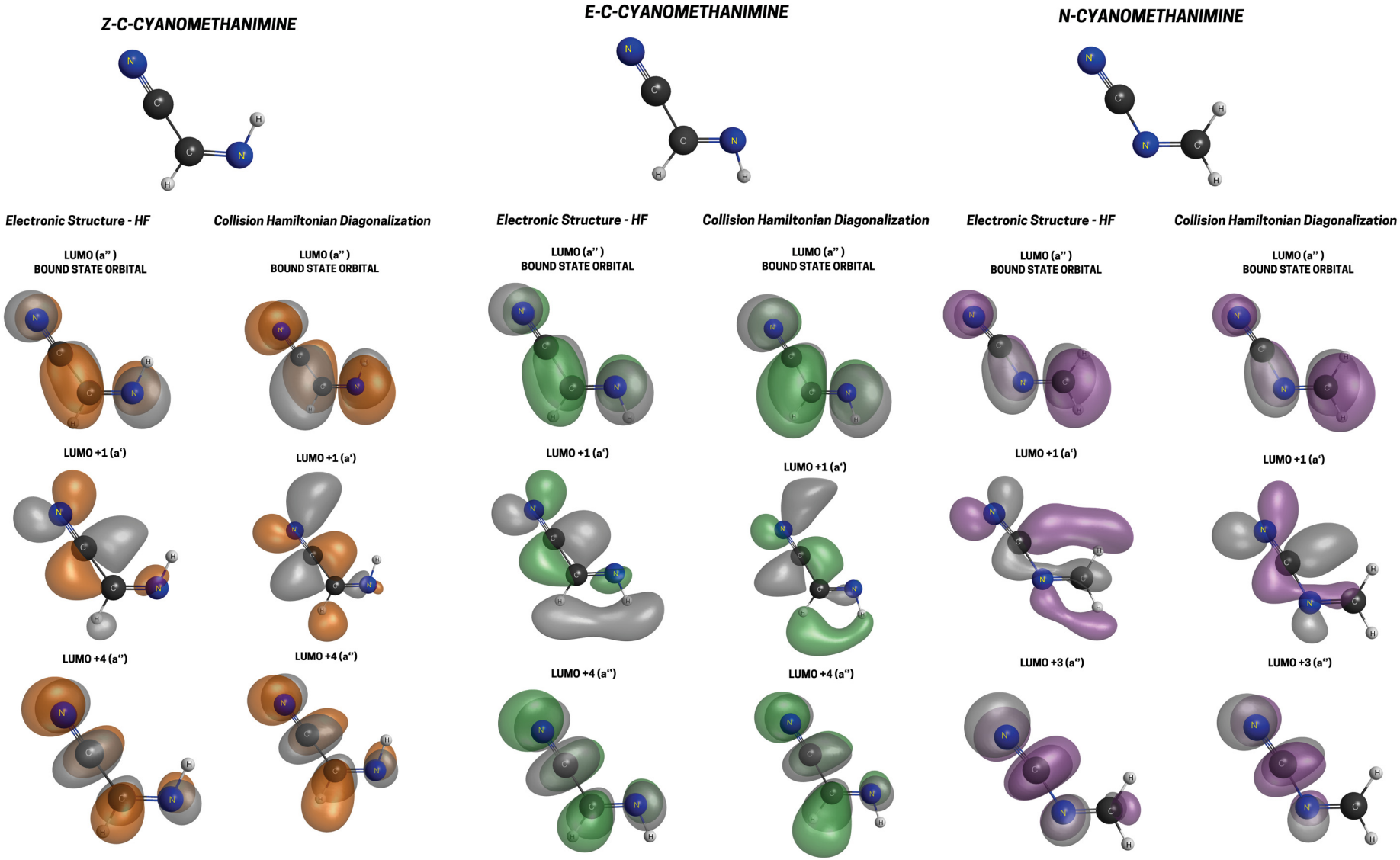

FIGURE 18 – Bound-state and resonance orbitals for the Z-, E-, and N-cyanomethanimine isomers. The left columns show the frontier molecular orbitals obtained at the Hartree–Fock (HF) level, while the right columns display the corresponding resonant orbitals obtained from collision Hamiltonian diagonalization. The LUMO (a'') represents the bound state orbital, and higher virtual orbitals (LUMO+n) correspond to the shape resonances relevant in the electron scattering process.

4.3.5 Born-Closure

To accurately account for the long-range dipole interaction absent in the static-exchange and static-exchange plus polarization approximations, the Born-Closure procedure was applied. This approach corrects the scattering amplitudes by incorporating the first-order Born term for the dipole potential, ensuring a physically meaningful description of the cross-sections, particularly at low energies and forward scattering angles. The resulting model significantly improves the reliability of the calculated electron scattering cross-sections for this polar molecules. The comparison between the integral and momentum transfer cross sections clearly illustrates the specific role of the Born closure correction. In the case of the integral cross section (ICS), which uniformly integrates contributions over all scattering angles, the Born closure is essential to recover the forward-scattering contribution associated with long-range dipole interactions. This results in significant differences between SEP and SEP+Born calculations, particularly at low energies, and ensures a physically consistent description of the scattering dynamics.

By contrast, the momentum transfer cross section (MTCS) suppresses forward scattering through its angular weighting, making the influence of the Born closure negligible. Consequently, the SEP and SEP+Born curves for the MTCS are practically indistinguishable, consistent with the theoretical expectation that Born corrections primarily affect the integral rather than the momentum transfer cross-section.

We begin our analysis of the isomers by examining the dominance of specific partial waves in the electron scattering process. The signatures of this dominance are the characteristic local minima and maxima visible in the differential cross sections (DCS) presented in the figures below. We will analyze each isomer separately.The Values of l_{SMC} for each isomer in the differential cross section are in table 12.

TABLE 12 – Converged partial-wave expansion parameters (l_{SMC}) for the Z, E, and N isomers of C-cyanomethanimine.

Energy (eV)	l_{SMC}		
	Z	E	N
1.00	2	2	3
2.00	4	3	4
4.00	5	5	5
6.00	5	5	5
8.00	6	6	6
10.0	7	7	7
12.0	7	7	8
15.0	7	7	8

4.3.5.1 Differential Cross Sections

For the Z-isomer (Figure19), the DCS in the 2–6 eV range exhibits a distinct double minimum, indicative of dominant *d*-wave contributions. At higher energies (8–15 eV), a pronounced triple minimum emerges, characteristic of *f*-wave behavior, a feature absent in the other isomers. Beyond this range, SE and SEP results remain comparable, while the Born correction primarily enhances forward scattering at small angles and lower impact energies.

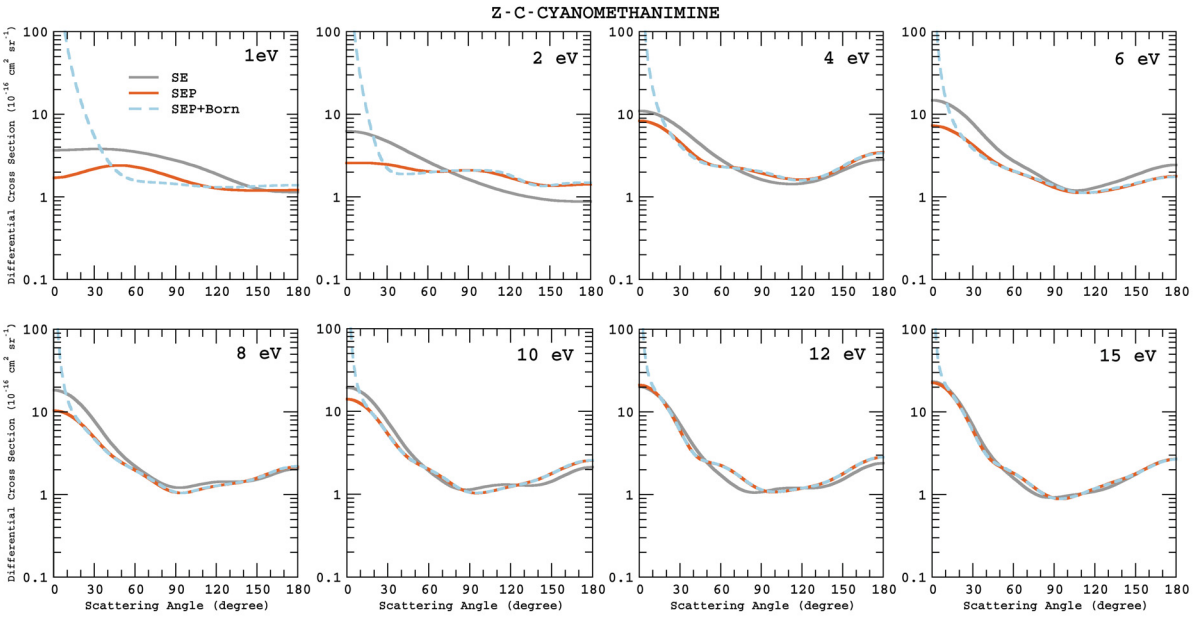

FIGURE 19 – Differential cross sections (DCS) for elastic electron scattering by the Z-isomer of C-cyanomethanimine at 1–15 eV, obtained in the SE (gray), SEP (orange), and SEP+Born (blue dashed) approximations.

For the E-isomer (Figure 20), the DCS between 1–2 eV displays a broad single minimum. As the energy increases, SE and SEP remain nearly indistinguishable, and the Born term enhances forward scattering without significantly modifying the overall angular distribution above 4 eV.

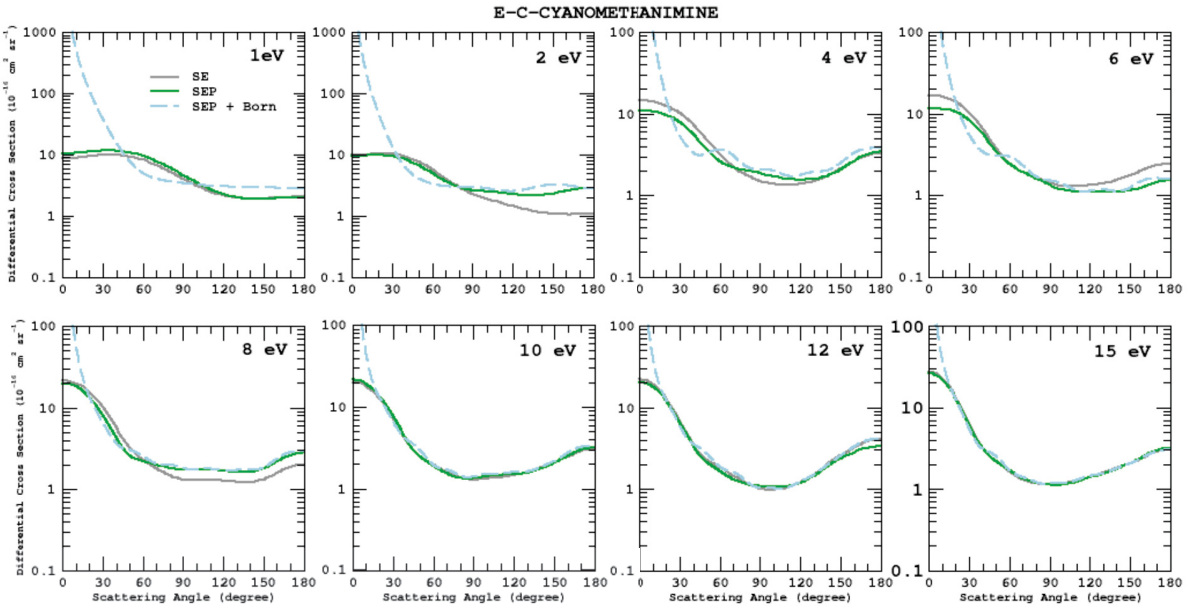

FIGURE 20 – DCS for the E-isomer at 1–15 eV, obtained in SE (gray), SEP (green), and SEP+Born (blue dashed) approximations.

For the N-isomer (Figure 21), the low-energy DCS (1–4 eV) are strongly influenced by long-range interactions. The inclusion of polarization (SEP) introduces additional structure relative to SE, while the Born correction consistently enhances forward scattering throughout the entire energy range.

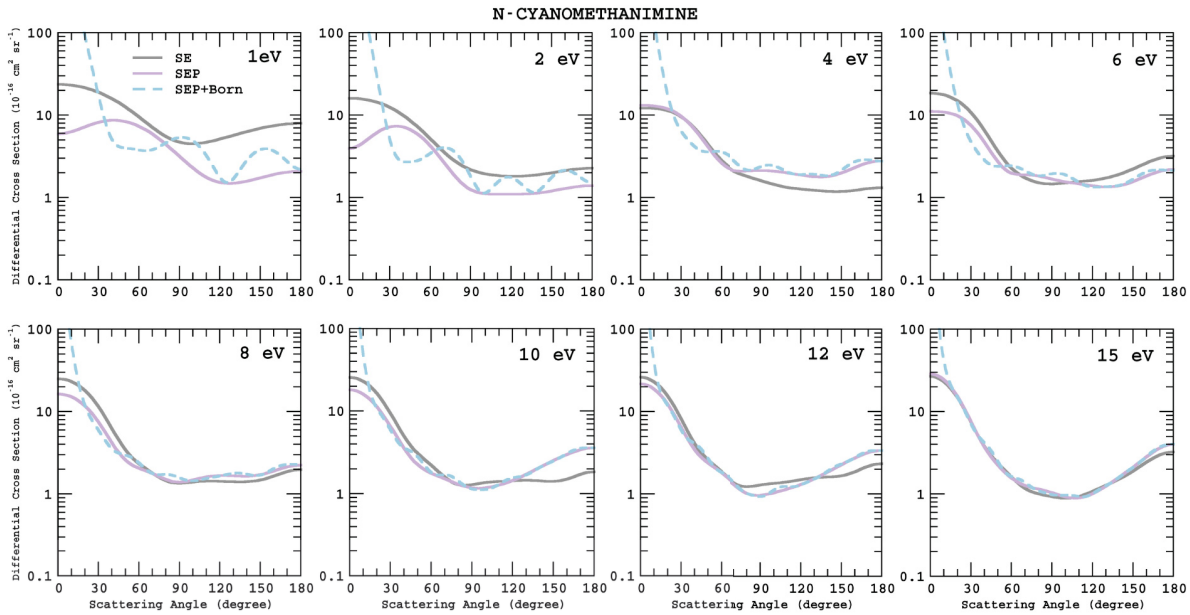

FIGURE 21 – DCS for the N-isomer at 1–15 eV, obtained in SE (gray), SEP (purple), and SEP+Born (blue dashed) approximations.

Overall, the Z-isomer exhibits a characteristic double-minimum angular profile arising from strong *d*-wave contributions. The E-isomer displays a smoother, less

structured single minimum, with forward scattering moderately enhanced by the Born term. The N-isomer, in turn, shows a markedly different behavior driven by its large dipole moment, which amplifies long-range effects and sustains strong forward scattering across the entire energy range.

4.3.5.2 Integral and Momentum Transfer Cross Sections

For the Z-isomer (Figure 22), the ICS exhibits sharp resonances below 6 eV, which are shifted to lower energies when polarization is included. The π^* resonances appear at similar positions but with enhanced intensity due to the Born term. A pseudo-resonance near 4 eV likely arises from neglected open channels treated as closed within the present model. The MTCS follows the same resonance pattern as the ICS, though with reduced magnitude, and the Born correction remains indistinguishable from the SEP results.

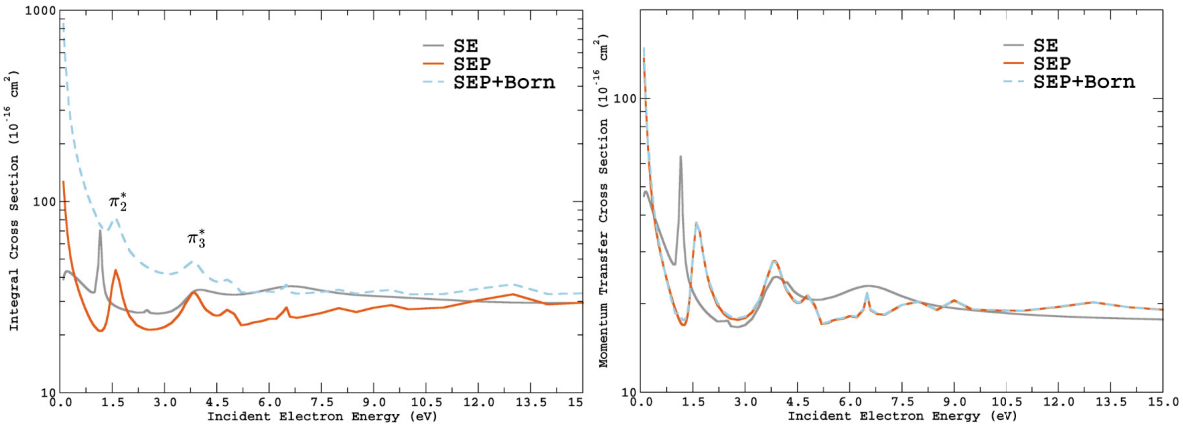

FIGURE 22 – (Left) ICS and (Right) MTCS for the Z-isomer, obtained in SE (gray), SEP (orange), and SEP+Born (blue dashed).

For the E-isomer (Figure 23), the ICS displays two dominant resonance features between 1 and 5 eV: a near-threshold peak and a broader structure around 4–5 eV. The π^* resonances appear at similar energies to those of the Z-isomer, but the overall ICS shows a stronger Born-induced enhancement. As in the Z-isomer, a pseudo-resonance near 4 eV is likely associated with open channels incorrectly treated as closed in the SEP approximation.

The MTCS, however, shows minimal dependence on the Born correction: SEP and SEP+Born curves are nearly coincident, confirming that the momentum-transfer cross section remains largely unaffected by long-range dipole contributions.

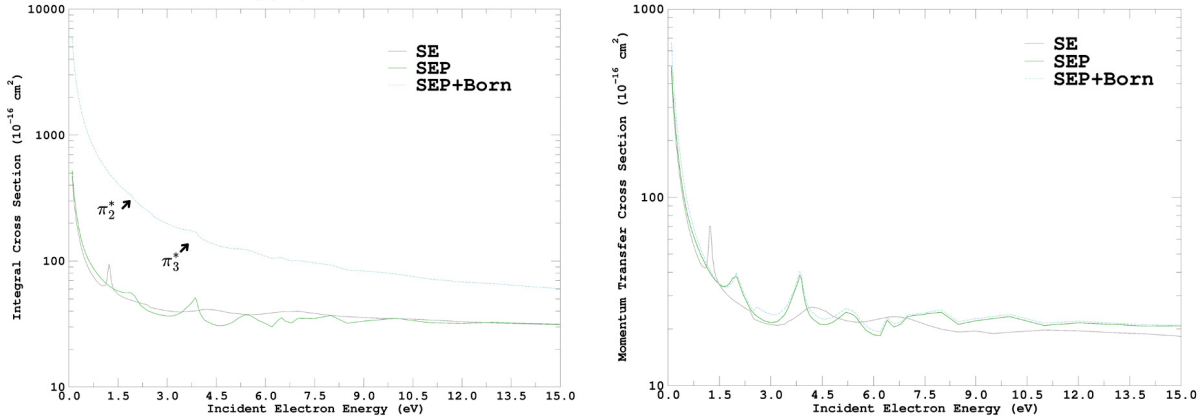

FIGURE 23 – (Left) ICS and (Right) MTCS for the E-isomer, obtained in SE (gray), SEP (green), and SEP+Born (blue dashed).

For the N-isomer (Figure 24), the ICS is markedly enhanced—more so than in the Z and E isomers, by the Born correction across the full energy range, consistent with its large permanent dipole moment (≈ 5.3 D). Two structures between 2.5 and 4.5 eV correspond to π^* resonance behavior. In contrast to the ICS, the MTCS is not significantly affected by the Born term: the SEP and SEP+Born curves remain essentially identical throughout the entire energy range, indicating that the forward-scattering enhancement is strongly angle-dependent and does not substantially alter the momentum-transfer cross section.

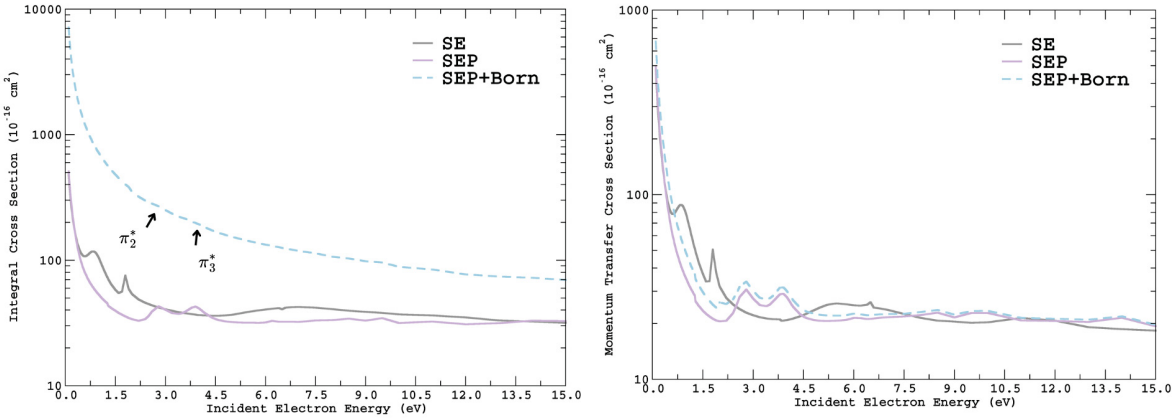

FIGURE 24 – (Left) ICS and (Right) MTCS for the N-isomer, obtained in SE (gray), SEP (purple), and SEP+Born (blue dashed).

In summary, the Z-isomer exhibits *d*- and *f*-wave dominance in the DCS, which governs the resonance structure in the ICS. The E-isomer is primarily characterized by *p*-wave features where they can be distinguished, while the N-isomer shows mixed *d*-, *f*-, and *g*-wave contributions amplified by its strong dipole field. Overall, molecular geometry controls the scattering behavior in the Z and E isomers, whereas dipole strength dominates in the N-isomer. Remaining limitations include pseudo-resonant

artifacts and the l_{SMC} cutoff in the 1–15 eV range, which should be addressed in future work through improved channel coupling.

4.3.6 Maxwell-Boltzmann Distribution of Gas Molecules

In order to evaluate the relative abundances of the different isomers of cyanomethanimine in the gas phase, it is essential to account for the thermal distribution of molecular populations. At thermal equilibrium, the number of molecules occupying a given isomeric state is governed by the Maxwell–Boltzmann distribution [35, 49], which relates the population of each state to its relative energy with respect to the ground state and the ambient temperature.

This statistical framework provides a straightforward connection between the total energies obtained from our calculations and the expected equilibrium fractions of the Z-, E-, and N-isomers. The resulting analysis not only clarifies which species are thermodynamically favored under laboratory conditions, but also provides a basis for understanding which isomers are likely to be observable in astrophysical environments.

We begin by consider the total number of molecules of HNCHCN in the gas phase as

$$N = N_Z + N_E + N_N, \tag{4.3}$$

where N_i are the populations of each isomer (Z-isomer, E-isomer, and N-isomer). Dividing through by N, we obtain

$$1 = \frac{N_Z}{N} + \frac{N_E}{N} + \frac{N_N}{N}. \tag{4.4}$$

Defining the fractional populations of each isomer as

$$n_Z = \frac{N_Z}{N}, \quad n_E = \frac{N_E}{N}, \quad n_N = \frac{N_N}{N}, \tag{4.5}$$

the expression becomes

$$1 = n_Z + n_E + n_N. \tag{4.6}$$

According to the Maxwell–Boltzmann distribution, the number of molecules is proportional to the energy difference between the neutral ground states of each isomer:

$$n_E = n_Z \exp\left[-\frac{(E_E - E_Z)}{k_B T}\right], \qquad n_N = n_Z \exp\left[-\frac{(E_N - E_Z)}{k_B T}\right], \tag{4.7}$$

where $k_B = 1.38 \times 10^{-23}$ J/K is the Boltzmann constant and $T = 298.15$ K. [8]

[8] Within the framework of this approximation, the use of the Maxwell-Boltzmann statistics is justified. For the typical temperature and density ranges encountered in standard molecular gas experiments. Under this condition, quantum statistical effects are negligible, and the classical Maxwell-Boltzmann description remains valid.

From our DFT calculations, the ground-state electronic energies (in eV) were found as:

$$E_Z = -5081.9983, \quad E_E = -5081.9847, \quad E_N = -5081.7561.$$

Using $k_B T = 0.025702\,\text{eV}$, the relative energy differences are

$$(E_E - E_Z) = 0.013606\,\text{eV}, \quad (E_N - E_Z) = 0.242182\,\text{eV}.$$

substituting into Eq.(4.5), we obtain

$$n_E = n_Z \times 0.588997, \qquad n_N = n_Z \times 8.086812 \times 10^{-5}. \tag{4.8}$$

Applying Eq.(4.1), the normalization gives

$$n_Z = \frac{1}{1 + 0.588997 + 8.086812 \times 10^{-5}} \approx 0.629305.$$

Therefore,

$$n_E \approx 0.37064, \qquad n_N \approx 5.60 \times 10^{-5}.$$

As percentages of the total population of HNCHCN isomers at 298.15 K:

TABLE 13 – Calculated percentage of Cyanomethanimine isomers in a gas.

Isomers	%	Dipole (Db)
Z-C	62.931	1.628
E-C	37.063	4.645
N	0.0061	5.324

At 298.15 K, the Boltzmann population analysis based on our DFT electronic energies shows that the Z- and E-isomers dominate the gas-phase distribution of cyanomethanimine, with fractions of approximately 63% and 37%, respectively, while the N-isomer contributes less than 0.01%. Although the N-isomer indeed supports genuine shape resonances, its large dipole moment also enhances background scattering, making the interpretation of its low-energy features less straightforward. More importantly, its vanishingly small equilibrium fraction explains why this isomer is not expected to be detectable in the interstellar medium (ISM), despite the theoretical presence of resonant structures. In contrast, the Z-isomer is the most stable and abundant species, while the E-isomer appears as a secondary but still significant component in the gas-phase distribution.

CHAPTER 5

CONCLUSION

This dissertation presented a systematic computational study of low-energy electron scattering by the Z, E, and N isomers of C-cyanomethanimine. The calculations identified and characterized the main shape resonances associated with the π^* orbitals and confirmed their positions through a combination of scaling laws, SE and SEP stabilization energies, and Hamiltonian diagonalization.

For the Z isomer, the π_2^* (a') resonance shifts from 4.01 eV (SE) to 1.60 eV (SEP), while the π_3^* (a'') decreases from 6.84 eV to 3.90 eV. The π_1^* (a'') state at 1.59 eV in SE becomes a bound state in SEP, consistent with its negative eigenvalue from Hamiltonian diagonalization (-1.06 eV). The E isomer exhibits a similar pattern: π_2^* shifts from 4.21 eV to 1.80 eV, π_3^* from 6.82 eV to 3.59 eV, and π_1^* becomes bound (-0.98 eV). For the N isomer, whose large dipole moment induces stronger polarization effects, the π_2^* resonance moves from 2.80 eV to 1.10 eV, π_3^* from 7.16 eV to 3.79 eV, and π_1^* likewise becomes a bound state (-0.94 eV).

Beyond resonance positions, the analysis of resonance widths (Γ) reinforces these trends. In the SE approximation, the Z isomer shows the narrowest widths for π_1^* and π_2^* (0.61 and 1.09 eV), indicating longer-lived temporary anions, whereas the N isomer displays shorter-lived resonances (1.30 and 0.42 eV). For the π_3^* resonance, however, the N isomer presents the longest lifetime (from 1.68 eV in SE to 1.35 eV in SEP), revealing a distinct scattering behavior driven by its strong dipole moment. In the SEP approximation, the π_2^* widths converge for Z and E (0.93 and 0.49 eV), while N becomes significantly broader (1.18 eV), and the π_3^* resonance remains narrowest for N. These variations highlight how polarization modifies the coupling of the incoming electron to each molecular geometry.

Taken together, the consistent energy shifts and systematic width variations confirm both the predictive power of the scaling law and the robustness of Hamiltonian diagonalization in validating the resonance dynamics. The results also differentiate the scattering behavior across isomers: Z is dominated by clear d-wave features and longer-lived temporary anions, E displays smoother s/p-wave scattering, and N is strongly influenced by dipole-induced polarization and broad background contributions.

Structurally, the calculations confirm the stability ordering

$$E_Z < E_E \ll E_N,$$

with Z as the global minimum, E slightly higher in energy (~ 0.014 eV), and N substantially less stable (~ 0.24 eV above Z). Boltzmann analysis at 298 K predicts populations of 63% (Z), 37% (E), and $< 0.01\%$ (N), demonstrating that only Z and E contribute meaningfully under astrophysical conditions, despite all three being local minima on the potential-energy surface.

High isomerization barriers further preserve Z and E as distinct, kinetically trapped structures in the interstellar medium (ISM), a key factor in environments far from equilibrium. Although all three isomers have been detected in the ISM, the present calculations show that the N isomer is not only thermodynamically disfavored but also exhibits less stable resonance patterns, suggesting that its abundance is likely maintained by non-equilibrium production pathways rather than by intrinsic stability.

Overall, this work provides a detailed characterization of cross sections, resonance energies, and resonance lifetimes for the C-cyanomethanimine isomers, establishing that the π_1^* orbital supports bound anionic states, whereas π_2^* and π_3^* form short-lived resonances. The results connect molecular structure, dipole strength, and scattering dynamics, offering essential theoretical input for astrochemical modeling of electron-driven processes. A natural extension of this study would be the investigation of dissociative electron attachment (DEA) pathways mediated by the π_2^* and π_3^* resonances, including mapping anionic potential-energy surfaces and computing DEA cross sections and branching ratios with advanced scattering methods.

REFERENCES

1. M. C. BOYER, N. RIVAS, A. A. TRAN, C. A. VERISH e C. R. ARUMAINAYAGAM. “The role of low-energy (20 eV) electrons in astrochemistry”. Em: *Surface Science* 652 (2016), pp. 26–32. DOI: 10.1016/j.susc.2016.04.014 (Citado 3 vez na página).

2. G. A. GALLUP, P. D. BURROW e I. I. FABRIKANT. “Electron-induced bond breaking at low energies in HCOOH and glycine: The role of very short-lived σ^* anion states”. Em: *Physical Review A* 79.4 (2009), p. 042701 (Citado 1 vez na página).

3. G. J. SCHULZ. “Resonances in electron impact on diatomic molecules”. Em: *Reviews of Modern Physics* 45.3 (1973), pp. 423–486. DOI: 10.1103/RevModPhys.45.423 (Citado 3 vez na página).

4. I. KLAIMAN S.and GILARY. “On Resonance: A First Glance into the Behavior of Unstable States”. Em: *Advances in Quantum Chemistry*. Vol. 63. Elsevier, 2012, pp. 1–31 (Citado 1 vez na página).

5. M. T. d. N. VARELLA. “O método multicanal de Schwinger aplicado ao espalhamento de elétrons I: Aspectos formais”. Em: *Revista Physicae* 1 (2000), pp. 45–58 (Citado 3 vez na página).

6. T. N. RESCIGNO, C. S. TREVISAN e A. E. OREL. “Comment on "electron-induced bond breaking at low energies in HCOOH and glycine: The role of very short-lived σ^* anion states"”. Em: *Physical Review A* 80.4 (2009), p. 046701 (Citado 1 vez na página).

7. B. BOUDAÏFFA, P. CLOUTIER, D. HUNTING, M. A. HUELS e L. SANCHE. “Resonant formation of DNA strand breaks by low-energy electrons”. Em: *Science* 287.5458 (2000), pp. 1658–1660. DOI: 10.1126/science.287.5458.1658 (Citado 1 vez na página).

8. B. SEDMIDUBSKÁ e J. KOČÍŠEK. “Interaction of low-energy electrons with radiosensitizers”. Em: *Physical Chemistry Chemical Physics* 26.12 (2024), pp. 1–25 (Citado 1 vez na página).

9. R. D’AGOSTINO. *Plasma Deposition, Treatment, and Etching of Polymers: The Treatment and Etching of Polymers*. 1ª ed. Boston: Academic Press, 1990 (Citado 1 vez na página).

10. M. CAPITELLI, R. CELIBERTO, G. COLONNA, F. ESPOSITO, C. GORSE, K. HASSOUNI, A. LARICCHIUTA e S. LONGO. *Fundamental Aspects of Plasma Chemical Physics*. 1ª ed. Vol. 85. Springer Series on Atomic, Optical and Plasma Physics. New York: Springer, 2016. DOI: 10.1007/978-1-4419-8182-0 (Citado 1 vez na página).

11. A. J. LICHTENBERG e M. A. LIEBERMAN. *Principles of Plasma Discharge and Materials Processing*. 2ª ed. Hoboken: Wiley-Interscience, 2005. DOI: 10.1002/0471724254 (Citado 1 vez na página).

12. J. N. MOSS e C. D. SCOTT, ed. *Thermophysical Aspects of Re–Entry Flows*. 1ª ed. New York: American Institute of Aeronautics e Astronautics, 1986. DOI: 10.2514/4.865770 (Citado 1 vez na página).

13. F. F. CHEN. “Industrial applications of low-temperature plasma physics”. Em: *Physics of Plasmas* 2.6 (1995), pp. 2164–2175. DOI: 10.1063/1.871477 (Citado 1 vez na página).

14. P. GIUNGATO, M. C. FERRARA, F. MUSIO e R. D’AGOSTINO. “Plasma Polymerized Thiophene for Sensing Volatile Chemicals: Synthesis, Chemical Characterization, and Low–Frequency Resistance Measurements”. Em: *Plasmas and Polymers* 1.4 (1996), pp. 283–297. DOI: 10.1007/BF02532827 (Citado 1 vez na página).

15. W. YANG. “A Tutorial Overview of the Angular Scattering Models of Electron–Neutral, Ion–Neutral, Neutral–Neutral, and Coulomb Collisions in Monte Carlo Collision Modeling on Low–Temperature Plasma”. Em: *Plasma Sources Science and Technology* 33.2 (2024), p. 023001. DOI: 10.1088/1361-6595/ad2491 (Citado 1 vez na página).

16. W. M. HUO e Y. K. KIM. “Electron Collision Cross–Section Data for Plasma Modeling”. Em: *IEEE Transactions on Plasma Science* 27.5 (1999), pp. 1225–1240. DOI: 10.1109/27.799798 (Citado 1 vez na página).

17. G. S. SELWYN, H. W. HERRMANN, J. PARK e I. HENINS. “Materials Processing Using an Atmospheric Pressure, RF–Generated Plasma Source”. Em: *Contributions to Plasma Physics* 41.6 (2001), pp. 610–619. DOI: 10.1002/1521-3986(200111)41:6<610::AID-CTPP610>3.0.CO;2-L (Citado 1 vez na página).

18. L. G. CHRISTOPHOROU e J. K. OLTHOFF. “Electron Collision Data for Plasma–Processing Gases”. Em: *Advances in Atomic, Molecular, and Optical Physics* 44 (2001), pp. 59–98. DOI: 10.1016/S1049-250X(01)80029-X (Citado 1 vez na página).

19. S. F. BOYS. “THE INTEGRAL FORMULAE FOR THE VARIATIONAL SOLUTION OF THE MOLECULAR MANY–ELECTRON WAVE EQUATION IN TERMS OF GAUSSIAN FUNCTIONS WITH DIRECT ELECTRONIC CORRELATION”. Em: *Proceedings of the Royal Society A* 258 (1960), p. 402 (Citado 1 vez na página).

20. C. J. JOACHAIN. *Quantum Collision Theory*. 1ª ed. Amsterdam: North-Holland Physics Publishing, 1975 (Citado 8 vez na página).

21. K. TAKATSUKA e V. MCKOY. “Extension of the Schwinger variational principle beyond the static-exchange approximation”. Em: *Physical Review A* 24 (1981), p. 2473 (Citado 2 vez na página).

22. K. Takatsuka e V. McKoy. “Theory of electronically inelastic scattering of electrons by molecules”. Em: *Physical Review A* 30.4 (1984), pp. 1734–1740. DOI: 10.1103/PhysRevA.30.1734 (Citado 2 vez na página).

23. R. F. DA COSTA et al. “Electron scattering by molecules using pseudopotentials: recent applications of the SMC method”. Em: *The European Physical Journal D* 69.7 (2015), p. 159. DOI: 10.1140/epjd/e2015-60243-5 (Citado 1 vez na página).

24. NRAO. *Discoveries Suggest Icy Cosmic Start for Amino Acids and DNA Ingredients*. National Radio Astronomy Observatory. Acesso em: 11 set. 2025. Socorro, NM, fev. de 2013. Disponível em: https://public.nrao.edu/news/pressreleases/icy-cosmic-start/ (Citado 2 vez na página).

25. M. MELOSSO, A. MELLI, C. PUZZARINI, C. CODELLA, L. SPADA, L. DORE, C. DEGLI ESPOSTI, B. LEFLOCH, R. BACHILLER, C. CECCARELLI, J. CERNICHARO e V. BARONE. “Laboratory measurements and astronomical search for cyanomethanimine”. Em: *Astronomy & Astrophysics* 609 (2018), A121. DOI: 10.1051/0004-6361/201731657 (Citado 1 vez na página).

26. C. PUZZARINI. “J. Phys. Chem. A”. Em: *The Journal of Physical Chemistry A* 119.47 (2015), pp. 11614–11622. DOI: 10.1021/acs.jpca.5b06843 (Citado 4 vez na página).

27. D. P. ZALESKI et al. “ApJL”. Em: *The Astrophysical Journal Letters* 765.1 (2013), p. L10. DOI: 10.1088/2041-8205/765/1/L10 (Citado 2 vez na página).

28. V. M. RIVILLA et al. “Monthly Notices of the Royal Astronomical Society: Letters”. Em: *Monthly Notices of the Royal Astronomical Society: Letters* 483.1 (2019), pp. L114–L119. DOI: 10.1093/mnrasl/sly223 (Citado 2 vez na página).

29. D. SAN ANDRÉS, V. M. RIVILLA, L. COLZI, I. JIMENEZ-SERRA, J. MARTIN-PINTADO, A. MEGIAS, Á. LOPEZ-GALLIFA, A. MARTINEZ-HENARES, S. MASSALKHI, S. ZENG, M. SANZ-NOVO, B. TERCERO, P. DE VICENTE, S. MARTIN, M. A. REQUENA TORRES, G. MOLPECERES e J. GARCIA DE LA CONCEPCION. “First Detection in Space of the High-energy Isomer of Cyanomethanimine: H_2CNCN”. Em: *The Astrophysical Journal* 967.1 (mai. de 2024). 15 pages, p. 39. DOI: 10.3847/1538-4357/ad3d5b (Citado 2 vez na página).

30. A. SZABO e N. S. OSTLUND. *Modern Quantum Chemistry: Introduction to Advanced Electronic Structure Theory*. 1ª ed. Mineola: Dover Publications, 1996 (Citado 5 vez na página).

31. C. C. J. ROOTHAAN. “New developments in molecular orbital theory”. Em: *Reviews of Modern Physics* 23.2 (1951), pp. 69–89. DOI: 10.1103/RevModPhys.23.69 (Citado 1 vez na página).

32. W. J. HUNT e W. A. GODDARD. “Excited States of H_2O using improved virtual orbitals”. Em: *Chemical Physics Letters* 3.6 (1969), pp. 414–418. DOI: 10.1016/0009-2614(69)87037-7 (Citado 2 vez na página).

33. C. W. BAUSCHLICHER. “The construction of modified virtual orbitals (MVO’s) which are suited for configuration interaction calculations”. Em: *The Journal of*

Chemical Physics 72.2 (1980), pp. 880–883. DOI: 10.1063/1.438938 (Citado 3 vez na página).

34. M. H. F. BETTEGA. “Espalhamento de Elétrons por Moléculas através de Pseudopotenciais Local Density”. Tese de Doutorado. Universidade Estadual de Campinas, 1993 (Citado 3 vez na página).

35. I. N. LEVINE. *Quantum Chemistry*. 5ª ed. Upper Saddle River, New Jersey: Prentice Hall, 1970 (Citado 3 vez na página).

36. J. SCHWINGER. “On a variational principle for scattering problems”. Em: *Physical Review* 72.8 (1947), pp. 742–749. DOI: 10.1103/PhysRev.72.742 (Citado 3 vez na página).

37. S. GELTMAN. *Topics in Atomic Collision Theory*. 1ª ed. New York: Academic Press, 1969 (Citado 1 vez na página).

38. M. A. P. LIMA e V. McKOY. “Aspects of the Schwinger multichannel variational formulation”. Em: *Physical Review A* 38.1 (1988), pp. 501–504. DOI: 10.1103/PhysRevA.38.501 (Citado 1 vez na página).

39. J. J. SAKURAI. *Modern Quantum Mechanics*. 2ª ed. Boston: Addison-Wesley Publishing Company, 1995 (Citado 1 vez na página).

40. M. H. F. Bettega, L. G. Ferreira e M. A. P. Lima. “Transferability of local-density norm-conserving pseudopotentials to electron-molecule-collision calculations.” Em: *Physical Review A* 47.2 (1993), pp. 1111–1118. DOI: 10.1103/PhysRevA.47.1111 (Citado 2 vez na página).

41. G. B. BACHELET, D. R. HAMANN e M. SCHLÜTER. “Pseudopotentials that work: From H to Pu”. Em: *Physical Review B* 26.8 (1982), pp. 4199–4228. DOI: 10.1103/PhysRevB.26.4199 (Citado 1 vez na página).

42. X. ZHANG et al. “Monthly Notices of the Royal Astronomical Society”. Em: *Monthly Notices of the Royal Astronomical Society* 497.1 (2020), pp. 609–625. DOI: 10.1093/mnras/staa1875 (Citado 1 vez na página).

43. R. PANICO, W. H. POWELL e J. C. RICHER. *A guide to IUPAC Nomenclature of Organic Compounds*. Ed. por R. Panico, W. H. Powell e J. C. Richer. Recommen-

dation 7.1.2. IUPAC/Blackwell Science, 1993. ISBN: 0-632-03488-2 (Citado 1 vez na página).

44. G. M. J. BARCA et al. “J. Chem. Phys.” Em: *The Journal of Chemical Physics* 152.15 (2020), p. 154102. DOI: 10.1063/5.0005188 (Citado 1 vez na página).

45. B. M. BODE e M. S. GORDON. “MacMolPlt: a graphical user interface for GAMESS”. Em: *Journal of Molecular Graphics and Modelling* 16.3 (1998), pp. 133–138. DOI: 10.1016/S1093-3263(99)00002-9 (Citado 1 vez na página).

46. M. H. F. BETTEGA, A. A. P. NATALENSE, M. A. P. LIMA e L. G. FERREIRA. “Note on the Generation of Gaussian Bases for Pseudopotential Calculations”. Em: *International Journal of Quantum Chemistry* 60.4 (1996), pp. 821–829. DOI: 10.1002/qua.560460822 (Citado 1 vez na página).

47. S. W. STALEY e J. T. STRNAD. “J. Phys. Chem.” Em: *The Journal of Physical Chemistry* 98.1 (1994), pp. 116–121. DOI: 10.1021/j100052a020 (Citado 2 vez na página).

48. F. VAZZART et al. “Journal of Chemical Theory and Computation”. Em: *Journal of Chemical Theory and Computation* 11.3 (2015), pp. 1165–1171. DOI: 10.1021/ct501083z (Citado 1 vez na página).

49. R. K. Pathria e P. D. Beale. *Statistical Mechanics*. 3rd. Singapore: Elsevier, 2011, pp. 583–586. DOI: 10.1016/B978-0-12-382188-1.00015-3 (Citado 1 vez na página).

50. L. H. Thomas. “The calculation of atomic fields”. Em: *Mathematical Proceedings of the Cambridge Philosophical Society* 23.5 (1927), pp. 542–548. DOI: 10.1017/S0305004100011683 (Citado 1 vez na página).

51. E. Fermi. “Eine statistische Methode zur Bestimmung einiger Eigenschaften des Atoms und ihre Anwendung auf die Theorie des periodischen Systems der Elemente”. Em: *Zeitschrift für Physik* 48.1–2 (1928), pp. 73–79. DOI: 10.1007/BF01351576 (Citado 1 vez na página).

52. W. Kohn e L. J. Sham. “Self-consistent equations including exchange and correlation effects”. Em: *Physical Review* 140.4A (1965), A1133–A1138. DOI: 10.1103/PhysRev.140.A1133 (Citado 2 vez na página).

53. P. A. M. Dirac. “Note on Exchange Phenomena in the Thomas Atom”. Em: *Mathematical Proceedings of the Cambridge Philosophical Society* 26.3 (1930), pp. 376–385. DOI: 10.1017/S0305004100016108 (Citado 1 vez na página).

54. R. O. Jones e O. Gunnarsson. “The density functional formalism, its applications and prospects”. Em: *Reviews of Modern Physics* 61.3 (1989), pp. 689–746. DOI: 10.1103/RevModPhys.61.689 (Citado 1 vez na página).

55. J. P. Perdew, A. Ruzsinszky, L. A. Constantin, J. Sun e G. I. Csonka. “Some Fundamental Issues in Ground-State Density Functional Theory: A Guide for the Perplexed”. Em: *Journal of Chemical Theory and Computation* 5.4 (2009), pp. 902–908. DOI: 10.1021/ct900032g (Citado 1 vez na página).

56. W. Kohn. “Nobel Lecture: Electronic structure of matter-wave functions and density functionals”. Em: *Reviews of Modern Physics* 71.5 (1999), pp. 1253–1266. DOI: 10.1103/RevModPhys.71.1253 (Citado 1 vez na página).

57. L. V. S. Dalagnol. “O Método da Teoria do Funcional da Densidade (Estático e Dinâmico)”. Unpublished manuscript. 2025 (Citado 1 vez na página).

58. J. F. Janak. “Proof that $\partial E/\partial n_i = \epsilon_i$ in density–functional theory”. Em: *Physical Review B* 18.12 (1978), pp. 7165–7168. DOI: 10.1103/PhysRevB.18.7165 (Citado 1 vez na página).

APPENDIX **A**

THE DENSITY FUNCTIONAL THEORY

Density Functional Theory (DFT) is a variational method based on the self-consistent field approach [35, 50–55]. Unlike Hartree–Fock, which relies on the many-body wave function, DFT uses the electronic density as the fundamental variable to minimize the energy functional of the ground state ($|\Phi_0\rangle$) for a system of N interacting particles under an external potential (e.g., interaction with nuclei). Developed in the 1960s this theory builds upon the Thomas–Fermi–Dirac atomic theory and simplifies complex quantum systems using the Born–Oppenheimer approximation and atomic Hartree units.

The central idea of Density Functional Theory [56] is that the desired energy can be regarded as a functional of the electronic density, $\rho(\vec{r})$. For closed-shell systems, the electronic density, sometimes called the electronic probability density, for a system of N electrons is defined as[1].

$$\rho(\vec{r}) \equiv \sum_{i=1}^{N} \langle \Phi_0 | \, \hat{\delta}(\vec{r} - \vec{r}_i) \, | \Phi_0 \rangle \,, \tag{A.1}$$

where $\hat{\delta}\left(\vec{r} - \vec{r}_i\right)$ is the Dirac delta operator. Using the completeness relation of the coordinate basis for an N-electron system, namely:

$$\mathbb{1}_N \equiv \prod_{j=1}^{N} \int d^3 r_j \; |\vec{r}_1, \vec{r}_2, \cdots, \vec{r}_i, \cdots, \vec{r}_N\rangle \, \langle \vec{r}_1, \vec{r}_2, \cdots, \vec{r}_i, \cdots, \vec{r}_N| \,, \tag{A.2}$$

we obtain:

$$\begin{aligned} \rho(\vec{r}) &\equiv \sum_{i=1}^{N} \langle \Phi_0 | \mathbb{1}_N \hat{\delta}(\vec{r} - \vec{r}_i) \, | \Phi_0 \rangle \\ &= \sum_{i=1}^{N} \prod_{j=1}^{N} \int d^3 r_j \; \langle \Phi_0 \mid \vec{r}_1, \vec{r}_2, \cdots, \vec{r}_i, \cdots, \vec{r}_N| \\ &\qquad \times \langle \vec{r}_1, \vec{r}_2, \cdots, \vec{r}_i, \cdots, \vec{r}_N | \, \hat{\delta}(\vec{r} - \vec{r}_i) \, | \Phi_0 \rangle \,, \end{aligned} \tag{A.3}$$

[1] For more details on the derivations of the equations presented in this dissertation, see the appendix of [57]

where $\delta\left(\vec{r}-\vec{r}_i\right)$ is the Dirac delta "function." Then, using the sifting property:

$$\begin{aligned}\rho(\vec{r}) &= \sum_{i=1}^{N}\prod_{j=1}^{N}\int d^3r_j\,\Phi_0^*\left(\vec{r}_1,\vec{r}_2,\cdots,\vec{r}_i,\cdots,\vec{r}_N\right)\delta\left(\vec{r}-\vec{r}_i\right)\Phi_0\left(\vec{r}_1,\vec{r}_2,\cdots,\vec{r}_i,\cdots,\vec{r}_N\right)\\ &= \sum_{i=1}^{N}\prod_{j\neq i}^{N}\int d^3r_j\,\Phi_0^*\left(\vec{r}_1,\vec{r}_2,\cdots,\vec{r},\cdots,\vec{r}_N\right)\Phi_0\left(\vec{r}_1,\vec{r}_2,\cdots,\vec{r},\cdots,\vec{r}_N\right),\end{aligned} \tag{A.4}$$

one can permute $\vec{r}_1$ with $\vec{r}$ in each term of the above equation, using the fact that Φ_0 must be antisymmetric, and then perform the sum to obtain:

$$\rho(\vec{r}) \equiv N\prod_{i=2}^{N}\int d^3r_i\,\Phi_0^*\left(\vec{r},\vec{r}_2,\vec{r}_3,\cdots,\vec{r}_N\right)\Phi_0\left(\vec{r},\vec{r}_2,\vec{r}_3,\cdots,\vec{r}_N\right), \tag{A.5}$$

and thus the integrations are performed over $\vec{r}_2,\vec{r}_3,\cdots,\vec{r}_N$. Before proceeding with the objective of expressing the energy as a functional of the electronic density, it is convenient to write the Hamiltonian operator in the following way:

$$H_N = -\sum_{i=1}^{N}\frac{1}{2}\nabla_i^2 - \sum_{i=1}^{N}\sum_{A=1}^{M}\frac{\mathcal{Z}_A}{\left|\vec{r}_i-\vec{R}_A\right|} + \sum_{i=1}^{N}\sum_{j>i}^{N}\frac{1}{|\vec{r}_i-\vec{r}_j|}, \tag{A.6}$$

Before proceeding with the goal of expressing the energy as a functional of the electronic density, it is convenient to rewrite the Hamiltonian operator as follows:

$$H_N = T + V + W \tag{A.1}$$

where T is the kinetic energy operator, defined as:

$$T \equiv -\sum_{i=1}^{N}\frac{1}{2}\nabla_i^2, \tag{A.7}$$

V is the electronic interaction operator, which includes Coulombic repulsion and all non-classical terms, defined as:

$$V \equiv \sum_{i=1}^{N}\sum_{j>i}^{N}\frac{1}{|\vec{r}_i-\vec{r}_j|}, \tag{A.8}$$

and W is the electron-nucleus interaction operator, often referred to as the external potential, given by:

$$W \equiv -\sum_{i=1}^{N}\sum_{A=1}^{M}\frac{\mathcal{Z}_A}{\left|\vec{r}_i-\vec{R}_A\right|}. \tag{A.9}$$

Assuming W defines the problem, an assumption justified by the universality of the operator $T+V$ for any multi-electronic system, it follows that W also defines the

wave function. Consequently, W determines the electronic density, which underpins the two fundamental theorems of Density Functional Theory: the Hohenberg–Kohn theorems:

Theorem A.1: First Hohenberg–Kohn Theorem: The external potential $W[\rho]$ experienced by the electrons is, up to an additive constant, a unique functional of the electronic density $\rho(\vec{r})$.

Theorem A.2: Second Hohenberg–Kohn Theorem: The ground-state energy is minimized for the exact density $\rho(\vec{r})$. That is, the functional $E_0[\rho]$, defined as:

$$\begin{aligned} E_0[\rho] &\equiv \langle \Phi_0 | \, H_N \, | \Phi_0 \rangle = \langle \Phi_0 | \, T + V + W \, | \Phi_0 \rangle \\ &= \langle \Phi_0 | \, T + V \, | \Phi_0 \rangle + \langle \Phi_0 | \, W \, | \Phi_0 \rangle \, , \end{aligned} \tag{A.10}$$

represents the ground-state energy of the electronic system. This functional is minimized for the exact ground-state electronic density $\rho(\vec{r})$ of the system under the influence of the potential W.

Theorems A.1 and A.2 establish how to determine the ground state of a system under a known potential W. The apparent challenges of the approach are resolved by imposing the following conditions on the electronic density: Non-negativity:

$$\rho(\vec{r}) \geq 0, \tag{A.11}$$

Normalization

$$\int d^3r \, \rho(\vec{r}) = N, \tag{A.12}$$

Finiteness

$$\int d^3r \, |\vec{\nabla} \sqrt{\rho(\vec{r})}|^2 < +\infty. \tag{A.13}$$

However, since the universal functional $F_{HK}[p]$ encompasses all purely electronic terms, including kinetic energy, Coulomb repulsion, exchange, and correlation, it must be handled with care. Furthermore, unlike the one-body problem, expressing the kinetic energy functional in terms of the electronic density is not straightforward. To address these challenges, Walter Kohn and Lu Jeu Sham developed an elegant and robust approach to circumvent this issue.

A.1 KOHN-SHAM EQUATIONS

To begin, the term with a classical analogue can be effectively isolated from $V[\rho]$:

$$V[\rho] = J[\rho] + K[\rho], \tag{A.14}$$

here, $J[\rho]$ represents the direct term, or the pure Coulomb repulsion term, which has a classical analogue and can be determined relatively easily, as it involves a two-particle operator. In contrast, $K[\rho]$ is a functional that includes all the terms of $V[\rho]$ that lack classical analogues.

$$J[\rho] = \frac{1}{2} \iint d^3r \, d^3r' \, \frac{\rho(\vec{r})\rho(\vec{r'})}{|\vec{r} - \vec{r'}|}. \tag{A.15}$$

What remains is the functional for the kinetic energy, $T[\rho]$, which cannot be trivially expressed in terms of the electronic density in many-body problems. It is within this context that Kohn and Sham introduced, in a remarkable manner, wave functions known as orbitals, allowing the kinetic energy to be computed relatively simply and with high accuracy, up to a small residual term that is negligible compared to the other terms. These orbitals, referred to as Kohn-Sham Orbitals and denoted as $\psi(\text{KS})(\vec{r})$ or $|\psi(\text{KS})\rangle$, describe a system of non-interacting electrons with a density exactly equal to $\rho(\vec{r})$. In other words, they represent a fictitious system of non-interacting electrons that produce the same electronic density $\rho(\vec{r})$. The desired ground state is described by a Slater determinant formed from the Kohn-Sham orbitals, given by:

$$\langle \vec{r}_1, \vec{r}_2, \ldots, \vec{r}_N \mid \Phi_0 \rangle = \frac{1}{\sqrt{N!}} \begin{vmatrix} \psi_1^{(\text{KS})}(\vec{r}_1) & \psi_2^{(\text{KS})}(\vec{r}_1) & \ldots & \psi_N^{(\text{KS})}(\vec{r}_1) \\ \psi_1^{(\text{KS})}(\vec{r}_2) & \psi_2^{(\text{KS})}(\vec{r}_2) & \ldots & \psi_N^{(\text{KS})}(\vec{r}_2) \\ \vdots & \vdots & \ddots & \vdots \\ \psi_1^{(\text{KS})}(\vec{r}_N) & \psi_2^{(\text{KS})}(\vec{r}_N) & \ldots & \psi_N^{(\text{KS})}(\vec{r}_N) \end{vmatrix}. \tag{A.16}$$

Even though the $\psi(\text{KS})_i(\vec{r}_i)$, for $i = 1, \ldots, N$, represent orbitals of a non-interacting electron reference system, the way they are constructed, in the context of the method, ensures that they correctly describe the interacting system's density.

When $\langle h\Phi_0|H_N|\Phi_0\rangle$ reaches an extremum, the electronic density obtained from the Kohn-Sham orbitals approaches the true electronic density of the ground state. To illustrate the brilliant approach developed by Kohn and Sham [52], it is helpful to begin with the exact formula for the kinetic energy of the ground state for the interacting particle system, derived using matrix elements involving Slater determinants,

$$T = -\frac{1}{2} \sum_{i=1}^{+\infty} \langle \Phi_0 | \, \nabla_i^2 \, | \Phi_0 \rangle = -\frac{1}{2} \sum_{a=1}^{+\infty} n_a \, \langle \psi_a^{(\text{KS})} | \, \nabla_i^2 \, | \psi_a^{(\text{KS})} \rangle \,, \tag{A.17}$$

where $\psi(\text{KS})$ refers to the natural orbitals, and n_a is the occupation number of each orbital. Since the system is fermionic, the Pauli exclusion principle requires that the occupation number, n_a, must lie between 0 and 1, i.e., $0 \leq n_a \leq 1$ for all $a = 1, 2, \ldots$. The electronic density can be obtained by:

$$\rho(\vec{r}) = \sum_{a=1}^{+\infty} n_a \, \langle \psi_a^{(\mathrm{KS})} | \, \delta(\vec{r}_i - \vec{r}) \, | \psi_a^{(\mathrm{KS})} \rangle = \sum_{a=1}^{+\infty} n_a \int d^3 r_i \, \psi_a^{(\mathrm{KS})*}(\vec{r}_i) \delta(\vec{r}_i - \vec{r}) \psi_a^{(\mathrm{KS})}(\vec{r}_i), \quad \text{(A.18)}$$

using the filtering property of the Dirac delta:

$$\rho(\vec{r}) = \sum_{a=1}^{+\infty} n_a |\psi_a^{(\mathsf{KS})}(\vec{r})|^2 \quad \text{(A.19)}$$

Note that for any interacting system of interest, there is an infinite number of terms in equations (A.16) and (A.17), as evidenced by the upper limit of the summation. However, Kohn and Sham showed that it is possible to simplify the equations (A.16) and (A.17) by assuming that:

$$n_a = \begin{cases} 1 & \text{if} \quad a \leq N \\ 0 & \text{if} \quad a > N \end{cases} \quad \text{(A.20)}$$

the formulas simplify to:

$$\begin{aligned} T_{\mathrm{KS}}[\rho] &= -\frac{1}{2} \sum_{a=1}^{N} \langle \psi_a^{(\mathrm{KS})} | \, \nabla_i^2 \, | \psi_a^{(\mathrm{KS})} \rangle \\ \rho(\vec{r}) &= \sum_{a=1}^{N} \left| \psi_a^{(\mathrm{KS})}(\vec{r}) \right|^2 \end{aligned} \quad \text{(A.21)}$$

This simplification leads to a more practical method for solving the many-body problem using Kohn-Sham orbitals, where only the occupied states (those with $a \leq N$) contribute to the density and the kinetic energy.

The kinetic energy can be separated into two terms:

$$T[\rho] = T_{\mathsf{KS}}[\rho] + T_{\mathsf{R}}[\rho], \quad \text{(A.22)}$$

where $T_{\mathsf{KS}}[\rho]$ is the kinetic energy of a fictitious non-interacting electron system defined by equation (A.21), but with the electronic density $\rho(\sim r)$, and $T_{\mathsf{R}}[\rho]$ is the residual term of the kinetic energy.

The functional of the ground-state energy is:

$$E_0[\rho] = T_{\mathsf{KS}}[\rho] + T_{\mathsf{R}}[\rho] + \frac{1}{2} \iint d^3 r \, d^3 r' \frac{\rho(\vec{r}) \rho(\vec{r'})}{|\vec{r} - \vec{r'}|} + K[\rho] + \int d^3 r \, w_M(\vec{r}) \rho(\vec{r}), \quad \text{(A.23)}$$

defining the exchange-correlation functional $E_{\mathsf{xc}}[\rho]$ as:

$$E_{\mathsf{xc}}[\rho] \equiv T_{\mathsf{R}}[\rho] + K[\rho], \quad \text{(A.24)}$$

so that $E_{\text{xc}}[\rho]$ contains not only the term that holds all the non-classical electronic interactions, but also the residual kinetic energy.

The electronic energy of the ground state, written as a functional of the density, is then:

$$E_0[\rho] = T_{\text{KS}}[\rho] + \frac{1}{2}\iint d^3r\, d^3r' \frac{\rho(\vec{r})\rho(\vec{r'})}{|\vec{r} - \vec{r'}|} + \int d^3r\, w_M(\vec{r})\rho(\vec{r}) + E_{\text{xc}}[\rho], \tag{A.25}$$

or, alternatively:

$$E_0[\rho] = T_{\text{KS}}[\rho] + \frac{1}{2}\iint d^3r\, d^3r' \frac{\rho(\vec{r})\rho(\vec{r'})}{|\vec{r} - \vec{r'}|} - \sum_{A=1}^{N} \mathcal{Z}_A \int d^3r \frac{\rho(\vec{r})}{|\vec{r} - \vec{R}_A|} + E_{\text{xc}}[\rho]. \tag{A.26}$$

Now, by applying the Hamiltonian principle solely to the functional in equation (A.25), we obtain the Kohn-Sham orbitals, which, in order to have physical meaning, must be normalized. Thus, the ground-state energy functional in terms of the N Kohn-Sham orbitals is:

$$E_0\left[\{\psi_c^{(\text{KS})*}(\vec{r}_i)\}\right] = -\frac{1}{2}\sum_{c=1}^{N}\int d^3r_i\, \psi_c^{(\text{KS})*}(\vec{r}_i)\nabla_i^2\psi_c^{(\text{KS})}(\vec{r}_i) + \sum_{c=1}^{N}\int d^3r_i\, \psi_c^{(\text{KS})*}(\vec{r}_i) v_{\text{KS}}(\vec{r}_i)\psi_c^{(\text{KS})}(\vec{r}_i), \tag{A.27}$$

where $i = 1, 2, \ldots, N$. From this, we can define an effective potential, known as the Kohn-Sham Effective Potential, $v_{\text{KS}}(\vec{r})$, which is given by:

$$v_{\text{KS}}(\vec{r}) = \frac{\delta E_0[\rho]}{\delta\rho(\vec{r})}. \tag{A.28}$$

This effective potential is the key component of the Kohn-Sham method, as it represents the potential that the fictitious non-interacting particles experience in order for their density to match the true electronic density of the real system. When applied to the definition of the Kohn-Sham Hamiltonian, these lead to the equations known as the non-canonical Kohn-Sham equations:

$$H_{\text{KS}}(\vec{r}_i)\psi_a^{(\text{KS})}(\vec{r}_i) = \sum_{b=1}^{N}\varepsilon_{ab}\psi_b^{(\text{KS})}(\vec{r}_i), \quad i = 1, 2, \ldots, N, \tag{A.29}$$

These unitary transformations are analogous to those in Hartree-Fock, as discussed in the previous section. Therefore, we obtain the following.

$$H_{\text{KS}}(\vec{r}_i)\psi_a^{(\text{KS})}(\vec{r}_i) = \varepsilon_a\psi_a^{(\text{KS})}(\vec{r}_i), \quad a = 1, 2, \ldots, N. \tag{A.30}$$

Although the Kohn-Sham equations are written as linear eigenvalue equations, they are actually pseudoeigenvalue equations because the Kohn-Sham Hamiltonian has functional dependence through the potential, necessitating iterative procedures. In practice, a basis set must be introduced and a suitable exchange-correlation functional must be selected. However, certain aspects of the eigenvalue equation remain independent of the basis set, such as the significance of the eigenvalues of the Kohn-Sham orbitals. The first to demonstrate this was electrical engineer James Franck Janak [58], and for this reason, the result he derived is known as Janak's Theorem, which is now stated as:

Theorem A.3: Janak's Theorem: Let $n_a \in \mathbb{R}$ be the occupation number of each of the Kohn-Sham orbitals, which can now take any real value in the closed interval [0, 1]; ε_a is the corresponding eigenvalue of the Kohn-Sham orbital, $\psi_a^{(\mathsf{KS})}(\vec{r})$, and $E_0[\rho]$ is the electronic energy functional of the ground state. The derivative of E_0 with respect to n_a is equal to the eigenvalue ε_a of the corresponding orbital $\psi_a^{(\mathsf{KS})}(\vec{r})$, and it is independent of the form of the exchange-correlation functional $E_{\mathsf{xc}}[\rho]$, that is:

$$\frac{\partial E_0[\rho]}{\partial n_a} = \varepsilon_a, \quad \forall a = 1, 2, \ldots, N \text{ and } \forall E_{\mathsf{xc}}[\rho]. \tag{A.31}$$

Using the theorem, we can derive the Kohn-Sham equations of the Hartree-Fock-Roothaan-Hall type. The natural development of these equations leads to the matrix equations of the Hartree-Fock-Roothaan-Hall type. The goal of this subsection is to describe the solution method for the equations in the case of closed-shell systems. The calculation of molecular orbitals can be reduced to solving the corresponding integral-differential equations.

$$\left[-\frac{1}{2}\nabla^2 + v_{\mathsf{KS}}(\vec{r})\right] \psi_b^{(\mathsf{KS})}(\vec{r}) = \varepsilon_b \psi_b^{(\mathsf{KS})}(\vec{r}), \quad b = 1, 2, 3, \ldots, \frac{N}{2}, \tag{A.32}$$

Defining the Kohn-Sham Fock-like operator as:

$$f_{\mathsf{KS}}(\vec{r}) \equiv -\frac{1}{2}\nabla^2 + v_{\mathsf{KS}}(\vec{r}), \quad b = 1, 2, 3, \ldots, \frac{N}{2}, \tag{A.33}$$

this simplifies to:

$$f_{\mathsf{KS}}(\vec{r})\psi_b^{(\mathsf{KS})}(\vec{r}) = \varepsilon_b \psi_b^{(\mathsf{KS})}(\vec{r}), \quad b = 1, 2, 3, \ldots, \frac{N}{2}. \tag{A.34}$$

Defining the elements of the Kohn-Sham Fock-like matrix as:

$$F_{\mu\nu}^{(\mathsf{KS})} \equiv \int d^3r\, \varphi_\mu^*(\vec{r}) f_{\mathsf{KS}}(\vec{r}) \varphi_\nu(\vec{r}), \tag{A.35}$$

where $F(\mathsf{KS})$ is a $k \times \kappa$ Hermitian matrix (usually real and symmetric if the basis is real, i.e., $F(\mathsf{KS})\mu v = F(\mathsf{KS})v\mu \Rightarrow F(\mathsf{KS})^\dagger = F(\mathsf{KS})$). The Kohn-Sham Fock operator is an

operator for a single electron, and any set of single-electron functions defines its matrix representation.

The Kohn-Sham Fock matrix is:

$$\boldsymbol{F}^{(\mathrm{KS})} = \begin{pmatrix} F_{11}^{(\mathrm{KS})} & F_{12}^{(\mathrm{KS})} & F_{13}^{(\mathrm{KS})} & \dots & F_{1\kappa}^{(\mathrm{KS})} \\ F_{12}^{(\mathrm{KS})*} & F_{22}^{(\mathrm{KS})} & F_{23}^{(\mathrm{KS})} & \dots & F_{2\kappa}^{(\mathrm{KS})} \\ F_{13}^{(\mathrm{KS})*} & F_{23}^{(\mathrm{KS})*} & F_{33}^{(\mathrm{KS})} & \dots & F_{3\kappa}^{(\mathrm{KS})} \\ \vdots & \vdots & \vdots & \ddots & \vdots \\ F_{1\kappa}^{(\mathrm{KS})*} & F_{2\kappa}^{(\mathrm{KS})*} & F_{3\kappa}^{(\mathrm{KS})*} & \dots & F_{\kappa\kappa}^{(\mathrm{KS})} \end{pmatrix}. \tag{A.36}$$

defining the elements of the overlap matrix as:

$$S_{\mu\nu} \equiv \int d^3r\, \varphi_\mu^*(\vec{r})\varphi_\nu(\vec{r}), \tag{A.37}$$

Assuming S is a $\kappa \times \kappa$ matrix that is Hermitian (or real and symmetric if the basis is real, which means, $S_{\mu\nu} = S_{\nu\mu} \Rightarrow S^\dagger = S$). The basis set is considered orthonormal and linearly independent, but it is not generally mutually orthogonal. As a result, the basis functions exhibit overlap such that $0 \leq |S_{\mu\nu}| \leq 1$. The diagonal elements are equal to 1, while the off-diagonal elements have magnitudes strictly less than 1. If the magnitude of any off-diagonal element approaches unity, it indicates complete overlap between the corresponding basis functions, leading to linear dependence.

Substituting the definitions, we have:

$$\sum_{\nu=1}^{\kappa} F_{\mu\nu}^{(\mathrm{KS})} C_{\nu b} = \sum_{\nu=1}^{\kappa} S_{\mu\nu} C_{\nu b} \varepsilon_b \quad b = 1, 2, \dots, \kappa \tag{A.38}$$

Thus, we can finally write the Kohn-Sham equations in the Hartree-Fock-Roothaan-Hall form:

$$\boldsymbol{F}^{(\mathrm{KS})} C = \boldsymbol{S}\boldsymbol{C}\boldsymbol{\varepsilon} \tag{A.39}$$

Finally, the orthogonalized Kohn-Sham Hartree-Fock-Roothaan-Hall equations are:

$$F'^{(\mathrm{KS})} \boldsymbol{C'} = C'\varepsilon \tag{A.40}$$

whose non-trivial solutions are given by:

$$\det\left[\boldsymbol{F}'^{(\mathrm{KS})} - \varepsilon\right] = \det\left[\boldsymbol{F}'^{(\mathrm{KS})} - \varepsilon_a \not{\mathbb{1}}\right] = 0, \tag{A.41}$$

which is an eigenvalue problem. However, it is a pseudo-eigenvalue-eigenvector problem because, as $F(\mathrm{KS})$, C, and ε are matrices, this is strictly an eigenvalue-eigenmatrix problem.